Grain Growth and Extended Defects in Multicrystalline Silicon Grown from Microcrystalline Silicon Template

Grain Growth and Extended Defects in Multicrystalline Silicon Grown from Microcrystalline Silicon Template

Ronit R. Prakash

Doctoral Program in Materials Science and Engineering

Submitted to the Graduate School of

Pure and Applied Sciences

in Partial Fulfillment of the Requirements

for the Degree of Doctor of Philosophy in

Engineering

at the

University of Tsukuba

Abstract

Multicrystalline silicon (mc-Si) is the dominant material for photovoltaic application, however existence of extended defects, such as grain boundaries (GB), dislocations and impurities lead to the reduction of the conversion efficiency. Control of these extended defects during growth process is important and is mainly done by controlling the initial stage of growth. However, grain structure evolution during growth can lead to the appearance of these undesired extended defects. Although, in recent years, mc-Si grown from small randomly oriented grains (called High Performance multicrystalline silicon HP mc-Si) has given promising results, the grain structure evolution in mc-Si is unclear and it needs to be understood in order to make further improvements. To investigate the grain structure evolution in mc-Si grown from small randomly oriented seeds, mc-Si was grown by directional solidification from a microcrystalline silicon (micro-Si) template, which has small randomly oriented grains. The grain structure of the grown mc-Si was investigated with respect to growth height using horizontal and vertical wafers. The work in this thesis can be broadly broken into three areas: grain structure evolution, impact of pulling rate and grain boundary interactions.

The grain structure evolution of the template grown ingot was carefully studied and was compared with another ingot grown by the conventional method at similar growth conditions. In the template grown ingot, the grain structure study showed three stages of growth. At the initial stage the grains are of spherical shape and although the grains are small initially, the grain size increases with growth height. Moreover, there is a high fraction of random (R) GBs which decreases with growth height. In the second stage, the grains elongate in the growth direction and become ellipsoidal, and the average grain size does not change. In the third stage the grain size increases with growth height and the grains have a columnar structure. In this stage grains with near orientations of <112> and <122> become dominant. The three growth stages are discussed with respect to impact of the template, preferential growth and impact of grain boundaries. On the other hand, conventional mc-Si has larger grains at the initial growth stage, and although the average grain size increases initially, it becomes almost constant at later stage of growth. As opposed to the template grown ingot, conventional mc-Si has a high fraction of Σ3 GBs, and some dominant orientations appear from the initial growth stage.

The impact of crucible pulling rate on the grain structure evolution was also investigated. Two ingots were grown from microcrystalline template, one with 15 mm/h and the other 45 mm/h pulling rate, and their grain structure evolution was studied. It was found that higher pulling rate enhanced columnar grain growth and the grain size was relatively smaller. It was also observed that the fraction of Σ3 GBs was higher at later growth stage in ingot grown with higher pulling rate. These results were explained

using increase in undercooling in the grain boundary grooves, and it was also suggested that GB interactions affected the grain structure evolution.

GB interactions were statistically studied in vertical wafers of template grown mc-Si. GB interactions that would lead to a decrease in GB density were defined as Annihilation, while interactions which increase GB density were defined as Generation. The frequency of GB interactions decreased as growth height increased. Although the fraction of Annihilation was always higher, there were three distinct regions of tendency change. These three regions were defined as stages **I**, **II** and **III** and it was suggested that although stages **I** and **II** may depend on the template, stage **III** is expected to hold true in general for mc-Si. From the statistics of GB interactions, it was found that although R GB interactions are high in stage **I**, it decreases in stage **II** and becomes almost constant in stage **III**. The dominant GB interaction was found to be that involving Σ3 GB. It was also found that Generation of Σ3 GB from an R GB led to the inclination of that R GB, which consequently increased the probability of that R GB to merge with other R GBs. This would lead to the annihilation of the R GBs leading to an increase in grain size. This also explained the larger grain size of twinned grains.

In summary, this thesis discusses the grain structure evolution in mc-Si grown from small randomly oriented grains. The importance of initial nucleation, grain alignment and impact of GBs, especially twins on grain structure evolution was highlighted. The impact of the crucible pulling rate was studied and a relationship between twinning, grain size and the pulling rate was discussed. Another important finding was the impact of interaction between grain boundaries on grain structure evolution, especially between Σ3 and R GB, which lead to increase in grain size. The findings in this thesis contribute to the understanding of grain structure evolution which is essential for optimization of mc-Si growth.

List of Abbreviations

CSL	Coincidence Site Lattice
EBIC	Electron Beam Induced Current
EBSD	Electron Backscatter Diffraction
GB(s)	Grain Boundary(ies)
HP mc-Si	High Performance Multicrystalline Silicon
IPF	Inverse Pole Figure
LA GB	Large Angle Grain Boundary
MAD	Misorientation Angle Distribution
Mc-Si	Multicrystalline Silicon
MCL	Minority Carrier Lifetime
Micro-Si	Microcrystalline Silicon
PR15	Ingot grown at Pulling Rate 15 mm/h
PR45	" " " " 45 mm/h
R GB	Random Grain Boundary
SA GB	Small Angle Grain Boundary

Crystallographic Notations used in this thesis

[*hkl*] **Crystallographic Direction**

<*hkl*> **Set of all direction** equivalent to [*hkl*] under the symmetry group of the crystal

(*hkl*) **Crystallographic Plane**

{*hkl*} **Set of all planes** equivalent to (hkl) under the symmetry group

Acknowledgment

The work in this thesis would not have been possible without the help of many individuals and groups and I wish to acknowledge them for their contributions.

First, I wish to thank my supervisor and group leader, Prof. Takashi Sekiguchi, for his advice and encouragement, especially for making himself available for discussions whenever needed. I also appreciate the members of Nano Device Characterization Group (NDCG) of National Institute for Materials Science (NIMS) : Prof. Sekiguchi and Dr. Chen Jun for their advice regarding electron beam induced current and defect etching, Dr. Jiptner, Dr. Harada and Mr. Miyamura for help and advice on crystal growth, carrier lifetime measurement and chemical processes.

With regards to crystal growth, I wish to thank Dr. Jiptner from NIMS for the long hours put in growth and for growing the ingot which became the motivation of this research. Also, I am grateful to Prof. Ohshita, Dr. Tachibana and Mr. Kojima of Toyota Technological Institute for letting us use their crystal growth facility. The minority carrier lifetimes were mainly measured at Meiji University and I wish to thank Prof. Ogura for letting me use their μ-PCD machine and Mr. Ikeno and Mr. R. Suzuki for their technical assistance. I also wish to thank Dr. Gao and Prof. Tsuchiya from the International Center for Young Scientists (ICYS) for letting me use their electron backscatter machine. MANA Foundry and their friendly staff are much appreciated for their assistance and for allowing me to use their clean room for chemical processes containing dangerous chemicals.

Mrs. Tomura from NDCG is greatly appreciated for taking care of the tremendous amount of official paperwork ranging from visa applications to official business trips. Dr. Watanabe, Ms. Yujin, Dr. Kimura, Dr. Li and Dr. Dierre also helped with the discussions during seminars. I wish to thank all members of my group for making my stay in Japan memorable and for always providing a positive atmosphere for research. I wish to thank the National Institute for Materials Science for giving me the opportunity to work as a Junior Researcher exposing me to world class research facilities. I am also very grateful to Prof. Akimoto, Prof. Fukata and Prof. Tsuchiya of Tsukuba University for joining Prof. Sekiguchi and Dr. Harada on my Ph.D. supervisory panel.

I wish to acknowledge that this work was partially supported by the New Energy and Industrial Technology Development Organization (NEDO) under the Ministry of Economy, Trade and Industry (METI).

Table of Contents

CHAPTER 1

Introduction

The increasing global energy consumption, together with the dwindling reserves of fossil fuels and its damaging impacts on the environment has pushed for a rapid development of renewable energy. Photovoltaics have gained considerable momentum in recent years and will continue to prosper in future. Crystalline silicon remains the dominant material for solar cells with about 90% market share [1-1]. The two major types of crystalline silicon are single crystalline (also called monocrystalline silicon, mono-Si) and the multicrystalline silicon (mc-Si). In recent years mc-Si grown by casting method, has overtaken single crystalline silicon to become the dominant material for solar cells having about 55% market share in 2013 [1-1]. This is due to the lower cost and higher productivity of mc-Si when grown by the casting method. However, due to the presence of extended defects such as grain boundaries, dislocations and impurities, the conversion efficiency is lower for solar cells made from mc-Si than that made from single crystalline silicon grown by Czochralski (CZ) or floating zone (FZ) method.

The cause for the lowered efficiency in mc-Si is localized regions of high minority carrier recombination. Studies have shown that transition metals can decrease the minority carrier diffusion length, which is a key parameter for determining the efficiency of solar-cell devices [1-2,1-3]. Some grain boundaries and dislocations heavily interact with the impurities and become gettering sites where the impurities precipitate and become difficult to take out by extrinsic gettering [1-4, 1-5]. These precipitates can become unlimited suppliers of the impurities during high temperature processes of cell fabrication. Impurity interaction with grain boundaries is known to depend on the character of the grain boundaries [1-6, 1-7]. Consequently, grain boundary engineering, where highly detrimental grain boundaries are reduced, has gained attention. The most common way of controlling grain boundaries in mc-Si is during the growth process.

Numerous techniques have been developed to grow mc-Si with a higher quality while keeping the cost as low as possible. One recent, technique is the so called High

Performance multicrystalline silicon (HP-mc), which grows from small randomly oriented seeds [1-8, 1-9]. The conversion efficiency of HP-mc solar cells has been reported to be higher and more uniform than conventional mc-Si. The dislocation density has also been reported to be lower than conventional mc-Si and this is suggested to be due to uniform grains and strain relaxation due to random grain boundaries. However with growth, the grain structure evolves and the grain size increases as well as the dislocation density [1-9]. The mechanism of grain structure evolution in mc-Si is unclear and remains an important area to conquer to enable a larger yield of high quality mc-Si.

1-1 Objective of the thesis

The aim of this thesis is to clarify the grain structure evolution in mc-Si grown by directional solidification from small randomly oriented seeds. For this purpose, mc-Si was grown from a microcrystalline template, which contains small randomly oriented grains, and the grain structure evolution was investigated with respect to the following:

1) Impact of template (microcrystalline template growth vs conventional mc-Si)
2) Impact of pulling rate
3) Impact of grain boundary interactions

1-2 Thesis Outline

Grain structure evolution in mc-Si grown from small randomly oriented seeds was investigated and is explained in this thesis. This thesis is composed of seven chapters where chapter 2 briefly discusses some fundamental knowledge related to this work and the concepts used in this thesis while chapter 3 introduces the experimental procedures. Chapters 4-6 focuses mainly on the original results obtained from this work and the discussions explaining the reasons behind the phenomena observed. Chapter 7 summarizes this thesis and also suggests some future work that can further contribute to this topic. The outline of the chapters is discussed in more detail below.

Chapter 2 introduces some fundamentals of multicrystalline silicon and extended defects which may be useful to understand the concepts used in other chapters. A brief introduction is given for topics such as the properties of crystalline silicon, grain boundaries, other extended defects and popular methods of defect control through growth optimization. Also discussed are the impacts of the extended defects on the efficiency of solar cells.

The background of the experimental procedures used in this thesis is discussed in Chapter 3. The first section discusses the setup and the parameters used for the crystal growth. This is followed by sample preparation and the characterization technique. The main characterization technique used is electron backscatter diffraction (EBSD)

Chapter 4 reports on the characteristics of mc-Si grown from the microcrystalline silicon template [1-10]. The grain structure is investigated with respect to distribution of grain size, grain boundary and grain orientation. It is compared with mc-Si grown by the conventional method

Chapter 5 discusses the impact of crucible pulling rate on the grain structure evolution. Ingots were grown from microcrystalline template with different crucible pulling rates, where one pulling rate was 15 mm/h and another 45 mm/h. The grain structure is discussed in terms of grain size, boundaries and orientation with respect to growth height.

The impact of grain boundary interactions on grain structure evolution is discussed in chapter 6 [1-11]. Grain boundary triple junctions were studied with respect to growth height and two main types of grain boundary interactions were defined. The distribution

of grain boundary interactions is demonstrated statistically and the impact of grain boundary interactions on the grain size evolution is discussed.

The summary of this thesis and some future work are discussed in Chapter 7. Regarding future work, additional experiments are proposed to further understand the grain structure evolution in mc-Si which may contribute to a general model for mc-Si growth.

1-3 References

[1-1] Fraunhofer Institute for Solar Energy Systems ISE, Photovoltaics Report, Freiburg, 24 October 2014

[1-2] Davis Jr, John Ransford, et al. "Impurities in silicon solar cells." *Electron Devices, IEEE Transactions on* 27.4 (1980): 677-687.

[1-3] Istratov, A. A., H. Hieslmair, and E. R. Weber. "Iron contamination in silicon technology." *Applied Physics A* 70.5 (2000): 489-534.

[1-4] Hamet, J. F., et al. "Precipitation at grain boundaries in silicon." *Materials Science and Engineering: B* 4.1 (1989): 143-145.

[1-5] Seibt, M., et al. "Interaction of metal impurities with extended defects in crystalline silicon and its implications for gettering techniques used in photovoltaics." *Materials Science and Engineering: B* 159 (2009): 264-268.

[1-6] Buonassisi, T., et al. "Metal precipitation at grain boundaries in silicon: Dependence on grain boundary character and dislocation decoration." *Applied Physics Letters* 89.4 (2006): 042102.

[1-7] Chen, Jun, et al. "Recombination activity of Σ3 boundaries in boron-doped multicrystalline silicon: Influence of iron contamination." *Journal of applied physics* 97.3 (2005): 033701-033701.

[1-8] Lan, C. W., et al. "Grain control in directional solidification of photovoltaic silicon." *Journal of Crystal Growth* 360 (2012): 68-75.

[1-9] Y. M. Yang, A. Yu, B. Hsu, W. C. Hsu, A. Yang, C. W. Lan, *Prog. Photovolt: Res. Appl.* (published online). http://dx.doi.org/10.1002/pip.2437 , 2013

[1-10] Prakash, Ronit R., et al. "Grain growth of cast-multicrystalline silicon grown from small randomly oriented seed crystal." *Journal of Crystal Growth* 401 (2014): 717-719.

[1-11] Prakash, Ronit R., et al. "Grain boundary interactions in multicrystalline silicon grown from small randomly oriented seeds." *Applied Physics Express* 8.3 (2015): 035502.

CHAPTER 2

Fundamentals of Multicrystalline Silicon and Extended Defects

2-1 Introduction

This chapter introduces the fundamentals of some of the concepts used extensively throughout this thesis. Crystal structure of silicon, grain boundaries, grain boundary engineering and impact of extended defects such as transition metal impurities on the conversion efficiency are some of the topics briefly discussed.

2-2 Silicon Crystal

Crystalline silicon remains the dominant material for commercial production of photovoltaic (PV) modules. It is abundant in supply (2nd most abundant element in earth's crust after oxygen), non-toxic and is a stable semiconductor. Moreover, the dominance of silicon in the microelectronics industry, has led to silicon being one of the most studied semiconductors. The transfer of the knowledge from the microelectronics industry is one of the reasons for the success of silicon in the photovoltaic industry.

Silicon has a diamond cubic structure and the unit cell of silicon is shown in Fig. 2-1. (a). The low index crystal planes (100), (110) and (111) are shown in Fig. 2-1 (b). As can be seen in Fig. 2-1, the atomic packing is different for different planes leading to the anisotropic nature. The anisotropy of the crystal surface is an important factor to consider. For example, in single crystalline silicon solar cells; due to the much faster etching rate of {100} in comparison to the {111} [2-1], selective etching can produce pyramids at the surface, which reduces the light reflection leading to an increased efficiency. However, in mc-Si due to the random orientation of the grains and presence of grain boundaries, surface texturization is not easy, although recent efforts have shown improvements [2-2, 2-3, 2-4].

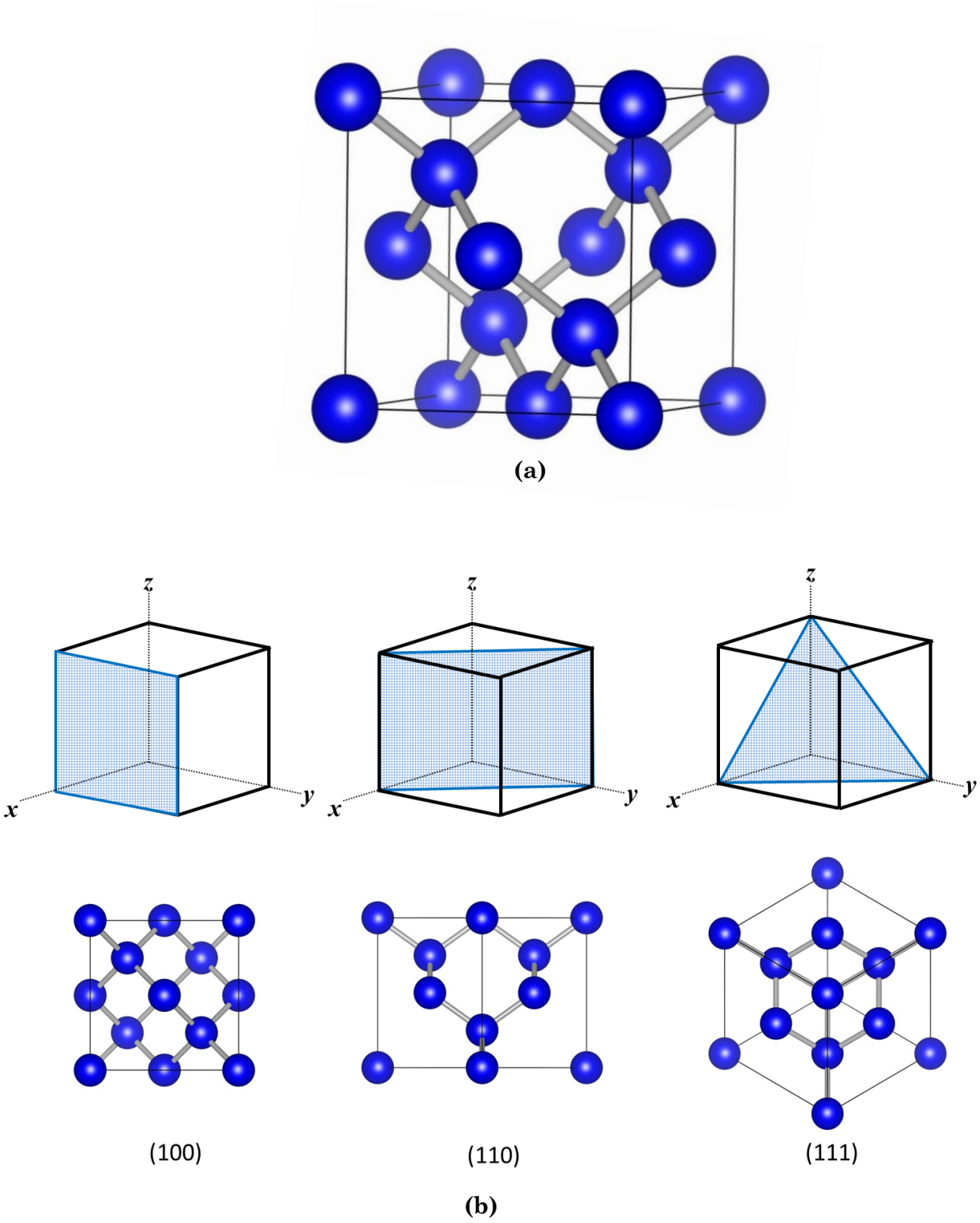

Figure 2-1. (a) Unit cell of silicon. (b) Crystal lattice planes of Si showing (100),(110),(111). (Drawn using VESTA 2.1.6 [2-5])

Not only is it important during processing, crystallographic anisotropy also plays an important role during nucleation and growth. In the classic nucleation theory the specific energy of the crystal/melt interface is assumed to be isotropic so a spherical nucleus forms. However, in case of silicon which is anisotropic, the shape of the critical nucleus of the crystal grown on a flat substrate is determined both by the surface tension and by the effective interfacial tension [2-6]. Fujiwara et al have suggested that the crystal growth shape of Si is octahedrally bounded by well-developed {111} facet planes, as {111} planes also have the lowest interfacial energy, (0.34 Jm^{-2} as calculated by Apte et al) [2-7, 2-8, 2-9].

Moreover according to the surface energy theory, based on the thermodynamic treatment of equilibrium states put forward by Gibbs: growing surface would assume that shape for which the surface energy is lowest [2-10]. Therefore, taking the surface energy into consideration is also important. Table 2.1 shows a summary of surface energies of some of the planes useful for this thesis. All the values are taken from the calculated values by Zhang et al [2-11], except for those inserted which are measured values from Jaccodine [2-12] and Gilman [2-13]. It can be seen that (111) has the lowest surface energy followed by (112), while (100) and (110) have relatively higher surface energy.

(*hkl*)	Surface Energy (ergs cm^{-2})	(*hkl*)	Surface Energy (ergs cm^{-2})
(100)	1880, (2130)[2-12]	(221)	1448
(110)	1536, (1510)[2-12]	(311)	2922
(111)	1254, (1230)[2-12], (1240)[2-13]	(321)	1886
(210)	1812	(433)	1397
(211)	1330	(511)	2589

Table 2-1. Surface energy values (ergs cm^{-2}) for various surfaces of silicon, taken from calculation of Zhang [2-11], measurements of Jaccodine[2-12] and Gilman [2-13].

2-3 Grain Boundaries

One big difference between single silicon and mc-Si is the presence of grain boundaries (GB) in mc-Si. Grain boundaries are the interface between two grains and are planar defects. Generally, GBs can be fully characterised by five independent parameters (degrees of freedom: DOF), three specify mutual misorientation of adjoining grains (rotation axis: 2 DOF, angle: 1 DOF), while two specify the orientation of the GB between the misoriented grains (2 DOF) [2-14]. Grain boundaries can be broadly characterized into small angle GB and large angle GBs. Small angle GBs have a low angle of misorientation, and this misorientation can be accommodated by an array of dislocations [2-15], however the misorientation angle has a limit at around 15°[2-16]. If the misorientation between two adjoining grains is above this limit, the grain boundaries can be classified as large angle grain boundaries. Large angle GBs can be further classified into coincidence site lattice (CSL), where lattice points of the misoriented grains coincide in a regular manner [2-17]. The reciprocal of the density of the coincidence sites, Σ, is an important parameter showing the coincidence between the lattice. Therefore a low Σ value means the coincidence is high. CSL are special because they have a given fraction of atoms in the grain boundary plane which are coincident to both planes [2-18]. For example in case of Σ3, one in 3 atoms at the coincident site will coincide. In mc-Si Σ3 is very common, and it has very low energy compared to other GBs [2-19, 2-20, 2-21]. A CSL boundary should have minimum energy when it lies in the most densely packed plane of coincidence lattice [2-18]. For cubic symmetry the Σ3 has an angle of 60°and an axis {111}. The Σ3 is a highly coherent GB, on the other hand a Random (R) GB is a non-coherent GB and is a mixture of both twist and tilt and do not follow Brandon's criteria [2-16]. Brandon's criteria is a criterion for proximity to a CSL structure :

$$\theta=\theta_0\Sigma^{-1/2} \qquad (1)$$

where proportionality constant θ_0 is generally taken to be 15^0 based on low to high angle transition.

There are often multiple misorientations that can achieve a given Σ value for example Σ27 can be achieved by a 31.59 degree rotation about [110] and 35.43 degrees about [210].

These descriptions are combined and various axis/angle descriptions corresponding to each Σ type for cubic symmetry (in this thesis until Σ27) are listed in Table 2.2 [2-22].

Σ Type	**Angle**	**Axis**
1	0	111
3	60	111
5	36.86	100
7	38.21	111
9	38.94	110
11	50.47	110
13a	22.62	100
13b	27.79	111
15	48.19	210
17a	28.07	100
17b	61.92	221
19a	26.53	110
19b	46.83	111
21a	21.78	111
21b	44.41	211
23	40.45	311
25a	16.26	100
25b	51.68	331
27a	31.59	110
27b	35.43	210

Table 2-2. Details of coincidence site lattice grain boundaries[2-22]

2-4 Feedstock for Multicrystalline Silicon Growth

In the early days of photovoltaic, the feedstock was the rejected scrap from the silicon produced for the microelectronics industry. However, due to the high demand in recent years, the main feedstock is now made by the conventional Siemens method. First the metallurgical grade silicon is produced by carbothermic reduction of quartz (as shown in equations (A)-(E)).

(A) SiO_2 (s) + 2C(s) $\rightarrow$Si(l) + 2CO(g)

(B) SiO(g) + 2C(s)$\rightarrow$SiC(s)+ CO(g)

(C) SiO_2(l)+Si(l)$\rightarrow$2SiO(g)

(D) SIC(s)+ 2$SiO_2$$\rightarrow$3SiO(g)+CO(g)

(E) SiC(s) + SiO(g) $\rightarrow$Si(l)+CO(g)

To get a high purity, the metallurgical grade Si is converted into silanes and then distilled and decomposed. The majority of the polysilicon produced today either use trichlorosilane (TCS) ($SiHCl_3$) or monosilane [2-23] which is purified by fractional distillation. The separated $SiHCl_3$ is decomposed and reduced on high purity rods at high temperature. The equation for the process is shown below:

(F) $SiHCl_3$ (g) + H_2(g) $\rightarrow$Si(s) + 3HCl(g)

2-5 Multicrystalline Silicon for Solar Cells

Although single crystalline silicon solar cells have a higher efficiency, the cost is high, so the lower cost multicrystalline silicon is used more often these days. Mc-Si for PV applications usually contain a variety of defects ranging from point defects of various origins to extended defects like dislocations, grain boundaries, micro-defects or second phase precipitates. Although generally grain boundaries are not electrically active at room temperature, grain boundaries decorated with metal impurities become electrically active even at room temperature [2-24, 2-25]. The electrical performance, mainly the minority carrier lifetime, is closely related to metal impurities present in the feedstock or introduced during crystal growth and solar cell processing [2-26, 2-27]. These impurities strongly interact with the defects to form complexes, accumulate at dislocations or grain

boundaries in different forms, or form silicide precipitates [2-28].Moreover, it has been found that Fe contamination of grain boundaries may enhance the electrical conductivity along grain boundaries, which also can potentially shunt the solar cells [2-29].

The carrier recombination is a major factor controlling Si solar cell performance, and one controllable but often dominant recombination mechanism is the defect assisted, Shockley Read Hall recombination [2-30]. Transition metal impurities are one of the major factors affecting the performance of solar cells, as they form deep levels in the silicon band gap and enhance recombination. Extended defects such as dislocations and high energy grain boundaries, which strongly interact with the impurities, make it easier for impurities to diffuse into the mc-Si during growth and make it difficult for the impurities to be taken out through extrinsic gettering.

Therefore, control of extended defects during the growth process in essential. Many growth technologies have been developed over the years to reduce the density of defects. Mainly, the initial region of growth is carefully controlled by the use of seeds or by optimization of temperature gradient to control undercooling.

2-6 Grain Boundary Engineering through Growth Optimization

To reduce the impact of GBs on the solar cell performance, it is desirable to avoid the formation of grain boundaries that interact strongly with metals. This would reduce diffusion of impurities from melt during growth and also make it easier to getter out impurities that do enter the bulk crystal. For this reason methods such as grain boundary engineering (GBE), to promote formation of special GBs (low Σ values) is considered. Although in metal alloys sequential thermomechanical processing is a common method, where often cold rolling is followed by annealing, since silicon is brittle this process is unsuitable and best methods of GBE may be during growth [2-31]. The most common way of controlling GBs has been controlling the initial stage of growth using seeds or undercooling. For example the dendritic growth method, where control of the undercooling at the initial stage of growth could induce large grains with same orientation to the growth direction at the bottom of the crucible (an alternative floating

cast has also been proposed) [2-32, 2-33, 2-34]. Apart from the large grains (low GB density), in this growth method a high fraction of Σ3 GBs exist. This technique however, needs precise control of temperature for undercooling and it was found to be difficult at industrial scale [2-35]. Wang et al proposed the spot cooling technique where they used crucible with notches. They also achieved large grained mc-Si with a high fraction of Σ3 GBs [2-36]. However, this technique also had its problems at industrial scale since the notches could induce crucible breakage [2-36]. To completely remove GBs, techniques to grow monocrystalline silicon by casting method were developed. One of the popular techniques was the seed-cast method, where monocrystalline silicon seeds were placed at the bottom of the crucible and unidirectional solidification enabled monocrystalline silicon to grow upwards from the seeds [2-37]. This method however, has the problem of dislocation generation from the gaps between seeds, and also mc-Si growth from the side of the crucible. Seed-cast using a single seed has also been proposed by Miyamura et al, aiming to reduce the dislocation density as well as to suppress mc-Si growth from side walls [2-38].

Although, to reduce impact of GBs most techniques concentrated on decreasing the GB density by increasing grain size, recently a technique using small randomly oriented seeds has gained much attention. Lan et al proposed, the high performance multicrystalline silicon (HP-mc), where small randomly oriented seeds are used to grow mc-Si [2-39, 2-40]. Although this technique has a high fraction of R GBs, it has been reported that lower dislocation density and uniform grain structure (grain size, defect distribution) exists, which enables solar cells with a higher and narrower distribution of efficiency [2-39-2-41] compared to conventional mc-Si. Although this technique has been developed recently, major silicon suppliers for mc-Si solar cells are considering HP-mc and it is expected to become the dominant mc-Si solar cell technology in future [2-42]. Although dislocation density has been reported to be low, in this technique it has been reported that dislocation density increases with growth and grain size also increases [2-39-2-41].

2-7 Transition Metal Impurities

Although in this thesis, transition metal impurities will not be focused, it will be briefly introduced in this section because of its strong impact on the performance of solar cells as well as its interaction with grain boundaries. In PV-Si transition metal impurities particularly Fe, Cr, Ni, and Cu can be present in concentrations as high as 10^{14} cm^{-3} in the as-grown substrates [2-43]. Transition metal impurities in the dissolved state are highly mobile with diffusivities close to 10^{-6} cm^2/s at typical process temperatures [2-44]. The main impurities found in Si belong to the 3d transition metals. Due to the high diffusivities, mc-Si can be easily contaminated by transition metals as grown-in (impurities in feedstock or during crystal growth), from chemicals (water, photo resist), from processing equipment (furnaces, rapid thermal annealing, polishing) and from handling [2-44]. Even low amounts of transition metal impurities can be detrimental to the solar cells. For example, Fe can deteriorate the efficiency of mc-Si solar cells even at a low concentration of 1ppb ($2.5x10^{13}cm^{-3}$) [2-44]. Davies J. R. et al investigated the effective solar cell efficiencies versus impurity concentration and the results are shown in Figure 2-2 [2-45].

As can be seen in Figure 2-2, that even small concentrations of transition metals can harm the solar cell efficiency. Therefore, introduction of transition metal impurities in Si must be avoided, or the effects of transition metals must be decreased through advance techniques. Impurity gettering and hydrogen passivation are some of the techniques to improve the material quality of Si for solar cells. However impurity gettering is sometimes difficult for precipitates.

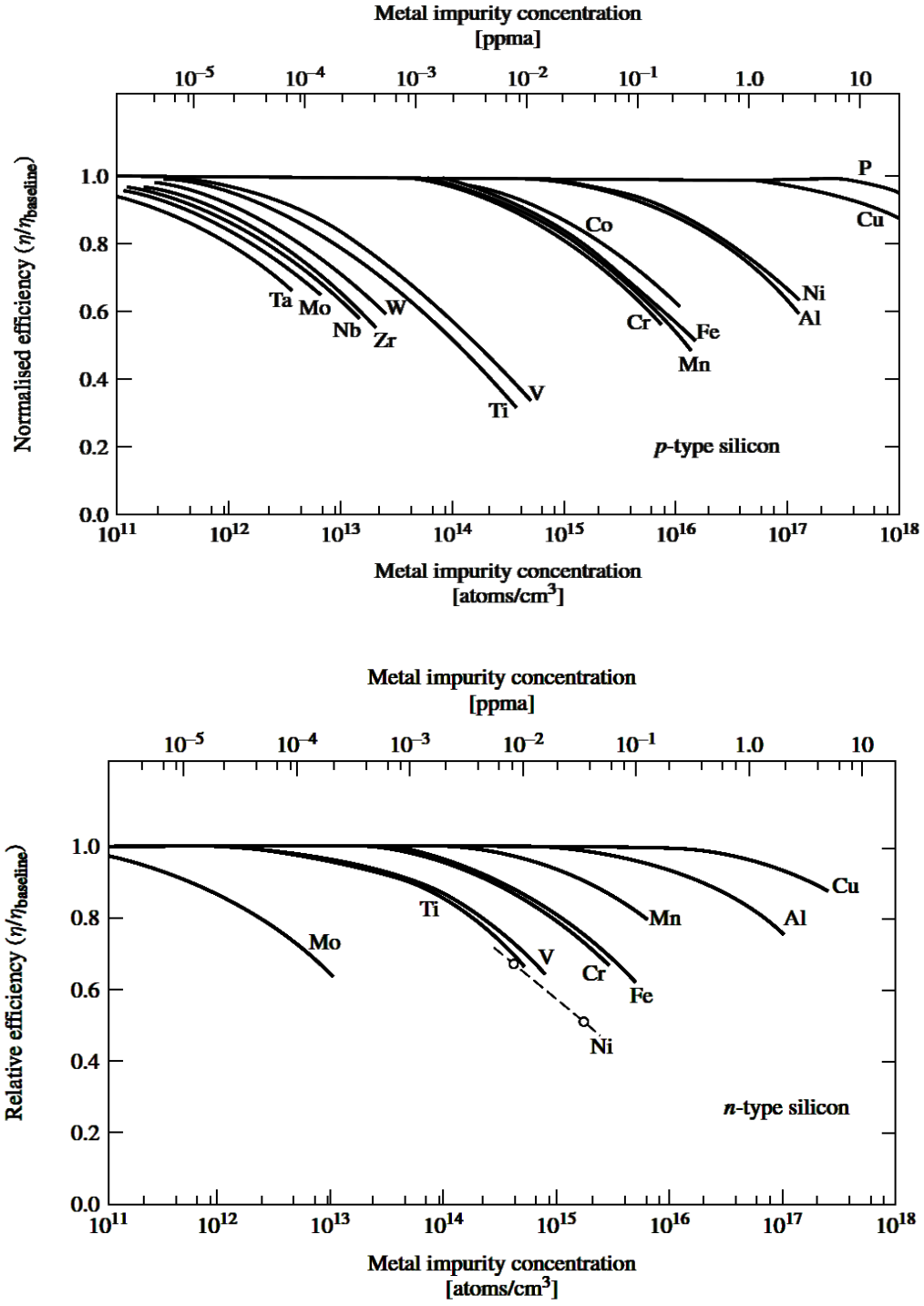

Figure 2-2 Solar cell efficiency versus impurity concentration for (a) 4 Ωcm p-base devices, (b) 1.5 Ωcm n-base devices. Reproduced from Impurities in Silicon Solar Cells, Davies J. R. et al. [2-45]

2-8 Directional Solidification and Impurity Incorporation

Directional solidification growth of Si (Bridgman, cast growth) is done in a quartz crucible which is coated with silicon nitride (Si_3N_4). Si_3N_4 serves as an anti-sticking layer preventing the adhesion of the silicon ingot to the quartz crucible walls, which is due to the volume expansion during crystallisation of the silicon material. This prevents the breaking of both the crucible and the silicon ingot.

Crystallisation starts at the bottom of the crucible by lowering the temperature below the melting point (1414°C) of Si. After solidification starts in the bottom region, the crystallisation front, the liquid-solid interface, moves in a vertical direction upwards through the crystallisation crucible.

During directional solidification it is assumed that a local equilibrium exists close to the solid-liquid interface. Most impurity elements are more soluble in liquid silicon that the solid phase and hence have a distribution coefficient, k_0, less than unity. These impurities segregate into the liquid keeping the solidified region clean, however at the top region the impurities get saturated and the melt in the top region when solidified has high concentration of impurities. This region is usually not used for solar cells.

Impurities such as transition metals and light elements diffuse from the crucible and coating into the melt and also into the solidified Si. Crucible and coating used for low cost silicon growth are known to contain impurities.

Elements with high diffusivity in Si, such as transition metals, can diffuse easily into the solidified Si, from the crucible and coating. However, slow diffusers such as light elements, do not diffuse into the solidified Si, hence are distributed mainly according to segregation. Therefore, concentration of impurities varies with height of the ingot.

2-9 Summary

This chapter discussed some of the fundamentals about multicrystalline silicon for solar cells. The crystal structure of silicon and grain boundaries was introduced, followed by grain boundary engineering and the impact of transition metal impurities on the solar cell efficiency.

2-10 References

[2-1] Seidel, H., et al. "Anisotropic etching of crystalline silicon in alkaline solutions I. Orientation dependence and behavior of passivation layers." *Journal of the electrochemical society* 137.11 (1990): 3612-3626.

[2-2] Tsujino, K., M. Matsumura, and Y. Nishimoto. "Texturization of multicrystalline silicon wafers for solar cells by chemical treatment using metallic catalyst." *Solar energy materials and solar cells* 90.1 (2006): 100-110.

[2-3] Gangopadhyay, U., et al. "Comparative study of different approaches of multicrystalline silicon texturing for solar cell fabrication." *Solar Energy Materials and Solar Cells* 91.4 (2007): 285-289.

[2-4] Panek, P., M. Lipiński, and J. Dutkiewicz. "Texturization of multicrystalline silicon by wet chemical etching for silicon solar cells." *Journal of Materials Science* 40.6 (2005): 1459-1463.

[2-5] Momma, Koichi, and Fujio Izumi. "VESTA: a three-dimensional visualization system for electronic and structural analysis." *Journal of Applied Crystallography* 41.3 (2008): 653-658.

[2-6] Uwaha, Makio. "Equilibrium crystal shapes on a flat substrate." *Japanese journal of applied physics* 26.9R (1987): 1592.

[2-7] Yang, Xinbo, et al. "Crystal growth and equilibrium crystal shapes of silicon in the melt." *Progress in Photovoltaics: Research and Applications* 22.5 (2014): 574-580.

[2-8] Fujiwara, K., et al. "Effect of silicon/crucible interfacial energy on orientation of multicrystalline silicon ingot in unidirectional growth." *Journal of Applied Physics* 112.11 (2012): 113521.

[2-9] Apte, Pankaj A., and Xiao Cheng Zeng. "Anisotropy of crystal-melt interfacial free energy of silicon by simulation." *Applied Physics Letters* 92.22 (2008): 221903-221903.

[2-10] Dhanaraj, Govindhan, et al. Springer handbook of crystal growth. Springer Science & Business Media, 2010.Pg 5

[2-11] Zhang, Jian-Min, et al. "Anisotropy analysis of the surface energy of diamond cubic crystals." *Surface and interface analysis* 35.10 (2003): 805-809.

[2-12] Jaccodine, R. J. "Surface energy of germanium and silicon." *Journal of The Electrochemical Society* 110.6 (1963): 524-527.

[2-13] Gilman, John J. "Direct measurements of the surface energies of crystals." *Journal of Applied Physics* 31.12 (1960): 2208-2218.

[2-14] Lejcek, Pavel. Grain boundary segregation in metals. Vol. 136. Springer Science & Business Media, 2010. Pg 5

[2-15] Read, W. T., and W. Shockley. "Dislocation models of crystal grain boundaries." *Physical Review* 78.3 (1950): 275.

[2-16] Brandon, D. G. "The structure of high-angle grain boundaries." *Acta Metallurgica* 14.11 (1966): 1479-1484.

[2-17] Ranganathan, S. "On the geometry of coincidence-site lattices." *Acta Crystallographica* 21.2 (1966): 197-199.

[2-18] Brandon, D. G., et al. "A field ion microscope study of atomic configuration at grain boundaries." *Acta Metallurgica* 12.7 (1964): 813-821.

[2-19] Kohyama, Masanori, Ryoichi Yamamoto, and Masao Doyama. "Structures and Energies of Symmetrical〈 011〉 Tilt Grain Boundaries in Silicon." *Physica Status Solidi (b)* 137.1 (1986): 11-20.

[2-20] Kohyama, M., R. Yamamoto, and M. Doyama. "Reconstructed Structures of Symmetrical〈 011〉 Tilt Grain Boundaries in Silicon." *Physica Status Solidi (b)* 138.2 (1986): 387-397.

[2-21] Kohyama, M. "Structures and Energies of Symmetrical〈 001〉 Tilt Grain Boundaries in Silicon." *Physica Status Solidi (b)* 141.1 (1987): 71-83.

[2-22] Warrington, D. H., and P. Bufalini. "The coincidence site lattice and grain boundaries." *Scripta Metallurgica* 5.9 (1971): 771-776.

[2-23] Crystal growth of Si for solar cells. Springer Verlag, 2009. Pg 4

[2-24] Buonassisi, T., et al. "Metal precipitation at grain boundaries in silicon: Dependence on grain boundary character and dislocation decoration." *Applied Physics Letters* 89.4 (2006): 042102.

[2-25] Chen, J., et al. "Electron-beam-induced current study of grain boundaries in multicrystalline silicon." *Journal of Applied Physics* 96.10 (2004): 5490-5495.

[2-26] Istratov, Andrei A., et al. "Metal content of multicrystalline silicon for solar cells and its impact on minority carrier diffusion length." *Journal of Applied Physics* 94.10 (2003): 6552-6559.

[2-27] T. Buonassisi, A.A. Istratov, M.D. Pickett, M. Heuer, J.P. Kalejs, G. Hahn, M.A.

Marcus, B. Lai, Z. Cai, S.M. Heald, T.F. Ciszek, R.F. Clark, D.W. Cunningham, A.M.

Gabor, R. Jonczyk, S. Narayanan, E. Sauar, E.R.Weber, *Prog. Photovolt: Res. Appl.*14 (2006) 513

[2-28] Buonassisi, T., et al. "Transition metal co-precipitation mechanisms in silicon." *Acta Materialia* 55.18 (2007): 6119-6126.

[2-29] Miremadi, Bijan K., and S. Roy Morrison. "Conductance along iron-doped silicon grain boundaries." *Journal of Applied Physics* 55.10 (1984): 3658-3663.

[2-30] Shockley, We, and W. T. Read Jr. "Statistics of the recombinations of holes and electrons." *Physical Review* 87.5 (1952): 835.

[2-31] Lehockey, E. M., A. M. Brennenstuhl, and I. Thompson. "On the relationship between grain boundary connectivity, coincident site lattice boundaries, and intergranular stress corrosion cracking." *Corrosion Science* 46.10 (2004): 2383-2404.

[2-32] Fujiwara, Kozo, et al. "Growth of structure-controlled polycrystalline silicon ingots for solar cells by casting." *Acta Materialia* 54.12 (2006): 3191-3197.

[2-33] Fujiwara, Kozo, et al. "Directional growth method to obtain high quality polycrystalline silicon from its melt." *Journal of Crystal Growth* 292.2 (2006): 282-285.

[2-34] Usami, Noritaka, et al. "Implementation of faceted dendrite growth on floating cast method to realize high-quality multicrsytalline Si ingot for solar cells." *Journal of Applied Physics* 109.8 (2011): 083527.

[2-35] T.F. Li, H.C Huang, H.W. Tsai, A. Lan, C. Chuck, C.W. Lan, “An enhanced cooling design in directional solidification for high quality multi-crystalline solar silicon”, *Journal of Crystal Growth* 340 (2012) 202-208.

[2-36] Wang, T. Y., et al. "Grain control using spot cooling in multi-crystalline silicon crystal growth." *Journal of Crystal Growth* 311.2 (2009): 263-267.

[2-37] Stoddard, Nathan, et al. "Casting Single Crystal Silicon: Novel Defect Profiles from BP Solar's Mono2 TM Wafers." *Solid State Phenomena* 131 (2008): 1-8.

[2-38] Miyamura, Y., et al. "Crystal growth of 50cm square mono-like Si by directional solidification and its characterization." *Journal of Crystal Growth* 401 (2014): 133-136.

[2-39] Y. M. Yang, A. Yu, B. Hsu, W. C. Hsu, A. Yang, C. W. Lan, Prog. Photovolt: Res. Appl. (published online). http://dx.doi.org/10.1002/pip.2437 , 2013

[2-40] Lan, C. W., et al. "Grain control in directional solidification of photovoltaic silicon." *Journal of Crystal Growth* 360 (2012): 68-75.

[2-41] Zhu, Didi, et al. "Seed-assisted growth of high-quality multi-crystalline silicon in directional solidification." *Journal of Crystal Growth* 386 (2014): 52-56.

[2-42] International Technology Roadmap for Photovoltaic, Fifth Edition 2014

[2-43] Istratov, A. A., H. Hieslmair, and E. R. Weber. "Iron and its complexes in silicon." *Applied Physics A* 69.1 (1999): 13-44.

[2-44] Istratov, A. A., H. Hieslmair, and E. R. Weber. "Iron contamination in silicon technology." *Applied Physics A* 70.5 (2000): 489-534.

[2-45] Davis Jr, John Ransford, et al. "Impurities in silicon solar cells." *Electron Devices, IEEE Transactions on* 27.4 (1980): 677-687.

CHAPTER 3:

Experimental Procedures

3-1 Introduction

Before presenting the experimental results, the growth process, sample preparation and the characterization techniques used in this thesis will be discussed in this chapter. First, the structure of the furnace and the growth setup is presented. Next, the sample preparation for characterization is introduced. Finally, characterization technique and analysis is briefly discussed.

3-2 Crystal Growth

We grew the ingots used in this study in a furnace at the Toyota Technological Institute. In this small lab-scale furnace, we grew test ingots of about 100 mm diameter via unidirectional solidification. The schematics of the furnace and the growth setup are shown in Fig. 3-1. [3-1,3-2]. The furnace has two compartments, the top area for heating and the bottom for cooling, which are separated by thermal insulators as shown in Fig 3-1. Although this furnace contains four heaters, two in heating (shown in Fig. 3-1) and two in the cooling compartment (not shown in Fig. 3-1), for this experiment we used only the two heaters in the heating compartment. Of these two heaters, one is situated above the crucible, and the other is on the side. The silicon is grown in a Si_3N_4 coated quartz crucible which is put inside a carbon crucible, with a felt in between the two crucibles. This crucible is then put on a pedestal which is stationery during growth (although this furnace allows rotation of the crucible we did not use this feature in our growth). The heat from the crucible is extracted by the pedestal, which is very important for unidirectional solidification, since the heat flow should be downwards into the bottom of the crucible for the crystal to grow upwards in one direction.

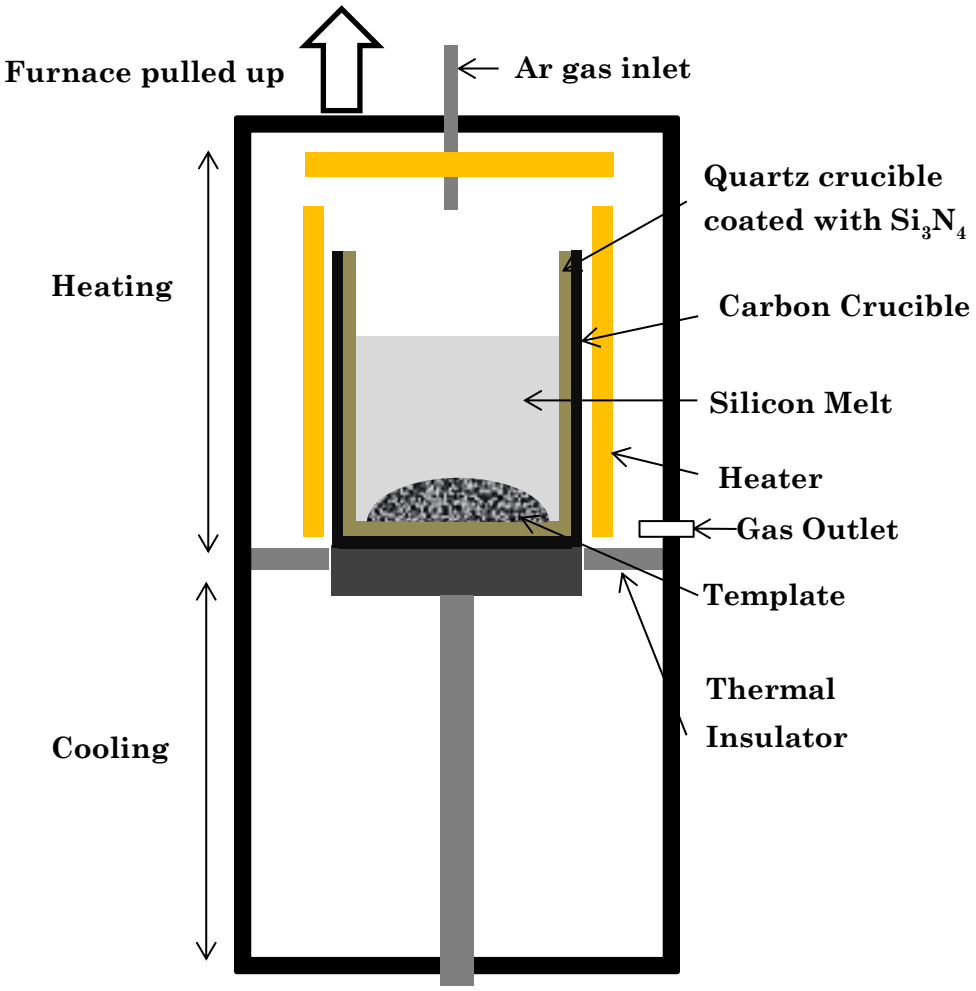

Figure 3-1. Schematics of the furnace for directional solidification [3-1, 3-2]

To prevent the silicon from sticking to the quartz crucible, the cylindrical quartz crucible was coated with Si_3N_4 powder [3-3]. The feedstock used for the growth is a high purity Siemens grown polycrystalline silicon. This polycrystalline silicon has an average grain size of about 100μm, hence will be called microcrystalline silicon (Note: not to be confused with nano-crystalline silicon which is a type of porous silicon). Due to this nature of small grains, which are also distributed randomly, the feedstock was also used as the template for growth. The feedstock was placed in the crucible as a whole, without breaking it into chunks. This is a much simpler and cleaner process than setting up different seeds or using small chunks of silicon. Dopants (highly boron doped silicon) were added to get a target resistivity of 2 Ωcm. The crucible was set in the furnace and was first heated to 1550 °C to melt the feedstock, however the growth setup was designed to

prevent complete melting of the feedstock. After the melting step the temperature was lowered to 1450 °C and the furnace was pulled upwards at a constant rate (15 mm/h or 45 mm/h). This means that by relative motion, the crucible is moving downwards out of the furnace and for simplicity from henceforth the pulling rate will be discussed in terms of the crucible position (not the furnace). The temperature gradient due to the crucible moving out of the furnace resulted in the solidification from the template upwards. An example of the growth process is shown in Fig. 3-2. The numerical simulation of the process in this type of furnace has been done by Gao et al [3-4,3-5]. During the entire process, Ar gas was passed into the crucible at 2 slm to suppress light element impurity transport in gas phase [3-6,3-7].

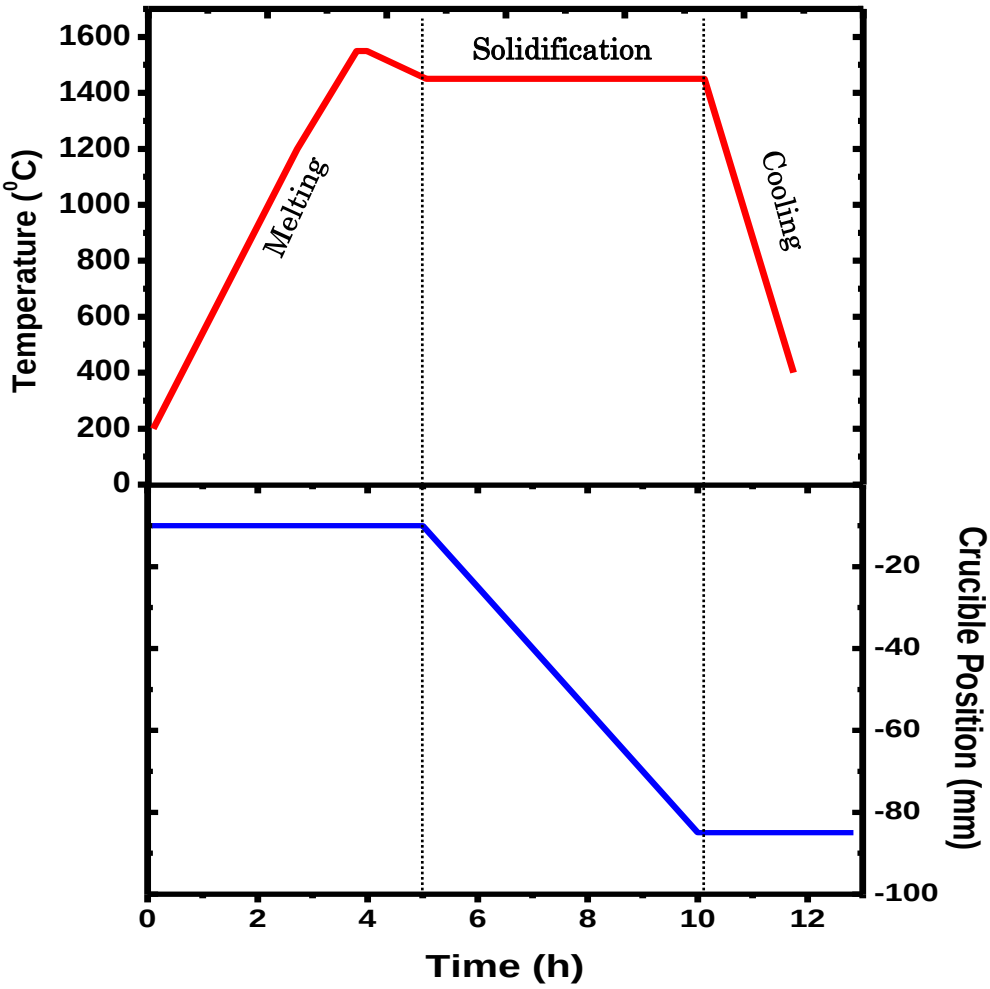

Figure 3-2. Example of a growth recipe

3-3 Sample Preparation

The ingots were cut into half vertically, with one half further cut into vertical wafers and the other into horizontal wafers. The vertical wafers are necessary to study the grain structure evolution continuously since it is parallel to the growth direction. On the other hand, horizontal wafers give a larger area per height by showing the area perpendicular to the growth direction. By using the vertical and horizontal wafers, a nearly three dimensional analysis is possible.

For characterization, electron backscatter diffraction (EBSD) was used, and to fit the sample into the holder of EBSD, the wafers were further cut into 13mm x 13mm pieces. Schematic of the cutting process is shown in Fig. 3-3. Since EBSD measurements need flat surfaces, the wafers were chemically-mechanically polished.

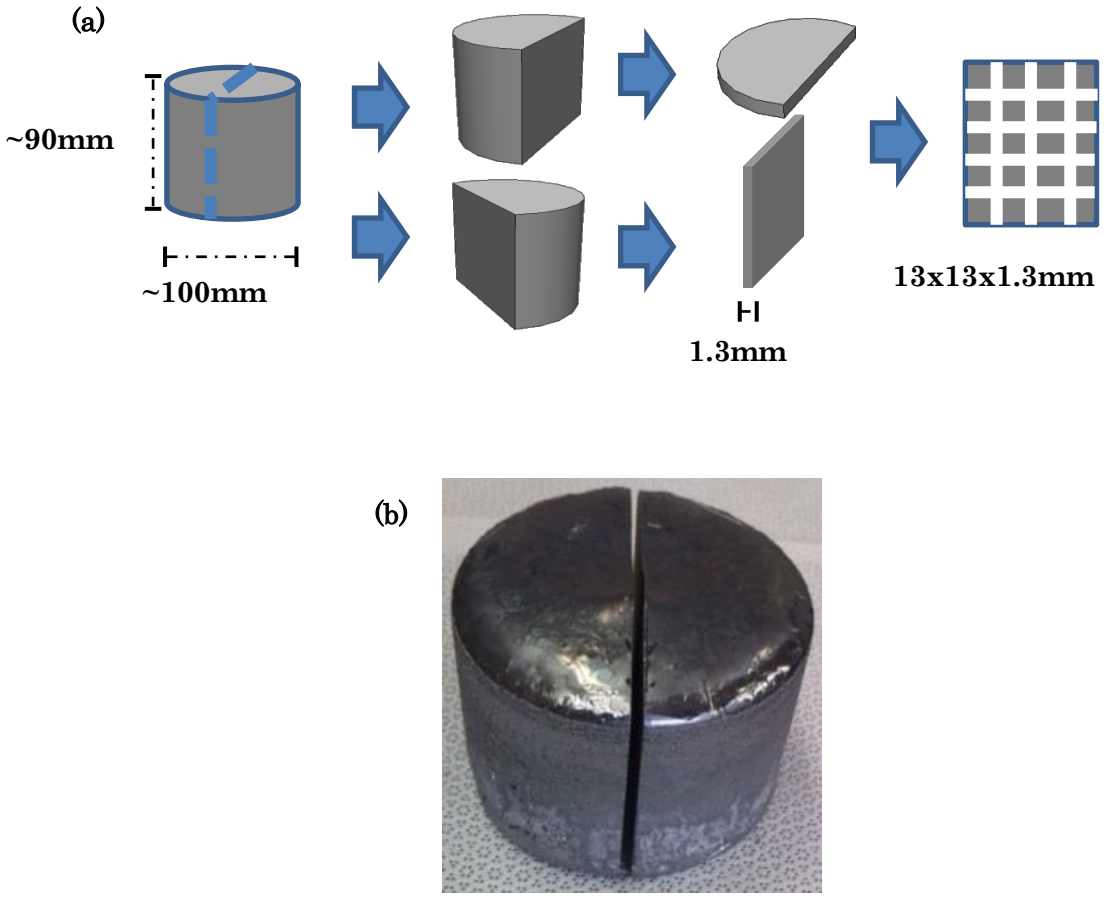

Figure 3-3. (a) Sample preparation schematics. (b) Grown ingot cut vertically into half.

3-4 Characterization: Electron Backscatter Diffraction

Electron backscatter diffraction (EBSD) is a powerful technique used for characterizing individual grain orientations, local texture, point-point orientation correlations etc. in polycrystals. It captures patterns from crystals to determine its grain morphology, crystallographic orientation etc. This section briefly discusses the experimental technique. The experiment conditions such as sample preparation are discussed in the experimental details section.

3-4-1 Electron Backscatter Diffraction (EBSD)

EBSD was used for grain boundary characterization. EBSD uses the interaction of electrons from an incident beam and a tilted (70°) crystalline sample. When the primary beam interacts with the lattice, low energy loss backscattered electrons are channelled and are subject to path differences that lead to constructive and destructive interferences. These patterns are detected and form visible lines called Kikuchi patterns. The mechanism by which the diffraction patterns are formed is complex, but principal features can be explained using the following model (Fig.3-4). The atoms in the material inelastically scatter a fraction of the electrons to form a divergent source of electrons close to the surface of the sample. Some of these electrons are incident on atomic planes at angles that satisfy the Bragg equation $nl = d \sin\theta$, where n is an integer, l is the wavelength of the electrons, d is the spacing of the diffracting plane, and θ is the angle of incidence of the electrons at the diffracting plane. These electrons are diffracted to form a set of paired large angle cones corresponding to each diffracting plane. The regions of enhanced electron intensity between the cones produce the Kikuchi patterns, which are automatically analysed and solved for phase and orientation [3-8]. EBSD is a commonly used technique and a good introduction of this technique can be found in ref. [3-9].

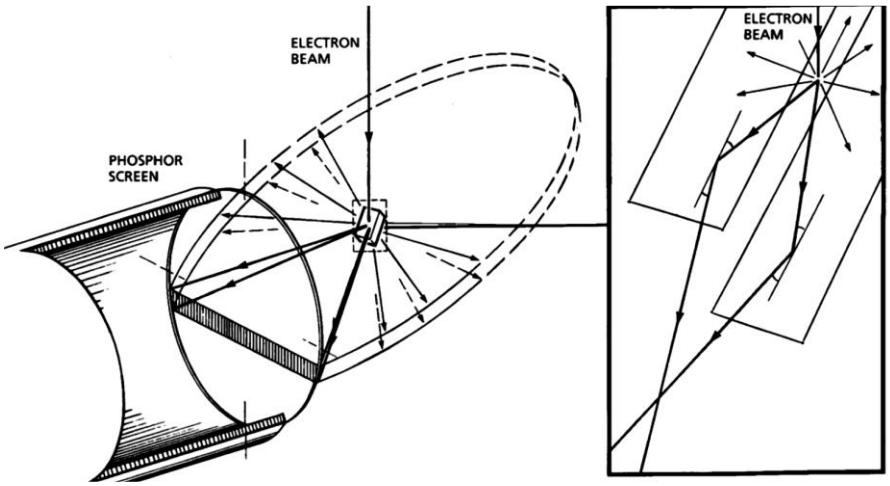

Figure 3-4. Mechanism of the formation of the electron backscatter diffraction pattern [3-8].

3-4-2 Experimental Details

For measuring the grain structure using the EBSD, the samples were chemically mechanically polished. The measurement was done in JSM-7001 Schottky field emission electron microscope. The acceleration voltage used was 20kV, with 18 mm work distance. The step size used for the measurements was 10μm except for the template when it was 5 μm.

3-5 Summary

This chapter discussed the experimental procedures used in this thesis. The crystal growth process and the sample preparation were discussed. The characterization techniques and the measurement details were briefly presented.

3-6 References

[3-1] Arafune, Koji, et al. "Directional solidification of polycrystalline silicon ingots by successive relaxation of supercooling method." *Journal of Crystal Growth* 308.1 (2007): 5-9.

[3-2] Jiptner, Karolin, et al. "Characterization of Residual Strain in Si Ingots Grown by the Seed-Cast Method." *Solid State Phenomena* 205 (2014): 94-99.

[3-3] Jiptner, Karolin, et al. "Effect of Si3N4 Coating on Strain and Fracture of Si Ingots." *Materials Science Forum*. Vol. 725. 2012.

[3-4]Gao, B., et al. "Crystal growth of high-purity multicrystalline silicon using a unidirectional solidification furnace for solar cells." *Journal of Crystal* Growth 312.9 (2010): 1572-1576.

[3-5]Gao, B., S. Nakano, and K. Kakimoto. "Global simulation of coupled carbon and oxygen transport in a unidirectional solidification furnace for solar cells." *Journal of the Electrochemical Society* 157.2 (2010): H153-H159.

[3-6] Miyamura, Y., et al. "Crystal growth of 50cm square mono-like Si by directional solidification and its characterization." *Journal of Crystal Growth* 401 (2014): 133-136.

[3-7] Li, Zaoyang, et al. "Effects of argon flow on impurities transport in a directional solidification furnace for silicon solar cells." *Journal of Crystal Growth* 318.1 (2011): 304-312.

[3-8] Tutorial: Electron Backscatter Diffraction in the Scanning Electron Microscope, Oxford Instruments Analytical

[3-9] Schwartz, Adam J., et al., eds. *Electron backscatter diffraction in materials science*. Vol. 2. New York: Springer, 2009.

CHAPTER 4

Multicrystalline Silicon Grown from Microcrystalline Template

4-1 Introduction

As discussed in Chapter 2, multicrystalline Silicon (mc-Si) is the dominant material for solar cells, however structural defects such as grain boundaries (GBs) and dislocations interact with transition metal impurities and limit the conversion efficiency [4-1, 4-2]. Transition metal impurities can be easily gettered by certain grain boundaries which consequently become sites for carrier recombination [4-3, 4-4]. Therefore it is desirable to avoid formation of grain boundaries that strongly interact with impurities. Several growth methods have been developed namely dendritic and spot cooling to reduce the density of grain boundaries by obtaining large grains [4-5, 4-6, 4-7, 4-8, 4-9]. Larger grain size is expected to give a higher efficiency and a common method to grow large grains is to start with large grains (seeds), often obtained by controlling nucleation through optimized undercooling. However, since the growth mechanism for mc-Si is not clear, control of grain structure during growth is difficult. Owing to this, several studies, both experimental [4-10, 4-11, 4-12] and simulations [4-13, 4-14], have attempted to explain grain growth mechanism in mc-Si grown from relatively large grains. On the other hand, high efficiency has also been obtained recently from mc-Si grown from small grains [4-15, 4-16, 4-17]. This type of mc-Si is called the high performance mc-Si (HP mc-Si) and is expected to play an important role in the future of the photovoltaic industry [4-18]. Therefore, it is very important to understand the grain growth mechanism of mc-Si grown from small randomly oriented grains.

In this study, we investigated the growth mechanism of mc-Si grown from a microcrystalline silicon template which has small randomly oriented grains of average size below 100 μm. The grain structure evolution was elucidated by examining the vertically cut (parallel to growth direction) and horizontally cut (perpendicular to growth direction) wafers from the grown ingot. The main structure characteristics discussed are

grain size, shape, boundary, and orientation distribution at different growth heights. To highlight the difference in the grain structure of microcrystalline template grown ingot, it was compared with a mc-Si that was grown by the conventional growth method (i.e. the grains grow from the bottom of the Si_3N_4 coated quartz crucible).

4-2 Experimental

Test ingot of 100 mm diameter was grown from a microcrystalline silicon template. This template is a high purity (11N) Siemens grown ingot of about 60 mm diameter, and was placed as a whole, i.e. without breaking into chunks. The template was also used as the feedstock; however the growth process was designed so that the feedstock would not melt completely, enabling it to be used as the seed from which solidification would begin. For comparison a conventional mc-Si was also grown at similar growth conditions, except that the whole feedstock was melted and the initial growth started from the bottom of the crucible. Both ingots were grown at a pulling rate of 15 mm/h and were boron doped with a target resistivity of 2 Ωcm. *(The growth is discussed in more detail in the Chapter 3)*

For characterization, the ingots were first vertically cut into half and one half was cut into vertical wafers while the other into horizontal wafers. The wafers were then mechanically and chemically polished before electron backscatter diffraction (EBSD) was used to study the grain structure. The step size for the EBSD measurement is 10 μm for all samples except for the microcrystalline template, where the step size is 5 μm.

Due to the design of the furnace, the template melted with a convex shape, therefore to reduce the impact of the growth interface shape, only the central region of the ingot where the interface is nearly flat was studied. The top part of the ingot is also not used to avoid the impact from impurity precipitation.

The grain size was measured using the line intercept method, where the actual number of grains intercepted by a number of test lines (i.e. the intersection of grain boundaries with the drawn lines), per unit length is used to calculate the average grain size.

4-3 Grown Ingot: Vertical and Horizontal Wafers

The images of vertically and horizontally cut wafers obtained by a digital scanner are shown in Fig. 4-1 and Fig. 4-2 for vertical and horizontal wafers respectively. The contrasts in the images represent different grains due the difference in scattering of light in grains with different orientation (in as-cut wafers). However, not all grains are visible separately, and different contrasts appear when the scans are done from different directions. Since in the following sections only the central region will be discussed, this section gives an overall view of the vertical and horizontal wafers. In this chapter, first the results will be shown and the discussion will be at a later stage.

4-3-1 Vertically and Horizontally Cut Wafers

Fig. 4-1 shows an image (scanned) of a vertically cut wafer from the microcrystalline template grown mc-Si. The different contrasts are related to different grains, however neighboring grains that have similar scattering behavior may look like a single grain. It can be observed that the template melted with a convex shape; therefore only the central region (which is flat), of the ingot was used to study the grain structure. The initial growth region is the interface between the microcrystalline template and the grains grown from it, as shown in Fig. 4-1 by Growth Height H = 0 mm.

Figure 4-1 Image of a vertically cut wafer from the center of the microcrystalline template grown ingot (Image obtained by digital scanner)

The scanned images of the horizontally cut wafers from the template grown mc-Si, taken from growth heights 1 mm, 17 mm and 24 mm are shown in Fig. 4-2. The enclosed semicircle area in Fig. 4-2 shows the region grown from the microcrystalline template.

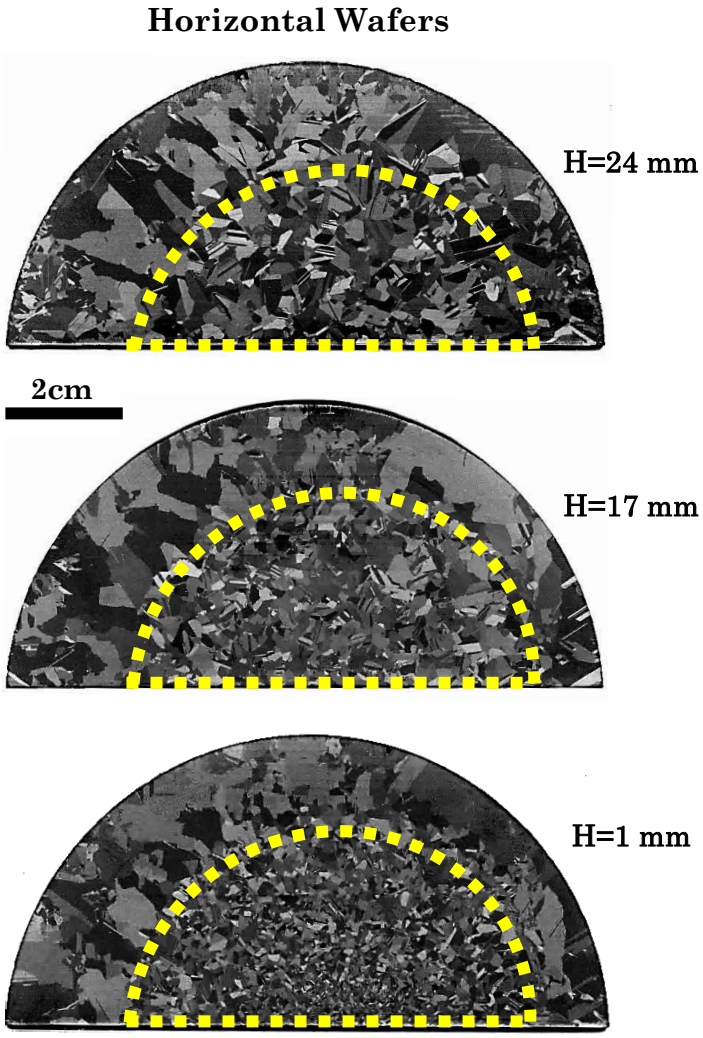

Figure 4-2 Images of horizontally cut wafers (from growth heights 1 mm, 7 mm and 24 mm) from the microcrystalline template grown ingot. Area enclosed by dotted semicircle shows the grains grown from the microcrystalline.

4-4 Grain Structure of the Template Grown Mc-Si

4-4-1 Grain Structure in Vertical Wafer

The grain structure of the microcrystalline template grown ingot was studied using electron backscattered diffraction (EBSD). Fig. 4-3 shows (a) inverse pole figure (IPF) and (b) GB mapping from a region with 10 mm width from the center of the vertical wafer. The color code for grain orientation is with respect to growth direction. In GB mapping, the color code for the GBs is as follows: Σ3= blue, R=black, Σ9=green, Σ27=red and other GBs = orange. Other GBs here refer to large angle GBs with Σ value less than 27 but not 3 or 9, and small angle grain boundaries, which have misorientation angle less than 15 °and more than 2 ° (As can be noticed in Others both large angle and small angle GBs

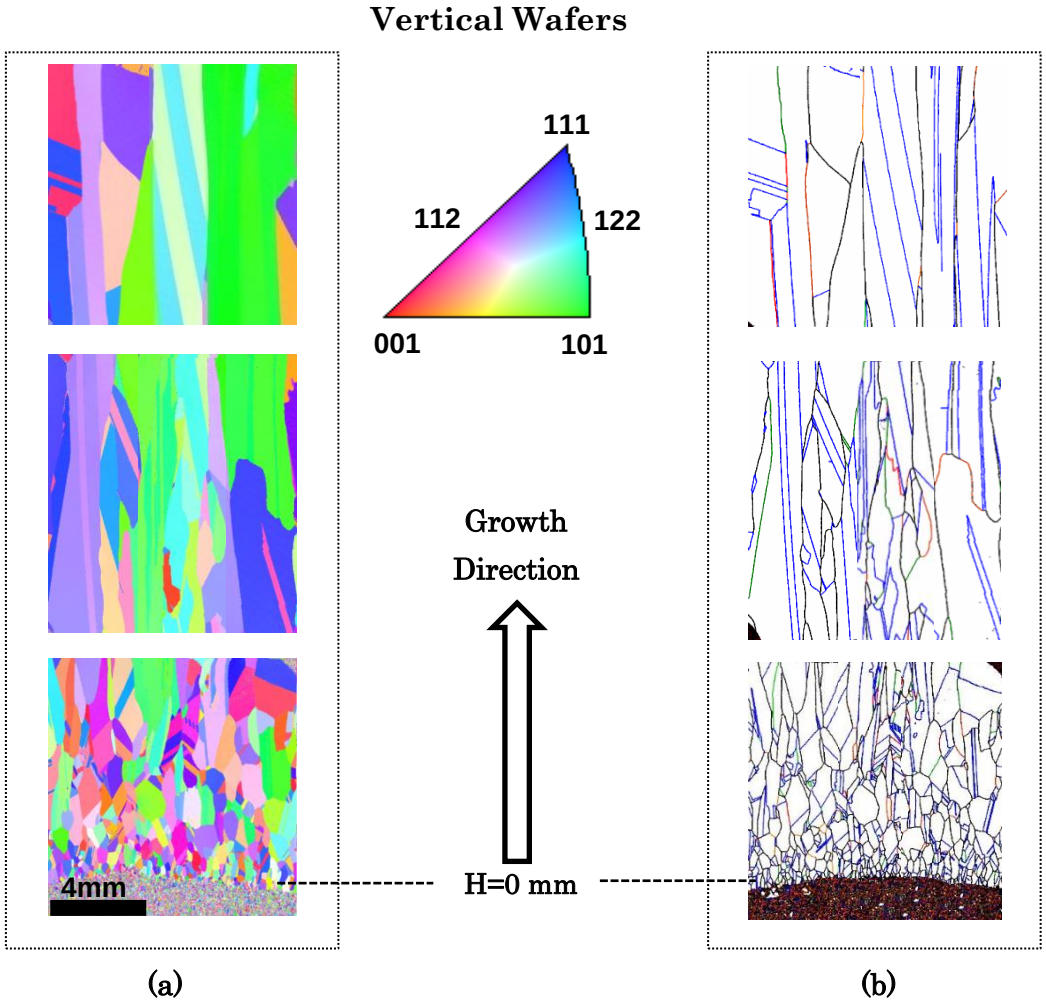

Figure 4-3. Inverse pole figures (IPF) (a) and grain boundary mapping (b) from the central region (~10 mm width) of a vertical wafer from the microcrystalline template grown ingot. Orientation direction is with respect to growth direction. GB color code in (b) Σ3=blue, R=black, Σ9=green, Σ27=red and other GBs = orange

are counted together, this because those GBs will not be focused on, in this chapter). Also, R GBs have been defined to include GBs with $\Sigma > 27$. From the images in Fig. 4-3, it can be noticed that initially small spherical grains exist; however as the growth height increases the grains elongate and become ellipsoidal before becoming columnar. From Fig. 4-3 (b) it can be seen that initially many curved GBs exist, which are mostly R GBs. However, as growth height increases most GBs become straight and follow the growth direction, although some inclined GBs do exist, most of which are $\Sigma 3$ GBs.

4-4-2 Grain Structure in Horizontal Wafers

Similarly, the grain structure in horizontal wafers was investigated and the IPF and GB mapping of wafers selected from growth heights 1 mm, 17 mm and 24 mm are shown in Fig. 4-4. The grain orientation code is with respect to growth direction (as shown in diagram) and the GBs have the same color code as in Fig. 4-3. The increase in grain size with growth height is clear. It can be seen that in wafer from growth height 1 mm, most grains are of similar size (uniform), however, in wafers from higher growth height especially H=24 mm, some grains are large, while some small grains also exist. From GB mapping, it can be seen that the GB density has dramatically decreased in wafer from growth height 24 mm compared to 1 mm.

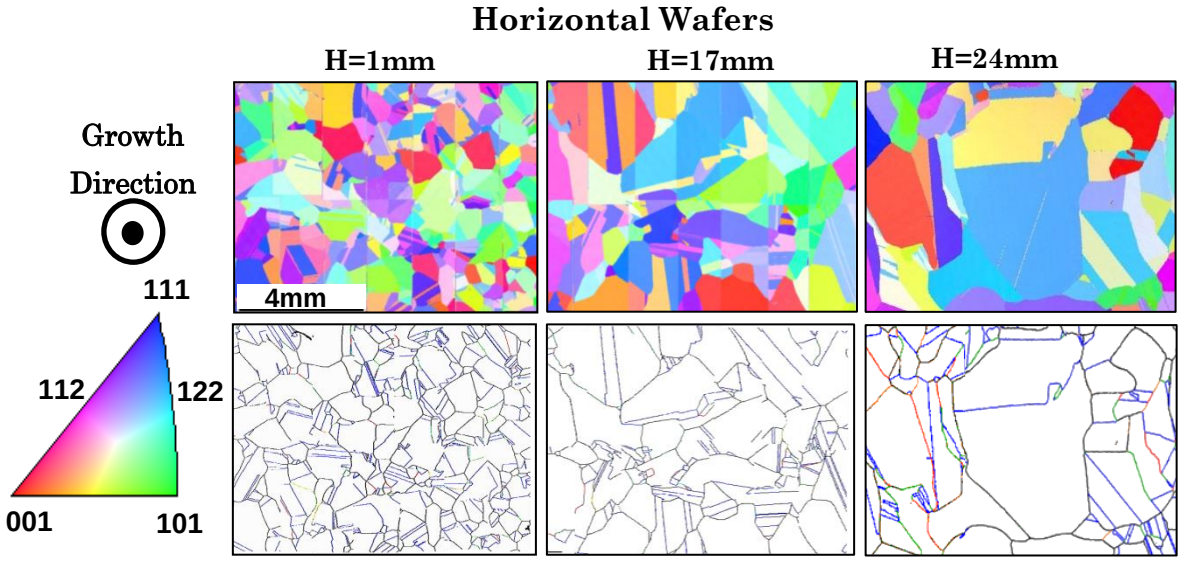

Figure 4-4. Inverse pole figures (top) and grain boundary mapping (bottom) from the central region (~10 mm width) of horizontal wafers from growth heights (H) 1 mm, 17 mm and 24 mm. Orientation direction is with respect to growth direction.
GBs: $\Sigma 3$ = blue, R = black, $\Sigma 9$ = green, $\Sigma 27$ = red and other GBs = orange

4-4-3 Grain Structure near the Interface of Template and Grown Grains

To understand the initial growth, the grain structure in the area near the interface of the microcrystalline template grown mc-Si was studied closely. Fig. 4-5 shows the EBSD measurement from a vertical wafer showing IPF (a) and GB mapping (b) of grains grown from the template, while that in (c) and (d) are of the grains in the template. The statistics related to GBs are shown in (e) grains grown from the template and (f) grains in the template. From (a) and (b) it can be seen that the interface between the template and grown grain s is not flat (as the dotted line shows, approximately). Moreover, the size of the grains grown from the template is much larger than the grains in the template.

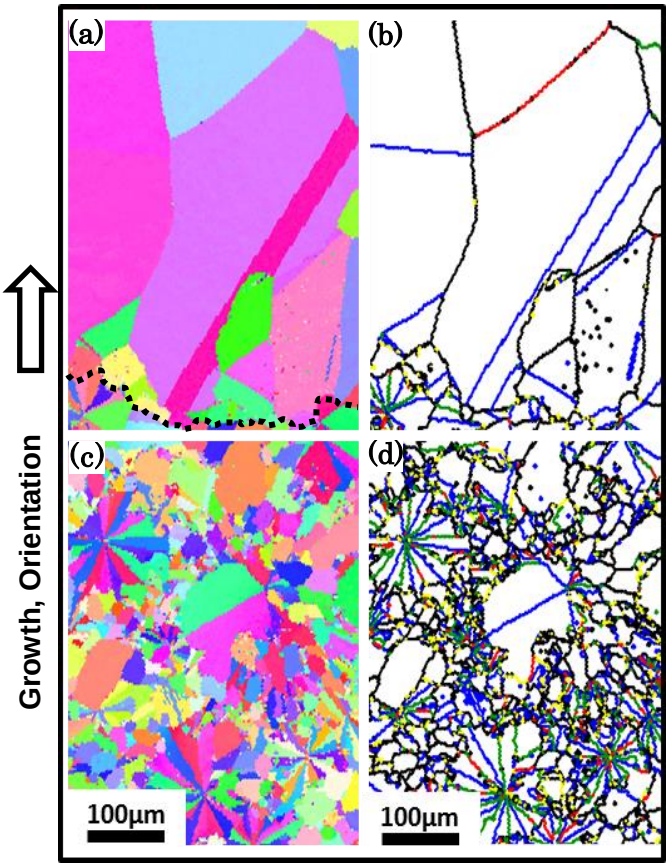

(e)	%	length (mm)	L/A (1/mm)
Σ3	31	1.5	6.3
Σ9	2	0.1	0.4
Σ27	4	0.2	0.8
Σ Other	2	0.1	0.4
R	61	2.9	12.5

(f)	%	length (mm)	L/A (1/mm)
Σ3	23	9.5	41.7
Σ9	11	4.6	19.9
Σ27	1	0.4	1.8
Σ Other	6	2.5	10.9
R	59	24.4	106.9

Figure 4-5 Inverse pole figures of vertical wafers at initial growth regions showing (a) growth region (dotted line=approximate interface) and (c) microcrystalline template. Grain boundary maps of (b) growth region and (d) microcrystalline template showing Σ3 (blue), Σ9 (green), Σ27 (red), Other Σ(Σ<27 but not 3 or 9) and random (black) grain boundaries. Tables (e) and (f) show the summary of grain boundaries from the regions showed in (b) and (d).

From the GB statistics, it can be seen that the total GB density of the grown grains decreases to become about 11% of that in the template. The ratio of GB density in grown grains divided the GB density in the template for different types of GBs are about 12 % for R GBs, 15 % for Σ3, 2% for Σ9, 44 % for Σ27 and 4 % for other Σ GBs. The largest decrease in GB density is for Σ9 GB. This is due to the flower-like structure that contains Σ3 and Σ9 GBs in the template, while the grown grains do not have that structure.

The grains which are perpendicular to the growth direction become the seeds for growth, hence horizontal wafers give a more accurate picture of the grain growth from the template. Horizontal wafers from the template and growth height 1 mm were studied in

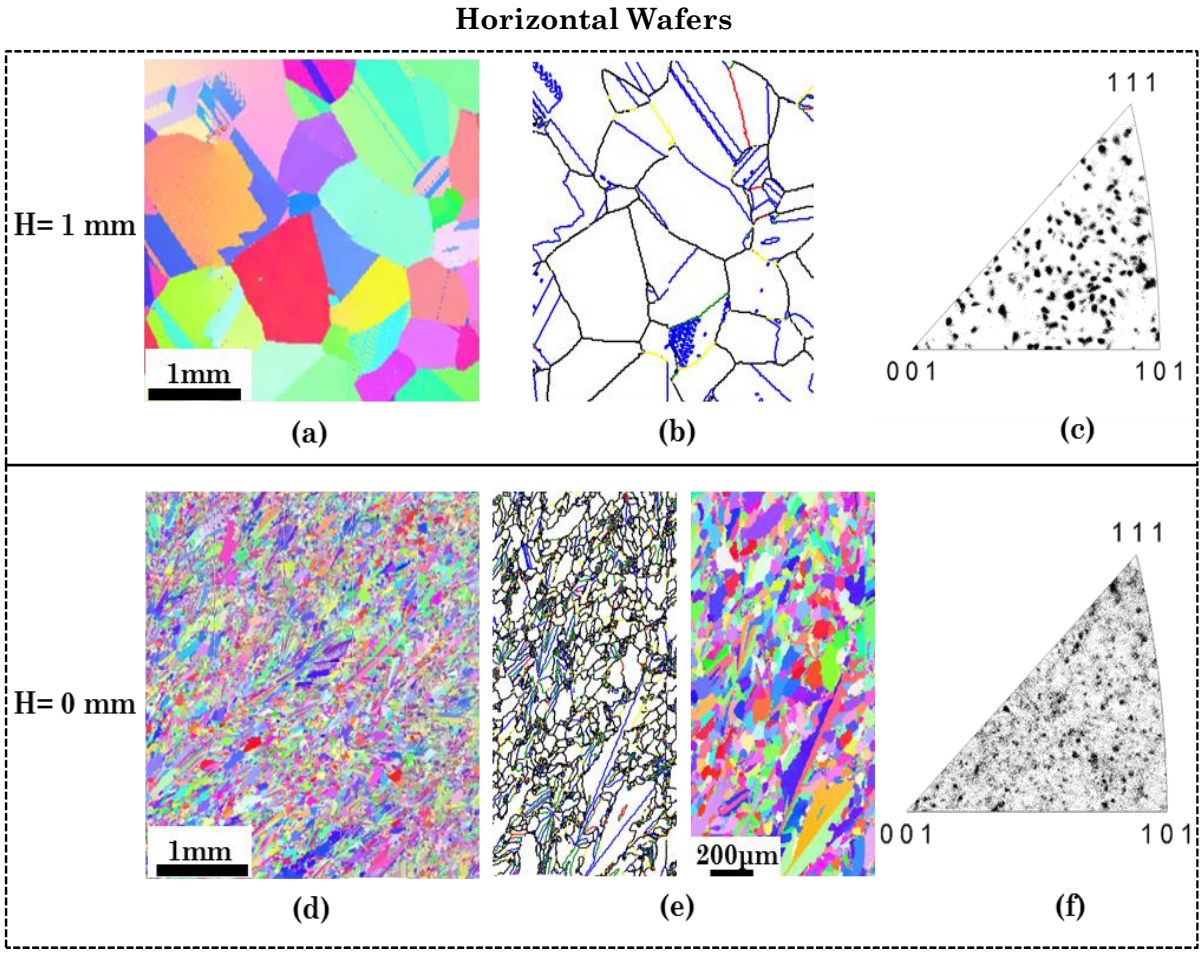

Figure 4-6 IPFs of horizontal wafers taken from (a) growth height H= 1mm and (d) microcrystalline template i.e. H=0. (b) Grain boundary mapping and (c) discrete plot of orientation (from 5 mm x 5 mm area) from IPF of wafer from growth height H=1 mm. (e) IPF and grain boundary mapping of a magnified region and (f) discrete plot of orientation(from 5 mm x 5 mm area) from the microcrystalline template.

more detail and are shown in Fig. 4-6. The IPF and GB mapping are shown in Fig. 4-6 (a), and (b) respectively, while a discrete plot of orientation from IPF (obtained from an area of 5 mm x5 mm) is shown in (c) for the wafer from growth height 1 mm. For the wafer from the template the IPF at same magnification as the wafer from 1 mm growth height is shown in (d). The IPF and the GB mapping of a magnified area from the template are shown in (d) and (e) respectively, and a discrete plot of orientation (obtained from an area of 5 mm x 5 mm) is shown in (f). As was seen in the vertical wafers, the H=1 mm wafer has much larger grains compared to the template. Moreover, although the template contains grains of various sizes and shapes (such as round or needle-like), the grown grains in wafer from 1 mm growth height look more equiaxed. In the template although there are some flower-like structures in horizontal wafers, it is much less than the vertical wafers, instead having need-like structures (which may be the upper view of the elongated flower-like structures). The discrete plot of orientation was taken for equal areas from the two wafers, and it can be seen that in 1 mm wafer, the spots are less randomly distributed compared to the template.

4-4-4 Grain Size Distribution

Grain size was measured by the line intercept method (discussed in experimental section 4-2) using IPFs obtained from EBSD measurements. Due to multiple intra-grain twins, the actual grain size is difficult to calculate, so in this calculation, multiple intra-grain twins were not considered. The average grain size (width of grains in vertical wafers perpendicular to growth direction) measured from vertical wafers is plotted with respect to growth height as shown in Fig. 4-7. The average grain size distribution in microcrystalline template grown ingot is generally increasing. This is consistent with that reported in HP mc-Si [4-15], as opposed to those reported in conventional mc-Si and dendritic growth, where grain size typically decreases with growth height [4-15, 4-19]. However, in this microcrystalline template growth, it can be observed that after initial increase (0-4 mm), average grain size becomes constant (4-8 mm), and then increases again (8 mm~), showing 3 stages in grain size distribution.

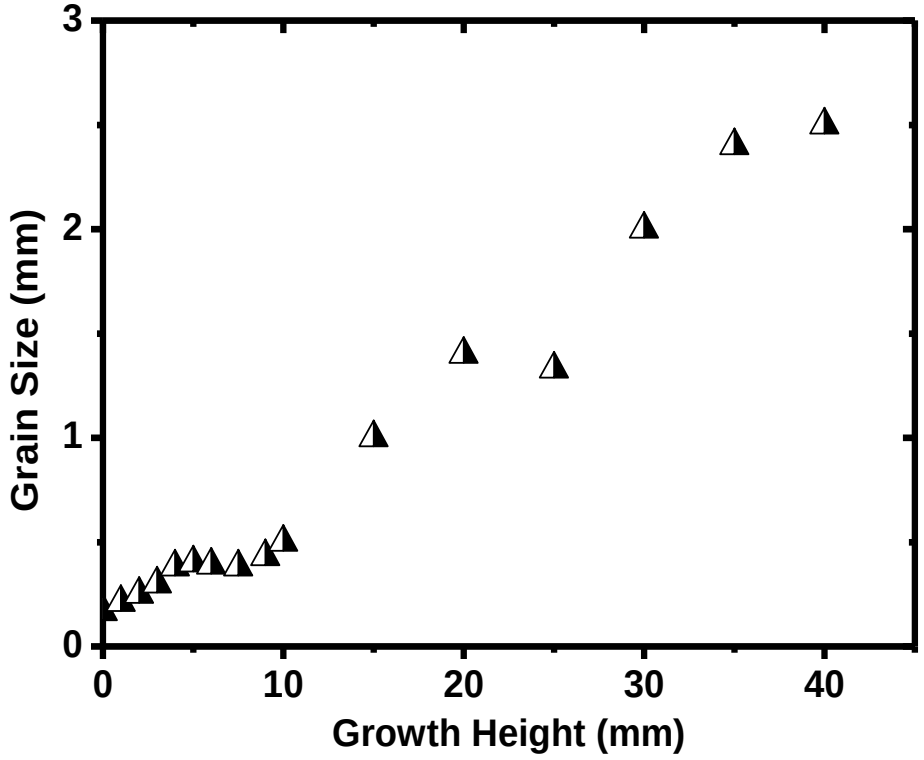

Figure 4-7 Plot of average grain size from vertically cut wafer of microcrystalline template grown mc-Si vs growth height. [4-20]

It was observed from the grain structure in Fig. 4-3 that the grains elongate as growth height increases. The aspect ratio of the grains with respect to the growth height was measured from the vertical wafer and is shown in Fig. 4-8. The grain size parallel to growth direction is defined as length (L) and that perpendicular is defined as width (W). It can be seen that the average aspect ratio increases with growth from about 5 mm growth height onwards, while at the initial stage the average aspect ratio seems to be constant. As shown by the schematics in Fig. 4-3, the grains are changing from being near-equiaxed at the initial stage to become columnar as the growth height increases.

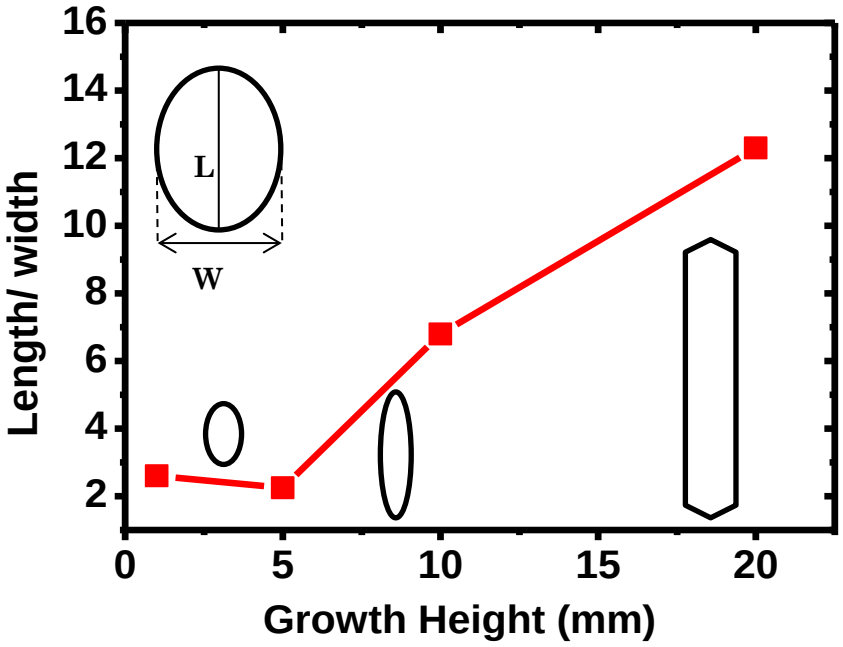

Figure 4-8 Plot of aspect ratio of grains from vertical wafer with respect to growth height. Inset: schematics showing grain shape. [4-20]

4-4-5 Grain Boundary Distribution

From the grain structure studies it was observed that the GB density decreases as growth height increases. Since the impurity gettering ability of the GBs is related to its character, the distribution of different types of GBs is an important factor to consider. Typically, the GB distribution is given by the fraction of the different types of GBs [4-15, 4-20, 4-21, 4-22]. Fig. 4-9 shows the GB distribution by the average fraction of different types of GBs, obtained from the vertical wafers for the region between H=0 mm to 16 mm. It can be seen that at the initial stage of growth the fraction of R GBs is very high >60 % (as seen earlier in Fig. 4-5), however the fraction decreases as growth height increases to a constant (Note: until 16 mm growth height). On the other hand, while Σ3 GBs have a low fraction (<30%) at the initial stage, the fraction increases with growth height to a constant (Note: until 16 mm growth height).

Since the GB density is changing with growth, the GB density distribution by character gives more a more detailed description. Moreover, when looking at GB distribution, due to the inclination of GBs, the GB fraction is different for horizontal wafers and vertical wafers. This is especially true when comparing Σ3 GBs and R GBs, since the multiple Σ3 GBs which are usually inclined, may not cut the vertical wafer if

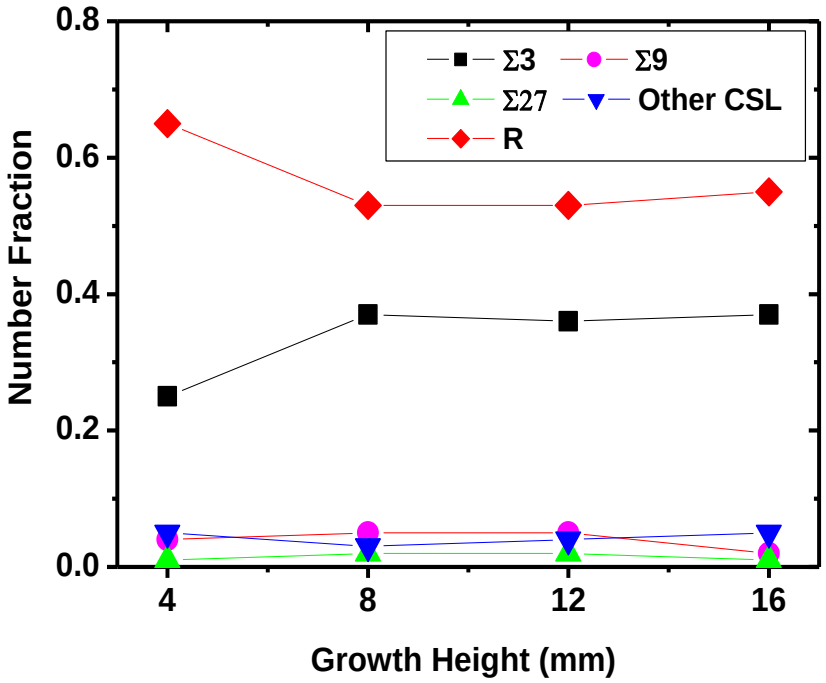

Figure 4-9 Average grain boundary Fraction distribution by character from vertically cut wafers of microcrystalline template vs growth height [4-20]

they are facing a different direction with respect to the vertical wafer, while R GBs more often follow the growth direction. The GB distribution is shown in Fig. 4-10 by GB density (i.e. GB length/ wafer area) with respect to growth height calculated from horizontal wafers. It should be noted that in Fig. 4-10, the measurement closest to the initial region is from a wafer taken from 1 mm growth height; hence the change in GB density from 0-1 mm is not included here. (The GB density near the initial growth region, calculated from a vertical wafer is shown in Fig. 4-5). The overall density of the major GBs, i.e. R and Σ3 decreases with growth, while other GBs show little change. Although, R GB and Σ3 have about the same GB density, the tendency of the decrease in R GBs is higher than Σ3 GBs leading to a higher fraction of Σ3 GBs at later stage of growth. In HP mc-Si, the reported GB fraction also shows that R GBs decrease with growth height, however the GB fraction of R GBs is much higher than Σ3 GBs (R GB~70%, Σ3~20%) [4-15]. On the other hand, Wong et al reported similar tendencies for growth from small spherical beads that were placed randomly [4-23].

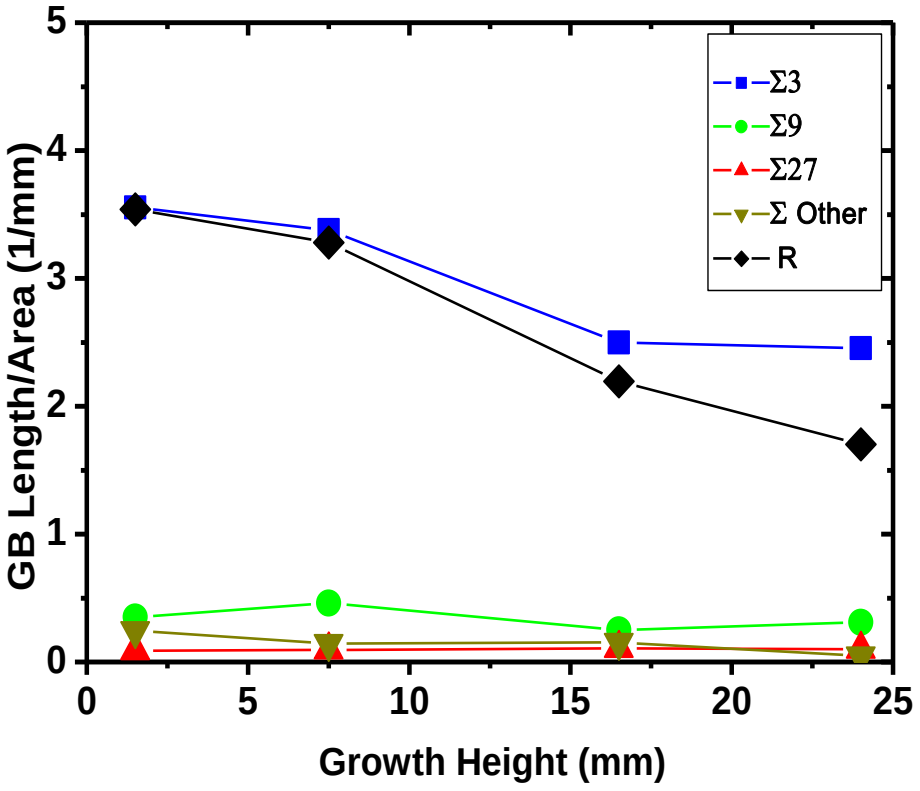

Figure 4-10 Average grain boundary density distribution by character from horizontally cut wafers of microcrystalline template vs growth height.

4-4-6 Grain Orientation Distribution

The distribution of the grains with respect to their orientations was investigated by measuring the misorientation between the neighboring grains and the fraction of the orientations at different growth heights in horizontal wafers. Fig. 4-11 shows the misorientation angle distribution (MAD) for wafers from the template (H=0 mm), growth height H= 1 mm and H=17 mm.

The graphs in the top half show the total fraction of the MAD and the bottom half show the area enclosed by the dotted squares in the graphs from the top half, for the sake of comparison with distribution of random grains. It can be seen that in the template the misorientation nearly follows the distribution of random grains based on the Mackenzie distribution [4-24]. However, there are slight deviations due to the peaks near 35° and 60° misorientation angles. The 60° can be attributed to the existence of Σ3 GBs, since the template has a Σ3 GB fraction of about 20% (from vertical wafer) as can be observed in Fig 4-5. The reason for the peak at 35° is not clear, but it may be due to the neighboring of grains with (110) and (111) planes, since the angle between these two planes is 35.26°. The misorientation angle distribution in wafer from 1 mm growth height shows a high fraction at 60° (>40%) in comparison to the template. This could be due to the increase in Σ3 GB fraction while there is a reduction of random GBs. The peaks at 39°and 31° can be attributed to Σ9 which has an angle/axis of 38.9°<110> and Σ27a which has 31.6°<110>. Overall, the misorientation angle is aligning towards certain angles, especially 60°, as growth height increases.

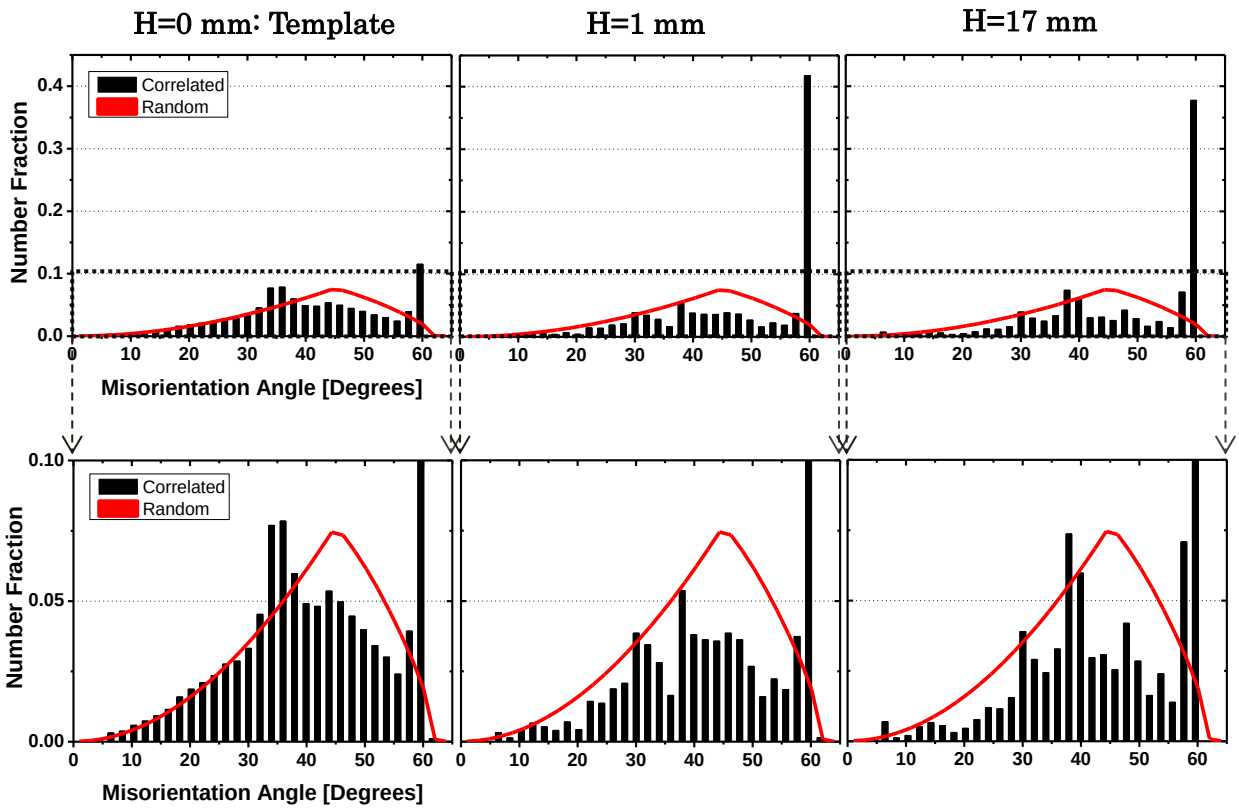

Figure 4-11 Misorientation angle distribution in horizontal wafers from template and growth heights H= 1 mm and H= 17 mm. Red line shows the Mackenzie distribution for random grains.

The orientation distribution of the grains with respect to growth direction was investigated from EBSD measurements using the crystal direction mode in Orientation Imaging Microcopy (OIM) software. The crystal direction of the grains was measured in horizontal wafers from the template, growth heights 1 mm, 17 mm and 24 mm. In Fig. 4-11 (a), the crystal orientations are plotted by area fraction with respect to some low index orientations (with a tolerance of 10°). Fig. 4-11 (b) shows the range of the orientations at 10° tolerance. It can be seen that at 10° tolerance a wide range of orientations will be included into one of the low index orientations considered here. Therefore the crystal orientations here are a collection of near-orientations. From this result, it can be seen that in the template, most orientations have similar distribution except for the low fraction of near-<110> and near-<111>. However, as the growth height

increases orientations such as near-<012>, near-<112> and near-<122> have a much higher fraction.

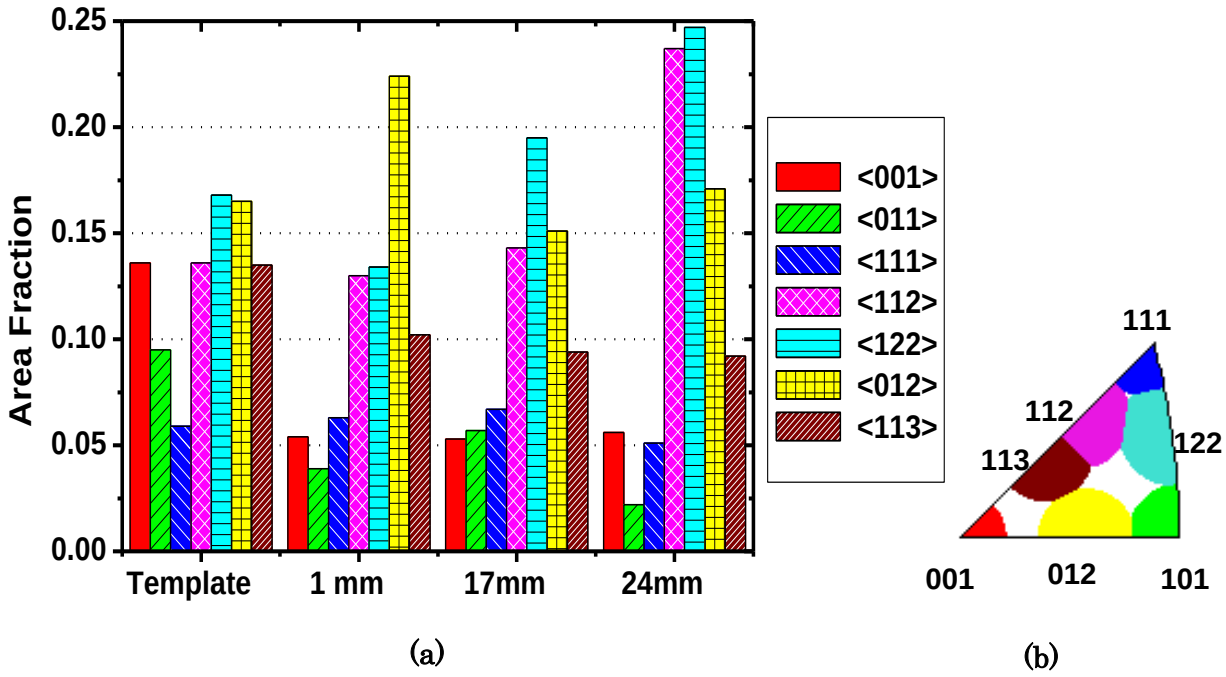

Figure 4-12 (a) Average crystal direction of grains by area fraction in horizontal wafers from template, growth heights 1 mm, 17 mm and 24 mm. (b) Schematics showing the range of the orientations plotted in (a), with a tolerance of 10°.

4-5 Conventional Multicrystalline Silicon (vs Microcrystalline Template Growth)

The structure of the microcrystalline template grown ingot has been discussed in the previous sections. However, how much does the grain structure differ from conventional mc-Si grown at similar conditions? We grew a conventional mc-Si at similar growth conditions and studied the grain structure for comparison. In this section, the grain structure of conventional mc-Si will be briefly discussed while highlighting the main difference between the two growths.

The grain structure of the conventional mc-Si can be seen from the vertically and horizontally cut wafers shown in Fig. 4-12. From the vertical wafer, the grains seem to have many inclined GBs and grain structure evolution is not clear. In contrast, the microcrystalline template had a much clearer grain structure evolution having a transition from small spherical grains to large columnar ones. Looking at the horizontal wafers, it can be seen that the wafers from the middle and near the top region looks to

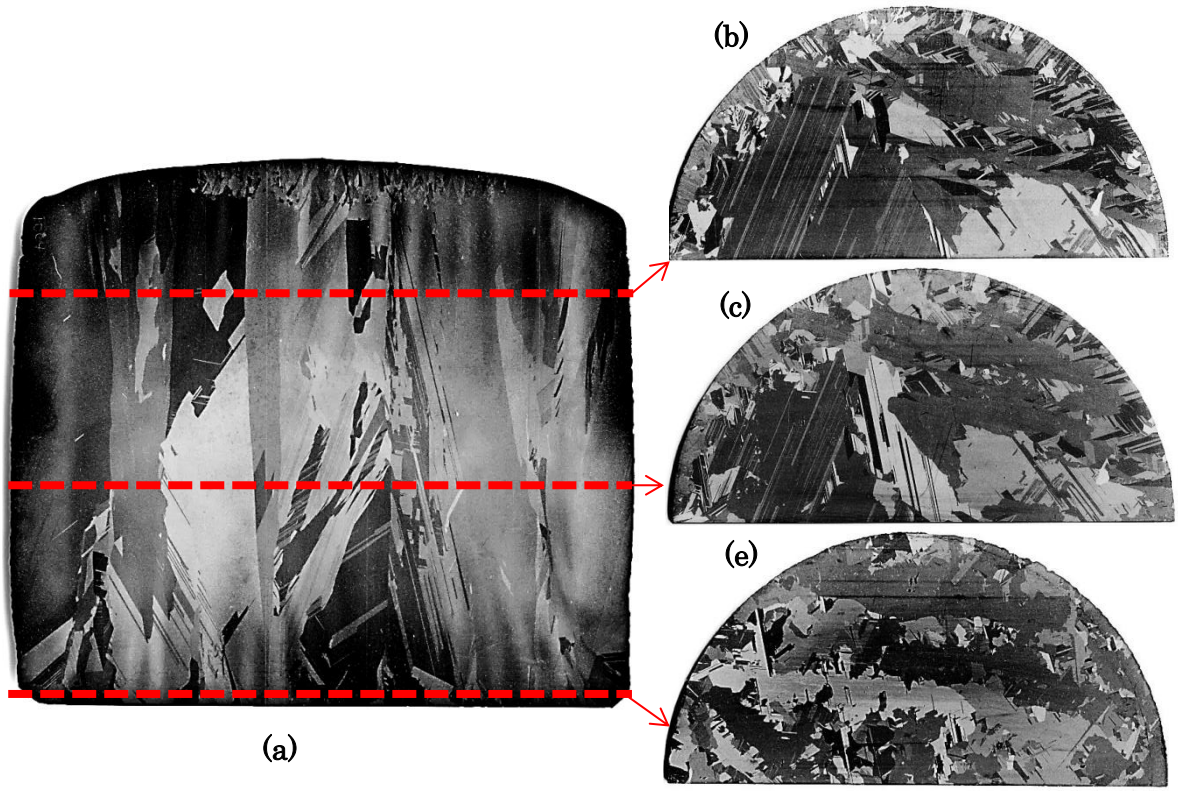

Figure 4-13 Image of (a) vertically cut wafer and (b), (c) and (d) horizontally cut wafers from growth height shown by dotted line in (a), from mc-Si grown by conventional method. (Image obtained using digital scanner)

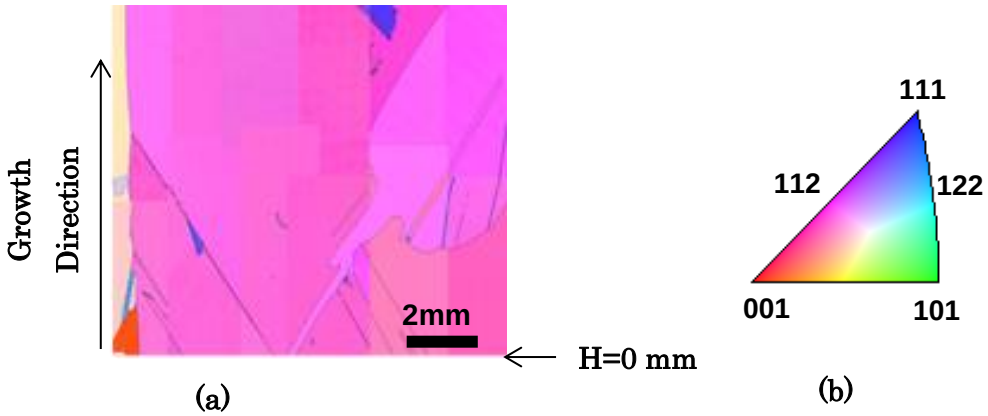

Figure 4-14 Inverse pole figure of area near initial growth stage and (b) color code for the grain orientation. Orientation is with respect to growth direction.

have similar grain structure, with many straight GBs. However, the wafer from the bottom region looks a little different, having many jagged grains. In contrast, the horizontal wafers from microcrystalline template grown ingots showed grains with a more uniform size.

The IPF from the area near the initial growth stage of conventional mc-Si obtained from vertical wafer is shown in Fig. 4-14 (a). It was also found that a near-<112>, and near-<113> grain orientation with respect to growth direction exists. These orientations are consistent with other reports for conventional mc-Si [4-25]. Moreover, many inclined straight GBs exist resulting in triangular shaped grains. The merging of the inclined GBs

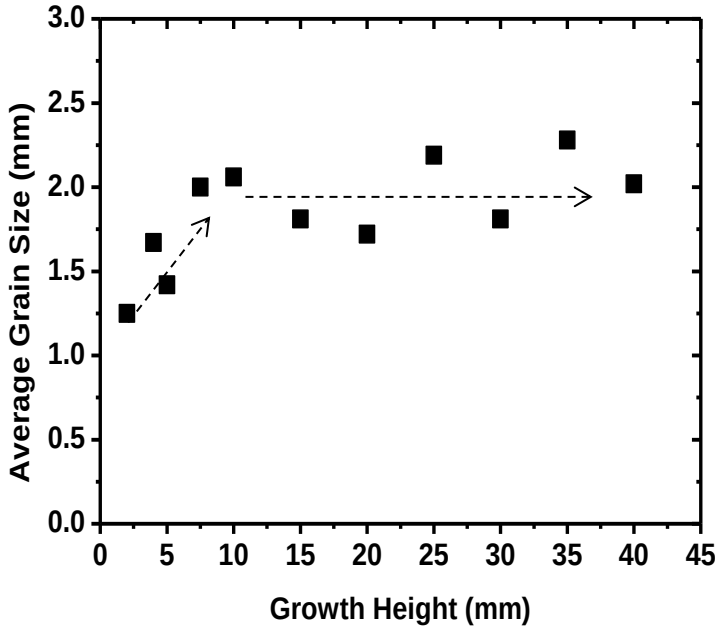

Figure 4-15 Average grain size vs growth height. (From vertical wafer of conventional mc-Si). Arrows are guide to show tendency of the plots in graph.

leads to the increase in grain size. The grain size calculated from the vertical wafer is shown in Fig. 4-15. It can be seen that the average grain size increases initially but becomes almost constant at later stage of growth. In comparison to the microcrystalline template grown ingot, in conventional mc-Si the average grain size near the initial stage of growth is much larger. Moreover, in conventional mc-Si the grains size becomes constant after an initial increase, showing only 2 stages, while in template grown mc-Si the average grain size increases with growth and shows 3 different stages.

The GB distribution measured (in vertical wafer) in conventional mc-Si is shown in Fig. 4-16, with respect to growth height for the region between 0 mm-20 mm. The fraction of Σ3 GBs is dominant throughout growth, at about 60%, although there is an increase initially and then a decrease, also suggesting that two stages of growth may exist in conventional mc-Si. The fraction of R GBs very slowly decreases, while Σ9 GB fraction was found to increase with growth height. In general the average fraction of the GB distribution by type is consistent with other reports from conventional mc-Si [4-21, 4-22]. In contrast, in template grown mc-Si, the GB distribution by character changes more drastically with growth and a higher fraction of R GBs exist, especially at initial stage (~60% see Fig 4-5).

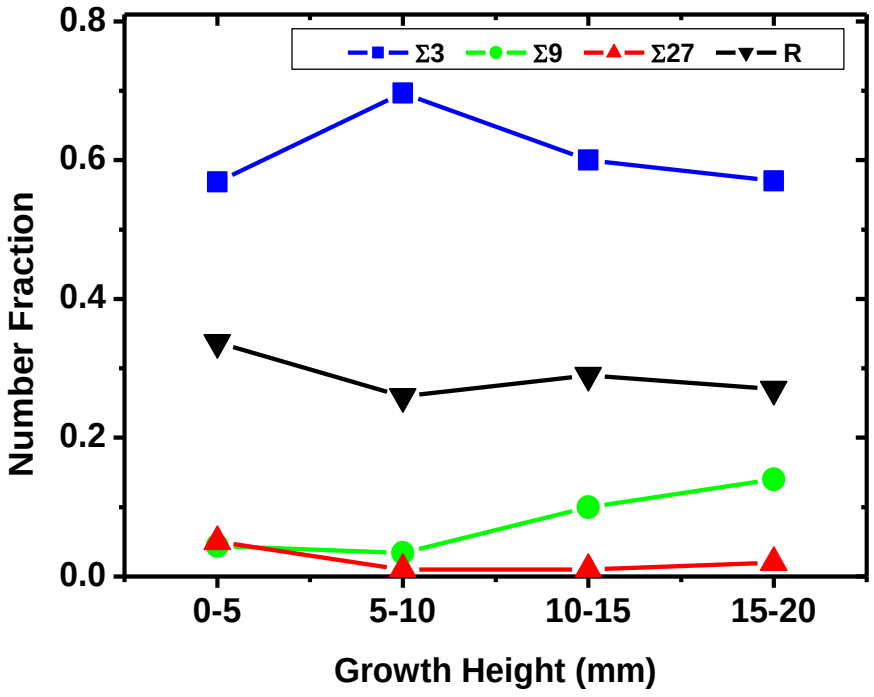

Figure 4-16 Average grain boundary fraction distribution by character from vertically cut wafers of conventional mc-Si with respect to growth height.

4-6 Discussion

4-6-1 Grain Structure Evolution in Template Grown Ingot

The grain structure analysis has clearly shown that in microcrystalline template grown ingot, the grain structure evolves as growth height increases. From the vertical wafers, it was observed that the grains are initially small and then elongate with growth, transitioning from spherical to ellipsoidal to columnar shape. The grain size distribution also showed that there is a 3 step increase in grain size. Based on the results, the grain growth can be explained in 3 stages.

Stage I: Initial Growth Stage

The initial growth stage is near the beginning of the solidification from the microcrystalline template. It was seen that the structure of the grown grains was different from the microcrystalline template (Fig 4-5, 4-6). The grown grains were found to be much larger than the grains in the template. This was also shown by the large decrease in GB density in grown grains compared to the template. The horizontal wafers (in Fig. 4-6) showed that although there were many needle-like grains in the template, most of the grains grown, even at 1 mm growth height, were equiaxed. It was also seen that the interface between the template and the grown grains was not flat. Considering these factors the nucleation at the initial stage of microcrystalline template growth can be explained by the schematics in Fig. 4-17. Due to the unevenness of the template (uneven melting of grains in template), the grains grow in several directions initially, and depending on the grain orientation and GB inclination some grains get annihilated while others grow larger. In many cases the grain boundaries which were inclined in the template, continued growing inclined and merged with other GBs, resulting in a decrease in GB density, which is in fact an increase in grain size. The probability of the GBs to merge is related to their inclination and the distance between the GBs. Therefore, if the grain size (i.e. distance between GBs) increases, it is expected that the probability of the GBs to merge will decrease. The interaction between GBs is an important factor affecting the grain structure evolution during growth (*discussed in detail in Chapter 6).* The spherical nature of the grains near the initial (seen in vertical wafer) stage may be due to the high fraction of R GBs, which do not need to follow the facet, thus have the freedom to

be curvy, enabling the spherical nature of grains (as can be seen in Fig 4-5 (b)). Stage I is thus heavily dependent on the template properties and the high fraction of R GBs.

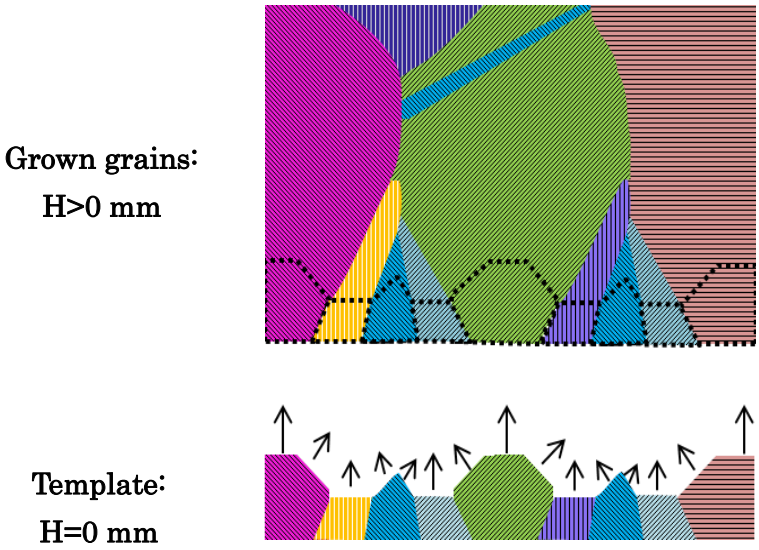

Figure 4-17. Schematics of nucleation for microcrystalline silicon template growth. Arrows indicating growth direction at initial stage H=0 mm from unevenly melted grains in template. In Grown grains at H>0 mm, dotted bold lines indicate interface between template and grown grains.

Stage II: Transient Growth Stage

In stage II, the average grain size (grain size perpendicular to growth direction) observed in vertical wafers, was nearly constant. It was also seen (Fig. 4-3) that the grains were elongating and becoming ellipsoidal, as shown by the aspect ratio of grains in vertical wafers (Fig. 4-8). In this region, it was observed in vertical wafers that the fraction of R GBs decrease while Σ3 GBs increase. From horizontal wafers, it was observed that the density of both R and Σ3 GBs decrease with growth height, however the tendency is gradual, and the density of R GBs become lower than Σ3 GBs (Note: horizontal wafers likely to show more Σ3 GBs). This region could be explained as a transient stage where fewer new grains are forming and fewer existing grains get annihilated, while the grains elongate in the growth direction. This is also evident with the curved R GBs becoming parallel to growth direction. Although it is not clear why this growth stage exists, it seems that at this stage the growth is becoming more stable than

stage I. Thus Stage II is a transition passage needed for the growth to evolve into Stage III from Stage I.

Stage III: Steady Growth Stage

In stage III, the average grain size increases with growth height. The grains elongate in growth direction and are mainly of columnar shape (from vertical wafers). The density of R GBs decreases more strongly than the Σ3 GBs. The misorientation between the grains is also aligning towards certain angles especially 60°. This is expected to be due to the higher fraction of Σ3 GBs. The growth seems to be steady with most GBs growing almost parallel to growth direction. In this region a high fraction of grains with <112> and <122> direction were found. The high fraction of <112> maybe due to (112) plane having the second lowest surface energy after the (111) plane [4-26]. (112) planes have also been found to be dominant in HP mc-Si, conventional and dendritic grown mc-Si [4-25, 4-6, 4-17, 4-23]. The high fraction of <122>, maybe due to the twinning of [001], since the twin orientation to [001] is [22-1] [4-27]. It was also observed that some grains that had twin boundaries (Σ3) also became larger *(See Chapter 6 for more details)*. The increase in certain grains over others also means that the grain size distribution is becoming non-uniform as growth height increases. In short, Stage III is governed by grain alignment and preferential growth of certain orientations as well as twinning.

4-6-2 Microcrystalline Silicon Template Growth vs Conventional Multicrystalline Silicon

The grain structure analysis in mc-Si grown from microcrystalline template showed the existence of 3 stages of growth, while in conventional mc-Si, the results suggested two stages. The initial stage of the conventional mc-Si has much larger grains, and there are many inclined Σ3 GBs, as opposed to the spherical grains with high fraction of R GBs in the microcrystalline template growth. The average grain size in conventional mc-Si initially increased, however became almost constant at later stage of growth, while in microcrystalline template growth the average grain size generally increases (except for stage II). Dominant grain orientations of near-<112> and near-<113> appear even at the initial stage of the conventional mc-Si while in microcrystalline template growth the dominant orientations of near-<112> and near-<122> appear at later stage. One

important difference between these two growths is the nucleation at the initial stage, which also affects the grain evolution. In conventional mc-Si, the initial grains are larger and due to the high fraction of inclined Σ3 GBs, the grain size increases rapidly due to the merging of those inclined GBs. On the other hand, in microcrystalline template growth, at the initial stage the grains are smaller and there are many R GBs, which are curvy at the initial stage, however they become parallel to growth direction later and thus less likely to merge with other GBs unless they are inclined. The comparison between the two techniques proves the importance of the initial growth stage, especially the types of GBs, grain size, and orientation with regards to grain structure evolution.

4-7 Summary

The grain structure evolution in multicrystalline silicon grown from a microcrystalline silicon template was studied with respect to grain size, boundary distribution, shape and orientations. It was found that generally the grain size increased and random grain boundary fraction decreased with growth height. At later stage of growth, grains align and grains with near orientation of <112> and <122> become dominant. The results suggested a three stage growth process.

In stage I (Initial stage), the grains are small and spherical with respect to growth direction and a high density of random grain boundaries exist. However, with growth the grain size increases, and the fraction of random grain boundaries decreases. This stage is heavily influenced by the template. In stage II, (Transient stage), the average grain size perpendicular to growth direction is almost constant, while grains elongate in growth direction becoming ellipsoidal. The R GBs become mostly parallel to growth direction. In stage III, (Steady stage), the average grain size steadily increases with growth height and the random grain boundary density decreases much faster than the Σ3 grain boundaries. The grains elongate towards the growth direction and become columnar. The grains align with growth and grains with near-orientations of <112> and <122> become larger than other grains.

The grain structure of the microcrystalline template grown ingot was compared with multicrystalline silicon grown by the conventional growth method. In conventional

multicrystalline silicon, there seems to be two growth stages. The grains at the initial stage are much larger than those at the initial growth region of the microcrystalline template grown ingot. There is also a high fraction of Σ3 grain boundaries, which are inclined and merge resulting in an increase in grain size, however due to formation of new Σ3 grain boundaries the overall average of grain size remains almost constant at later stage of growth. The comparison between the two growth methods highlighted the impact of the initial growth stage on the evolution of grain structure during growth.

From this study, the grain structure evolution in multicrystalline silicon grown from small randomly oriented grains was elucidated. The importance of initial nucleation, preference of low energy grain orientation and impact of GBs, especially twins on grain structure evolution was highlighted. Moreover, it is evident that the growth using the microcrystalline template is an easy, yet effective method not only to study grain structure evolution but also to control the grain structure in multicrystalline silicon.

4-8 References

[4-1] Benmohamed, Z., and M. Remram. "Effect of dislocation density on the efficiency of multicrystalline silicon solar cells." *Materials Science-Poland* 25.1 (2007): 243-249.

[4-2] Sopori, Bhushan, et al. "Performance limitations of mc-Si solar cells caused by defect clusters." *ECS Transactions* 18.1 (2009): 1049-1058.

[4-3] Chen, Jun, et al. "Electron-beam-induced current study of small-angle grain boundaries in multicrystalline silicon." *Scripta Materialia* 52.12 (2005): 1211-1215.

[4-4] T. Buonassisi, M. D. Pickett, A. A. Istratov, E. Sauer, T. C. Lommason, E. Marstein, T. Pernau, R. F. Clark, S. Narayanan, S. M. Heald and E. R. Weber, *Proc. 4th World Conf. Photovoltaic Energy Conversion*, 2006, p. 944.

[4-5] Nara, S., T. Sekiguchi, and J. Chen. "High quality multicrystalline silicon grown by multi-stage solidification control method." *The European Physical Journal Applied Physics* 27.1-3 (2004): 389-392.

[4-6] Fujiwara, Kozo, et al. "Growth of structure-controlled polycrystalline silicon ingots for solar cells by casting." *Acta Materialia* 54.12 (2006): 3191-3197.

[4-7] Fujiwara, Kozo, et al. "Directional growth method to obtain high quality polycrystalline silicon from its melt." *Journal of Crystal Growth* 292.2 (2006): 282-285.

[4-8] Usami, Noritaka, et al. "Implementation of faceted dendrite growth on floating cast method to realize high-quality multicrsytalline Si ingot for solar cells." *Journal of Applied Physics* 109.8 (2011): 083527.

[4-9] Wang, T. Y., et al. "Grain control using spot cooling in multi-crystalline silicon crystal growth." *Journal of Crystal Growth* 311.2 (2009): 263-267.

[4-10] Fujiwara, Kozo, et al. "In situ observation of Si faceted dendrite growth from low-degree-of-undercooling melts." *Acta Materialia* 56.11 (2008): 2663-2668.

[4-11] Fujiwara, Kozo, et al. "Grain growth behaviors of polycrystalline silicon during melt growth processes." *Journal of Crystal Growth* 266.4 (2004): 441-448.

[4-12] Fujiwara, K., et al. "Formation mechanism of parallel twins related to Si-facetted dendrite growth." *Scripta Materialia* 57.2 (2007): 81-84.

[4-13] Chen, P., Y. L. Tsai, and C. W. Lan. "Phase field modeling of growth competition of silicon grains." *Acta Materialia* 56.15 (2008): 4114-4122.

[4-14] Cantù, G., A. Popescu, and W. Miller. "Grain growth of silicon." *Acta Materialia* 60.19 (2012): 6755-6761.

[4-15] Y. M. Yang, A. Yu, B. Hsu, W. C. Hsu, A. Yang, C. W. Lan, Prog. Photovolt: Res. Appl. (published online). http://dx.doi.org/10.1002/pip.2437 , 2013

[4-16] Lan, C. W., et al. "Grain control in directional solidification of photovoltaic silicon." *Journal of Crystal Growth* 360 (2012): 68-75.

[4-17] Zhu, Didi, et al. "Seed-assisted growth of high-quality multi-crystalline silicon in directional solidification." *Journal of Crystal Growth* 386 (2014): 52-56.

[4-18] International Technology Roadmap for Photovoltaic, Fifth Edition 2014

[4-19] Miyahara, Hirofumi, et al. "Solidification Conditions at the Early Stages for Grain Control of Polycrystalline Silicon ingot." Photovoltaic Energy Conversion, Conference Record of the 2006 IEEE 4th World Conference on. Vol. 1. IEEE, 2006.

[4-20] Prakash, Ronit R., et al. "Grain growth of cast-multicrystalline silicon grown from small randomly oriented seed crystal." *Journal of Crystal Growth* 401 (2014): 717-719.

[4-21] Ratanaphan, Sutatch, Yohan Yoon, and Gregory S. Rohrer. "The five parameter grain boundary character distribution of polycrystalline silicon." *Journal of Materials Science* 49.14 (2014): 4938-4945.

[4-22] Chen, Jun, and Takashi Sekiguchi. "Carrier recombination activity and structural properties of small-angle grain boundaries in multicrystalline silicon." *Japanese Journal of Applied Physics* 46.10R (2007): 6489.

[4-23] Wong, Y. T., C. Hsu, and C. W. Lan. "Development of grain structures of multi-crystalline silicon from randomly orientated seeds in directional solidification." *Journal of Crystal Growth* 387 (2014): 10-15.

[4-24] Mackenzie, J. K. "Second paper on statistics associated with the random disorientation of cubes." *Biometrika* 45.1-2 (1958): 229-240.

[4-25] Brynjulfsen, I., et al. "Growth velocity and grain size of multicrystalline solar cell silicon." *Journal of Crystal Growth* 356 (2012): 17-21.

[4-26] Zhang, Jian-Min, et al. "Anisotropy analysis of the surface energy of diamond cubic crystals." *Surface and interface analysis* 35.10 (2003): 805-809.

[4-27] Wilhelm, F. "The orientation of high-order growth twins in diamond-type crystals." *Journal of Applied Crystallography* 4.6 (1971): 521-523

CHAPTER 5

Impact of Pulling Rate on Grain Structure Evolution

5-1 Introduction

Although, the initial growth stage is very important *(as discussed in Chapter 4)* the grain growth behavior during growth must also be optimized. To control the grain structure, Nara et al. changed the solidification speed after the initial stage and found that a high solidification rate at initial stage and a low solidification rate at the second stage are necessary to obtain large grained mc-Si [5-1]. Fujiwara et al. observed the silicon melt growth from bi-crystal seed and found that the cooling rate significantly affects the growth behavior [5-2]. Similarly, Tsai et al. did simulation on bi-crystals and agreed with Fujiwara et al., illustrating the competition between the interfacial and kinetic effects [5-3]. These studies show the fundamentals of crystal growth behavior in large grains with certain orientations and are useful to understand the grain competition during growth. Other growth rate related studies in mc-Si showed that the growth rate influenced impurity concentration [5-4, 5-5] and it was suggested that impurity precipitation also affects the grain structure during growth [5-6]. Indeed many studies have been done regarding the impact of growth rate in mc-Si, highlighting its importance. However, very few studies have been done on the impact of growth rate on the grain structure evolution in mc-Si grown from small randomly oriented grains. Wong et al, examined grain structure development in mc-Si grown from small randomly oriented silicon beads [5-7]. They found that grains with certain orientations become dominant at later stage of growth and the dominant orientation varies with the crucible pulling rate. Although, their result for similar crucible pulling rates as HP mc-Si shows a dominance of grains with {112} orientation, the tendency was opposite in their sample as the proportion of {112} increases while in HP mc-Si the dominant {112} orientation fraction is reported to decrease with growth height [5-8]. Moreover, Wong et al reported that although {112} orientation is dominant at low crucible pulling rate, {111} becomes dominant at high

pulling rates (although their results showed a higher proportion of {113} and {123} at later stage of growth). The inconsistencies in the results and lack of other literature warrant more studies to understand the grain structure evolution in mc-Si grown from small randomly oriented grains.

In this work, we investigate grain structure evolution in mc-Si grown from a microcrystalline silicon (micro-Si) template. This micro-Si template has an average grain size (<100μm) much smaller than the seeds used in other similar studies [5-7, 5-8]. Moreover, since the template is a high-purity Siemens grown micro-Si, and we use it without breaking it, it is expected to have lower impurities compared to seeds that are broken into chips. (Broken chunks can get contaminated easily during crushing and handling). The grain structure evolution of mc-Si grown from this template is discussed in Chapter 4. However, since the focus was on the impact of the template, the discussion was based on ingot grown at only one crucible pulling rate, which is 15 mm/h.

To understand the impact of crucible pulling rate in mc-Si grown from small randomly oriented seeds, in this chapter the grain structure evolution is investigated in mc-Si grown from micro-Si templates with two different pulling rates: 15 mm/h and 45 mm/h. For simplicity, henceforth ingots grown at these two crucible pulling rates will be termed as PR15 and PR45 for 15 mm/h and 45 mm/h pulling rates respectively.

5-2 Experimental

Test ingots of 100 mm diameter, with a target resistivity of 2 Ωcm, were grown in unidirectional solidification growth setup. The crucibles were pulled out of the furnace at 15mm/h and 45mm/h respectively for each growth. The growth process is discussed in more detail in Chapter 3.

For characterization, the ingots were first vertically cut into half and one half was cut into vertical wafers while the other into horizontal wafers. The wafers were then mechanically and chemically polished before electron backscatter diffraction (EBSD) was used to study the grain structure. The step size for the EBSD measurement is 10 μm for all samples except for the microcrystalline template, where the step size is 5 μm.

Due to the design of the furnace, the template melted with a convex shape, therefore to reduce the impact of the growth interface shape, only the central region of the ingot where the interface is nearly flat was studied. The top part of the ingot is also not used to avoid the impact from impurity precipitation.

5-3 Grain Structure Evolution in Microcrystalline Template Grown Ingots at 15 mm/h vs 45 mm/h

In Chapter 4, the grain structure evolution was investigated in mc-Si grown from a micro-Si template at a crucible pulling rate of 15 mm/h. In this section we investigate the impact of pulling rate on the grain structure of mc-Si grown from the template. Test ingots were grown with pulling rates of 15 mm/h and 45 mm/h at similar growth conditions, and their grain structure was studied using vertically and horizontally cut wafers.

5-3-1 Grain Structure of Ingots grown at 15 mm/h and 45 mm/h

The grain structure studied using EBSD in vertical wafers from the ingots grown at a pulling rate of 15 mm/h (PR15) and 45 mm/h (PR45) are shown in Fig. 5-1 (a) and (b) respectively. The regions shown in Fig 5-1 are from the center of the vertical wafers (~10mm width), that were cut from the center of the ingots.

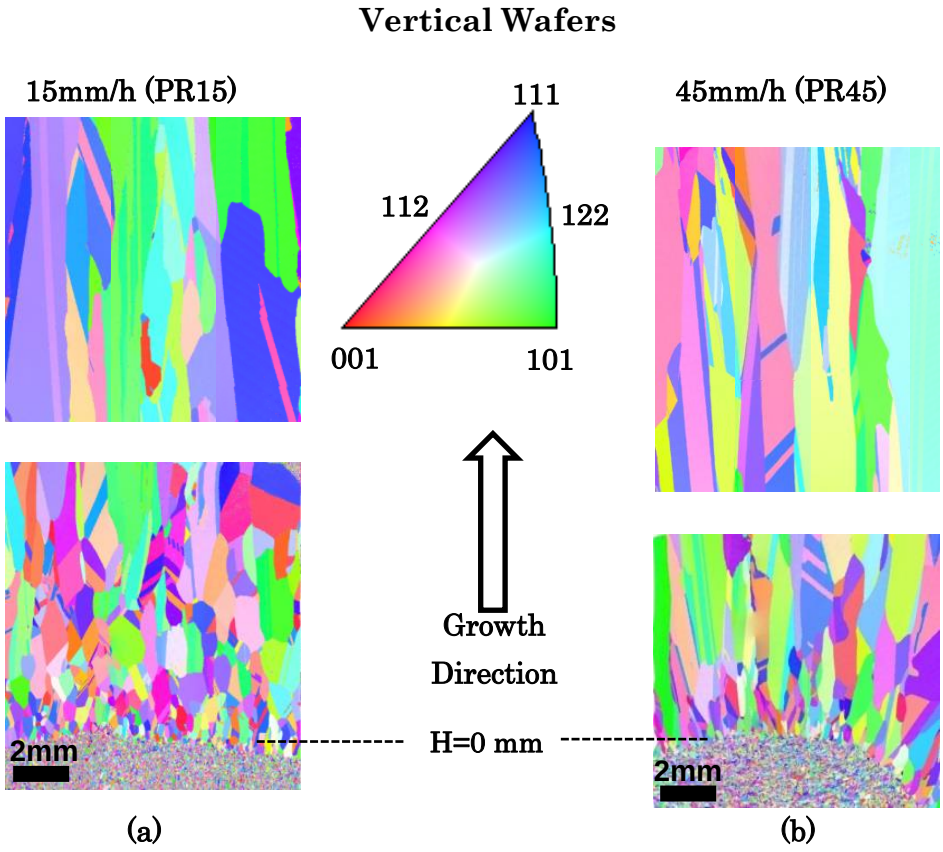

Figure 5-1. Inverse pole figures (IPF) of vertical wafers from ingots grown at pulling rate (a) 15 mm/h and (b) 45 mm/h (from the central region. Orientation direction is with respect to growth direction.

Unfortunately, for PR45 the template did not melt with a flat interface, and only a small region in the center is relatively flat, as can be seen in Fig. 5-1 (b). This means that the region used for analysis is small, since we try to reduce the the impact of the growth interface in our analysis. Nevertheless, the analysis is expected to give some tendencies regarding the growth rate impacts in mc-Si grown from micro-Si template. The inverse pole figures (IPF) of the two wafers, show a difference in grain structure, especially regarding the grain shape and size. In contrast to the spherical → ellipsoidal → columnar transition of grain shape with respect to growth direction in PR15, the grains in PR45 are elongated, and become columnar, from almost near the initial region, having many straight grain boundaries (GB)s and GBs that follow the growth direction. The grain size perpendicular to growth direction also looks smaller in PR45.

The IPFs of horizontal wafers from growth heights H=1 mm, and H=17 mm of PR15 and PR45 are shown in Fig. 5-2. Overall, the wafers from both ingots show similar grain structure, however, PR45 seems to have a higher density of twins (straight Σ3 GBs).

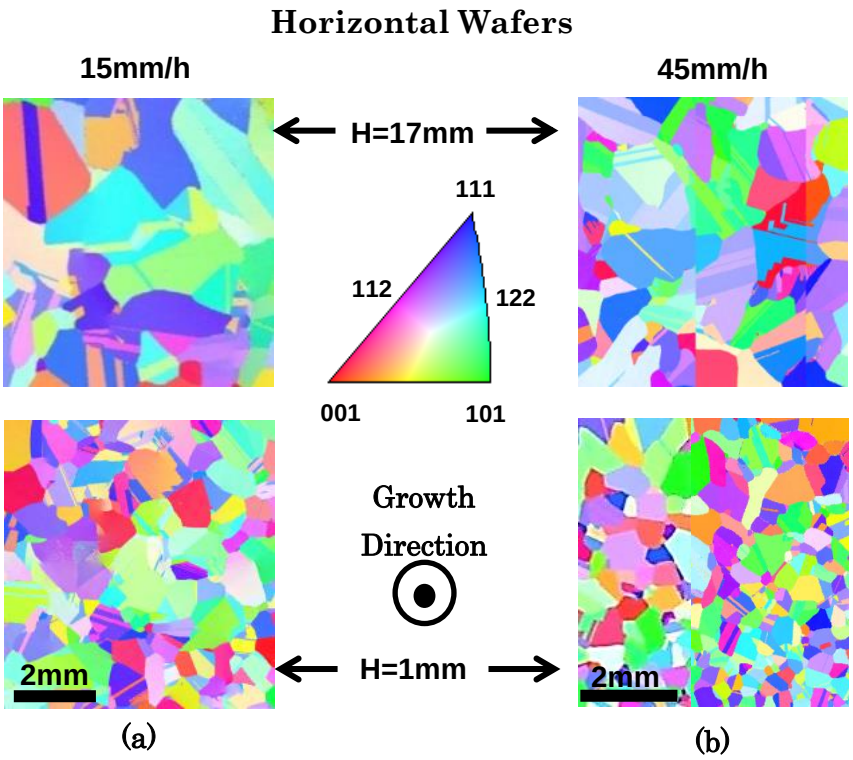

Figure 5-2. Inverse pole figures (IPF) of horizontal wafers from ingots grown at pulling rate (a) 15 mm/h and (b) 45 mm/h (from the central region of ingot). Orientation direction is with respect to growth direction.

5-3-2 Impact of Pulling Rate on Grain Size Distribution

The grain size distribution was measured and compared between PR15 and PR45. The line intercept method was used to measure the grain size (in vertical wafer it is the width of grain, i.e. perpendicular to growth direction) and although multiple twins were not counted (i.e. a grain containing a high density of multiple twins was counted as one grain), clearly visible single Σ3 GBs were counted.

The average grain size measured in vertical wafers from PR15 and PR45 is plotted in Fig. 5-3. For comparison, grain size measured in horizontal wafers from PR45 is also plotted in Fig. 5-3, showing similar results as the vertical wafer. The grain size distribution in PR45 seems to have two stages, where at initial stage, until 10 mm, the average grain size increases similar to that in PR15, however in the second stage the grain size increases slowly compared to the rapid increase in PR15.

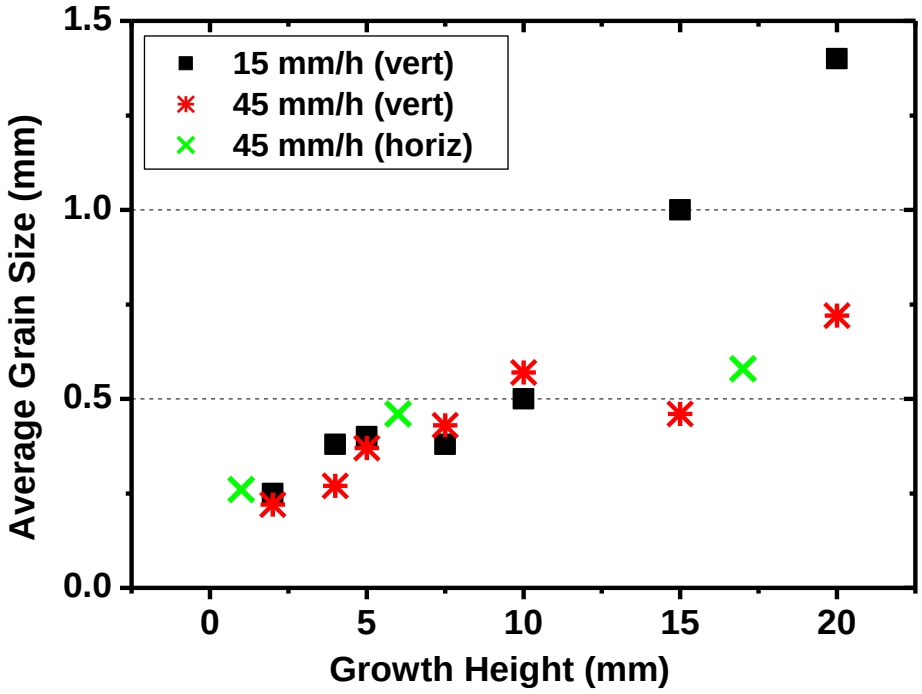

Figure 5-3. Average grain size measured in vertical wafers (vert) from ingots grown at 15 mm/h and 45 mm/h pulling rate plotted with respect to growth height. Grain size measured from horizontal (horiz) wafers for 45 mm/h also plotted.

5-3-3 Impact of Pulling Rate on Grain Boundary Distribution

The GB distribution by character was investigated with respect to growth height in horizontal wafers from both ingots. The results for PR15 is presented in Chapter 4 (Fig. 4-9). The GB distribution measured from horizontal wafers for the PR45 is shown in Fig. 5-4 (a). It shows that at the initial growth stage the GB fraction is constant, however as growth height increases the R GB fraction decreases while that of Σ3 GB increases. The other GBs did not show any significant change. Hence, the two main GBs, i.e. Σ3 and R

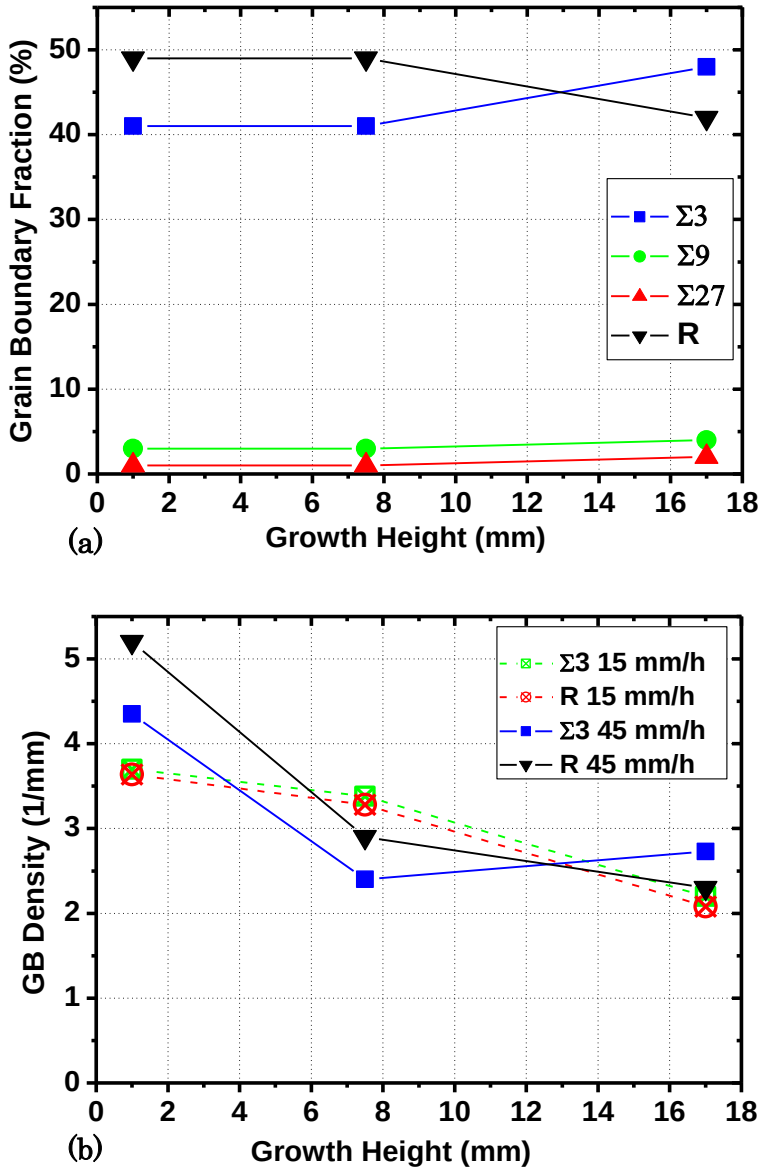

Figure 5-4. (a) Grain boundary distribution by character with respect to growth height in PR45. (b) Grain boundary density distribution for R GBs and Σ3 GBs with respect to growth height in PR15 and PR45 (all results from horizontal wafers).

GBs, were measured in horizontal wafers taken from the same growth heights of both ingots and is plotted in Fig.5-4 (b). It can be noted that in PR45 the density of R GBs is higher than Σ3 GBs near the initial stage (H=1 mm), while they are almost same in PR15. Although the GB density decreases with growth height in both ingots, the tendency is very different. For PR45, the GB density rapidly decreases to below that of PR15 at growth height 8 mm. However, thereafter the density of Σ3 GBs increased while R GB density decreased at a slower rate, leading to a higher overall GB density than PR15. This tendency is consistent with the grain size distributions in Fig. 5-3.

5-3-4 Impact of Pulling Rate on Grain Orientation Distribution

The orientation distribution of the grains with respect to growth direction was investigated from EBSD measurements using the crystal direction mode in Orientation Imaging Microcopy (OIM) software. The crystal direction of the grains was measured in horizontal wafers from growth heights 1 mm, 6 mm and 16 mm in PR45 and is plotted in Fig. 5.5 (a). The crystal orientations are plotted by area fraction with respect to some low index orientations (with a tolerance of 10°). The range of the orientations at 10° tolerance is shown in Fig 5-5 (b). Since the 10° tolerance includes a wide range of orientations, the orientations here will be considered as a collection of near-orientations. From this result,

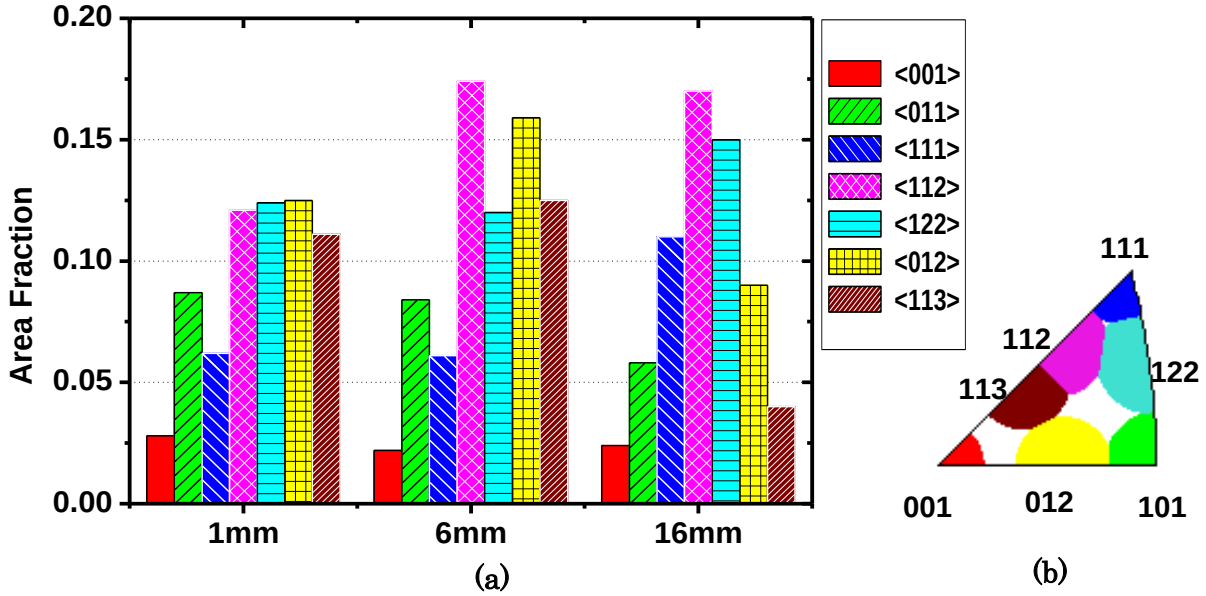

Figure 5-5(a) Average crystal direction of grains by area fraction in horizontal wafers from growth heights 1 mm, 6 mm and 16 mm. (b) Schematics showing the range of the orientations plotted in (a), with a tolerance of 10°.

it can be seen that near the initial growth stage, most orientations have similar distribution except for the low fraction of near-<001>. However, as the growth height increases orientations such as near-<111>, near-<112> and near-<122> have a higher fraction. Although, the dominance of <112> and <122> are similar to that in PR15 (shown in Chapter 4 Fig 4.12), it can be seen that in PR45 a high fraction of grains with near-<111> direction was also found at later stage (16mm).

The misorientation angle distribution (MAD) between grains was also measured in horizontal wafers from growth heights 1 mm, 6 mm and 16 mm of PR45 as shown in Fig. 5-6. It can be seen that in H=1 mm the misorientation angle distribution shows peaks at 60° and near 35°. This is similar to that observed in PR15 (Fig. 4-11). On the other hand, at later stage of growth (17 m growth height), in PR15 it was observed that a misorientation angle of near-40° was distinctly visible; however in PR45 the fraction of misorientation angles increases steadily between 30° and 40°.

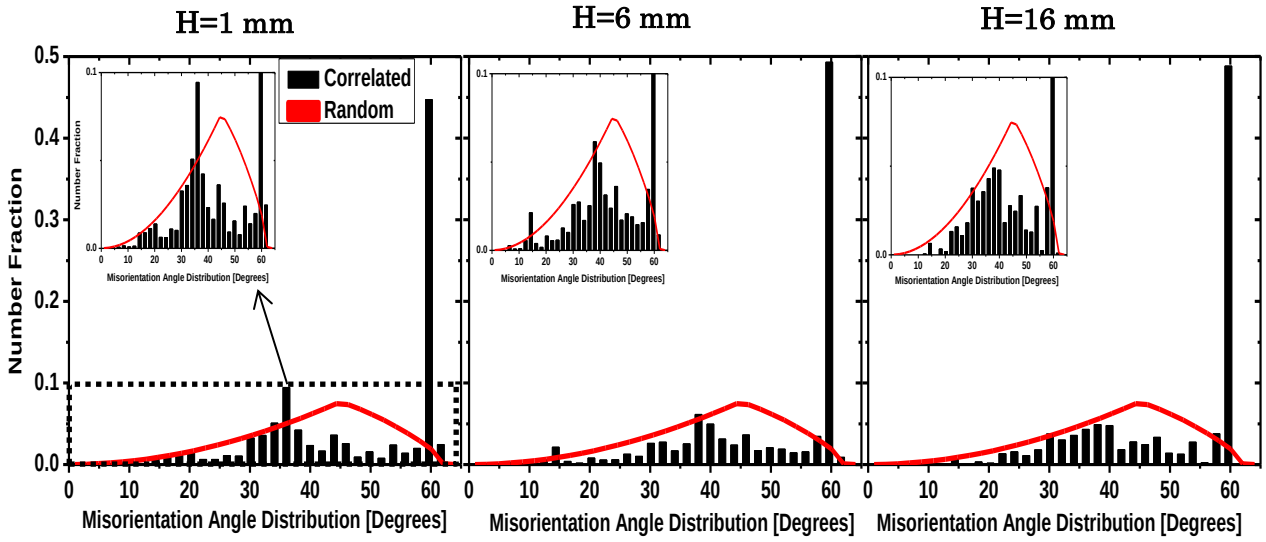

Figure 5-6 Misorientation angle distribution in horizontal wafers from template and growth heights H= 1 mm and H= 17 mm. Red line shows the Mackenzie distribution for random grains. Inset: same graphs with scale between 0 and 0.1 as shown in area enclosed by the dotted line.

5-4 Discussion

From the grain structure studied in PR15 and PR45, it was found that in PR45 the grains were columnar from near the initial growth region and the average grain size seems to increase in two stages. The GB density of both Σ3 and R GB in PR45 was higher than PR15 at the initial stage, however it decreased rapidly until a certain growth height and then decreased slowly thereafter. An increase in Σ3 GB density was also observed at later growth stage. With regards to crystal orientation, in PR45 near-<112> and near-<122> were dominant similar to PR 15, however at later stage of growth, a high fraction of near-<111> grains also appeared.

The reason for grain elongation from an early stage in PR45 is not clear; however it was observed that in contrast to PR15, the R GBs became almost parallel to growth direction from an early stage, leading to columnar grains. This suggests enhancement of grain growth in the growth direction. With respect to GBs, the slight increase in density of Σ3 GBs in PR45 showed that more twins form at a higher pulling rate. This may be due to an increase in undercooling at the groove between grains, which increases the probability of twin nucleation [5-9]. The fraction of grains with near-<112> and near-<111> direction may be due to its low interfacial energy. Near-<122> may be due to the twining of {001}, which gives {122}, even though twinning of {122} may bring back the {001} (high interfacial energy grain), subsequent twinning will once again bring {122}. This is visible in the appearance of {001} at later stage, however with a smaller fraction compared to the {122}.

Although the above explanation attempts to explain the results in terms of interfacial energy and twinning, the impact of the convex interface is not clear. Therefore, for a more accurate understanding, ingots with a flatter growth interface should be studied.

5-5 Summary

The impact of crucible pulling rate on the grain structure evolution in mc-Si grown from a microcrystalline Si template was investigated. It was found that higher pulling rate enhances growth of elongated columnar grains. The grain size distribution showed two stages, where initially the increase in grain size was similar for both growths. However, the lower pulling rate ingots showed a more rapid increase in grain size at the later stage. It was also found that higher pulling rate also enhances Σ3 GB fraction at later stage of growth. Although, the results were discussed in terms of twinning and interfacial energy, a major factor could also be the convex growth interface. It is therefore, suggested that ingots with a flatter growth interface may give more accurate results.

5-5 References

[5-1] Miyahara, Hirofumi, et al. "Solidification Conditions at the Early Stages for Grain Control of Polycrystalline Silicon ingot." *Photovoltaic Energy Conversion, Conference Record of the 2006 IEEE 4th World Conference* on. Vol. 1. IEEE, 2006.

[5-2] Fujiwara, Kozo, et al. "In-situ observations of melt growth behavior of polycrystalline silicon." *Journal of Crystal Growth* 262.1 (2004): 124-129.

[5-3] Chen, P., Y. L. Tsai, and C. W. Lan. "Phase field modeling of growth competition of silicon grains." *Acta materialia* 56.15 (2008): 4114-4122.

[5-4] Autruffe, Antoine, et al. "Influence of pulling rate on multicrystalline silicon ingots' properties." *Journal of Crystal Growth* 386 (2014): 199-203.

[5-5] Kvande, Rannveig, Øyvind Mjøs, and Birgit Ryningen. "Growth rate and impurity distribution in multicrystalline silicon for solar cells." *Materials Science and Engineering: A* 413 (2005): 545-549.

[5-6] Schmid, E., et al. "The effect of the growth rate on the microstructure of multi-crystalline silicon." *Journal of Crystal Growth* 359 (2012): 77-82.

[5-7] Wong, Y. T., C. Hsu, and C. W. Lan. "Development of grain structures of multi-crystalline silicon from randomly orientated seeds in directional solidification." *Journal of Crystal Growth* 387 (2014): 10-15.

[5-8] Y. M. Yang, A. Yu, B. Hsu, W. C. Hsu, A. Yang, C. W. Lan, Prog. Photovolt: Res. Appl. (published online). http://dx.doi.org/10.1002/pip.2437 , 2013

[5-9] Nadri, Amal, Yves Duterrail-Couvat, and Thierry Duffar. "Two-dimensional numerical modeling of grain structure in multi-crystalline silicon ingot." *Journal of Crystal Growth* 385 (2014): 16-21.

CHAPTER 6

Grain Boundary Interactions in Multicrystalline Silicon Grown from Small Randomly Oriented Seeds

6-1 Introduction

Grain boundaries (GBs) play an important role in the performance of multicrystalline silicon (mc-Si) solar cells. GBs can act as sinks for impurities and the gettering ability of GBs depend on the GB character. Non-coherent GBs preferentially getter transition metal impurities, which strongly enhance carrier recombination activity at GBs, while highly coherent GBs (Σ3) do not and are mainly electrically inactive. [6-1, 6-2]. Moreover, extended gettering (to remove impurities out of GBs) and hydrogen passivation has also shown to be difficult for GBs with lower coherency (higher Σ values) [6-3]. Hence not all GBs are severely detrimental to the performance of solar cells.

Until recently, most growth techniques were concentrating on decreasing the GB density by increasing grain size. However the high performance multicrystalline silicon (HP-mc), where small randomly oriented seeds are used to grow mc-Si has gained attention recently and is expected to become dominant in future [6-4, 6-5, 6-6, 6-7]. Although this technique has a high fraction of R GBs, it has been reported that lower dislocation density and uniform grain structure (grain size, defect distribution) exists, which enables solar cells with a higher and narrow distribution of efficiency [6-4, 6-5, 6-6] compared to conventional mc-Si. In HP-mc the dislocation density has been reported to be low, however it increases with growth [6-4, 6-5, 6-6]. Lan et al suggested that this increase in dislocation density may be due to the non-uniform grains appearing as grain size increases with growth [6-4, 6-5]. The mechanism of this grain structure evolution is not clear and need to be clarified to enable optimization of HP-mc. Wong et al studied grain

structure evolution in mc-Si grown from small spherical randomly oriented seeds. They discussed that grains with lower interfacial energy overgrow that with higher interfacial energy. However grains with high interfacial energy were also present at later stage and they suggest it is due to twinning [6-8]. These previous studies, however do not explain the grain structure evolution in HP-mc sufficiently. Moreover, the previous studies mainly looked at horizontal wafers and did not discuss how GB interactions during growth affect the grain structure evolution. Since GB density is decreasing and the GB fraction by character is also changing, it is expected that GBs interact with each other during growth.

In this chapter, GB interactions in mc-Si grown from small randomly oriented seeds will be discussed. GB triple junctions of more than 2000 GBs from vertical wafers of mc-Si grown from small randomly oriented seeds were statistical analyzed. Two main interactions were defined in terms of that which would increase (Generation) or decrease (Annihilation) GB density.

6-2 Experimental

6-2-1 Crystal Growth and Characterization

Test ingot of 100 mm diameter and 80 mm height was grown from microcrystalline template. The pulling rate used for this experiment is 15 mm/h. For characterization, the ingot was first vertically cut into half and one half was cut into vertical wafers while the other into horizontal wafers. The wafers were then mechanically and chemically polished before electron backscatter diffraction (EBSD) was used to study the grain structure.

6-2-2 Analysis Details

The GB triple junctions of more than 2000 GBs in vertically cut wafers (i.e. parallel to growth direction) were analyzed with respect to growth height as defined below (see Fig. 6-1):

1) **Generation**: GB interaction which leads to increase in total number of GBs
2) **Annihilation**: GB interaction which leads to decrease in total number of GBs

6-3 Grain Boundary Interactions during Growth

Fig. 6-1. shows the inverse pole figure (IPF) with GBs highlighted taken from the central region (10 mm width) of a vertical wafer (The gap between the two IPF's is due to wafers cut into small samples to fit into EBSD holder).

Looking at the highlighted GBs in Fig. 6-1, the curved GBs are mostly R GBs while the straight GBs are mostly Σ3 GBs. At the initial stage many spherical grains exist and the fraction of R GBs is high, while as growth height increased grains became columnar. (Grain size and GB fraction are discussed in more detail in Chapter 4).

The definition for Generation and Annihilation interaction is also shown clearly in Fig. 6-1. The interactions were defined in this way to clarify which GBs merge and reduce the GB density or which GBs are generated and increase GB density. This is expected to show how the GB fraction changes during growth.

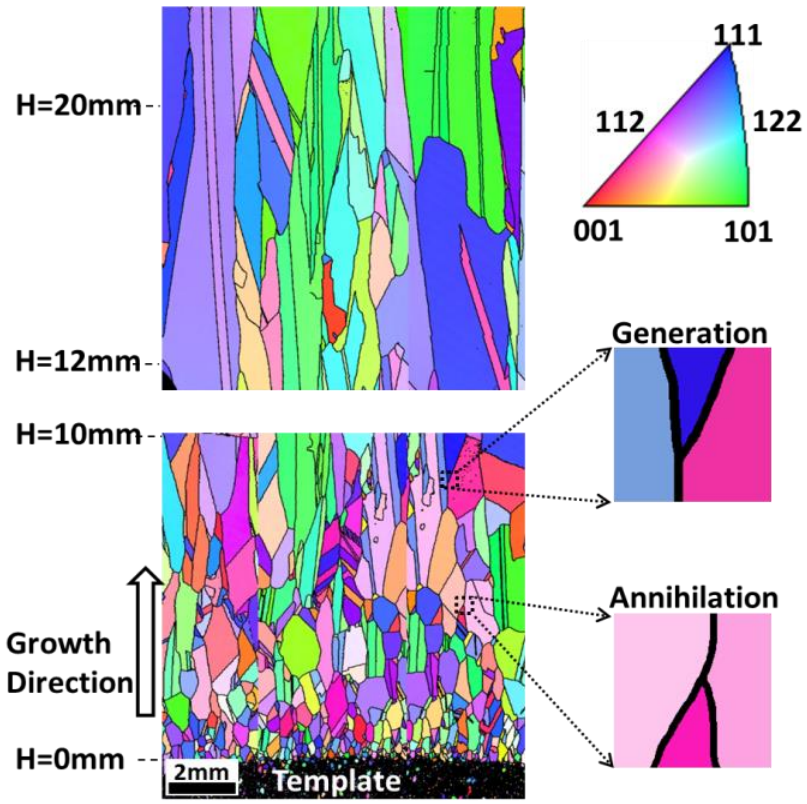

Figure 6-1. Inverse pole figure (IPF), with grain boundaries from the center of vertically cut wafer. The growth starts from the template upwards as shown in diagram. Color code shows crystal orientation with respect to growth direction. Definition of Generation and Annihilation also shown in diagram. [6-10]

6-3-1 Total Grain Boundary Interactions during Growth

Fig. 6-2. (a) shows the total number of GB interactions in terms of Generation and Annihilation with respect to growth height. The GB interactions are very high near the initial stage (0-1mm), with Generation slightly lower than Annihilation (Generation is about 90% of Annihilation). With growth the total number of interactions decreases rapidly until about 10 mm growth height, and then decreases steadily thereafter. This is inversely proportional to the trend shown by the increase in grain size with growth height, discussed in Chapter 4 [13].

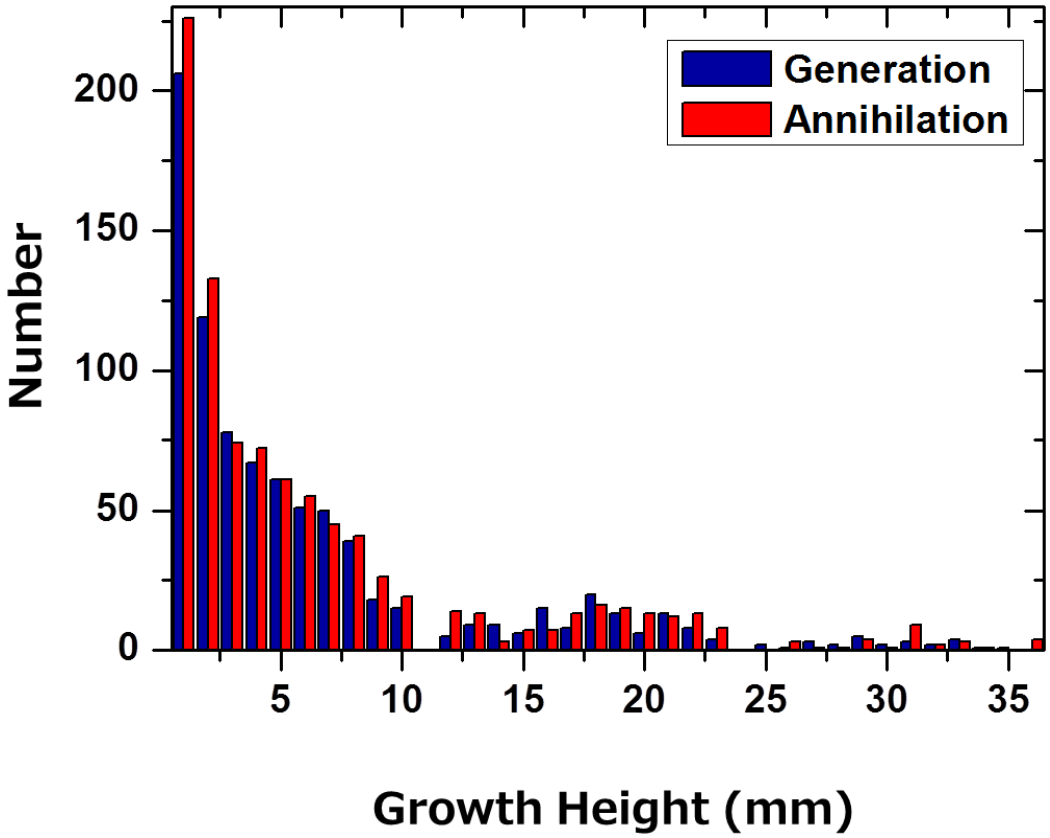

Figure 6-2. a) Total grain boundary interactions in terms of generation and annihilation. [6-10]

6-3-2 Fractions of Generation vs Annihilation

To compare the distribution of Generation vs Annihilation over growth height, the average fractions of Generation and Annihilation from total number of GB interactions were analyzed. Since the grains elongate with growth (as shown by the aspect ratio in Chapter 4), the interactions were averaged according to the grain size parallel to growth direction (vertical aspect of grain size). In other words, between growth height 0-1 mm the grain size parallel to growth direction is small, while between 25-36 mm grains are elongated and each grain covers a larger area. To reduce error due to the decrease in number of grains per unit area as the growth height increases, the average has been taken for a larger area with respect to growth height. If this type of average is not done, there would be error from comparing whole grains vs partial grains.

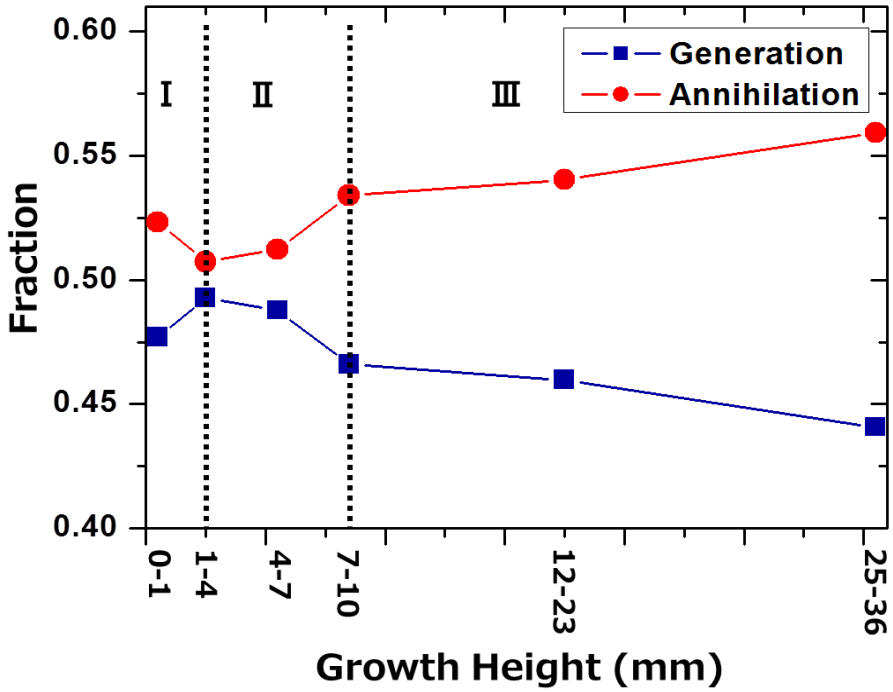

Figure 6-3. Average fractions of Generation and Annihilation interactions with respect to growth height. (Points plotted at the midpoint of averaged growth height, example 12-23 mm plotted at 17.5 mm) [6-10]

Fig. 6-3. Shows the fractions of Generation vs Annihilation averaged between growth heights with respect to the grain size in growth direction. This graph shows that generally the fraction of Annihilation is higher than that of Generation throughout growth, illustrating that decrease in GB density is favored. At initial stage (0-1mm and 1-4 mm), the fraction of Annihilation decreased with growth height. We define this region as stage **I**, as shown in Fig. 6-3. Between regions 1-4 mm to 7-10mm, defined stage **II**, the Annihilation fraction increases rapidly with growth, while after 7-10 mm there is a steady increase in the fraction of Annihilation, defined stage **III**. This change in the tendency at 3 stages, as defined stages **I**, **II** and **III**, is consistent with the 3 stages in grain size distribution [6-9].

6-3-3 Interaction between Different Types of Grain Boundaries

To understand how different types of GBs of interact during growth, GB Generation and Annihilation was investigated with respect to GB character vs growth height. For simplicity less coherent large angle GBs (Σ>27) were also considered as R GBs. Generation is plotted in Fig. 6-4 and Annihilation is plotted in Fig. 6-5 for the GB interactions as explained in Table 6-1.

Definition	Interaction	Description
Generation	R=>Σ3+R	R GB splitting into Σ3 and another R GB
	Σ9=>Σ3+Σ3	Σ9 splitting into two Σ3s
	GB=>GB+Σ3	Total of other interactions that increase number of Σ3, for example other Σ GB splitting into Σ3 and another Σ GB
	GB=>Σ9+GB	Generation increasing Σ9 GBs
	GB=>Σ27+GB	Generation increasing Σ27 GBs
	R=>R+R	One R GB splitting into two R GBs
	Other	Generation that do not fall into any previous category, e.g. small angle GBs, other CSL GBs
Annihilation	Σ3+R=>R	Σ3 GB merging with R GB to give R GB
	Σ3+Σ3=>Σ9	Two Σ3 GBs merging to give Σ9
	Σ3+GB=>GB	Σ3 GB Annihilation by GB interactions not mentioned previously
	Σ9+GB=>GB	Annihilation decreasing Σ9 GBs
	Σ27+GB=>GB	Annihilation decreasing Σ27 GBs
	R+R=>R	Two R GBs merge and give one R GB
	Other	All other Annihilations

Table 6.1. Summary of grain boundary interactions with respect to boundary character considered for the Generation and Annihilation interactions shown in Fig. 6-4 and 6-5

6-3-3-1 Fractions of Generation by Grain Boundary Character

Fig. 6-4. shows the average for Generation by GB character, as a fraction of total Generation, with respect to growth height. In case of R GBs, the dominant Generation is when one R GB splits into two R GBs (R=>R+R). This interaction is high at initial stage (0-1 mm), decreases until 10 mm, and then is almost constant thereafter. Generation leading to increase in Σ9, Σ27 and other GBs fluctuates initially, however remains low with growth. The dominant Generation involves the increase of Σ3 GBs. The total of Σ3 Generation fraction (i.e. sum of R=>Σ3+R, Σ9=>Σ3+Σ3 and GB=>GB+Σ3) at 0-1 mm is 55%, while at 25-36 mm it increases to 76%. This result statistically illustrates the favorability of low energy GB Generation (Σ3) over high energy GBs (R GBs) during growth.

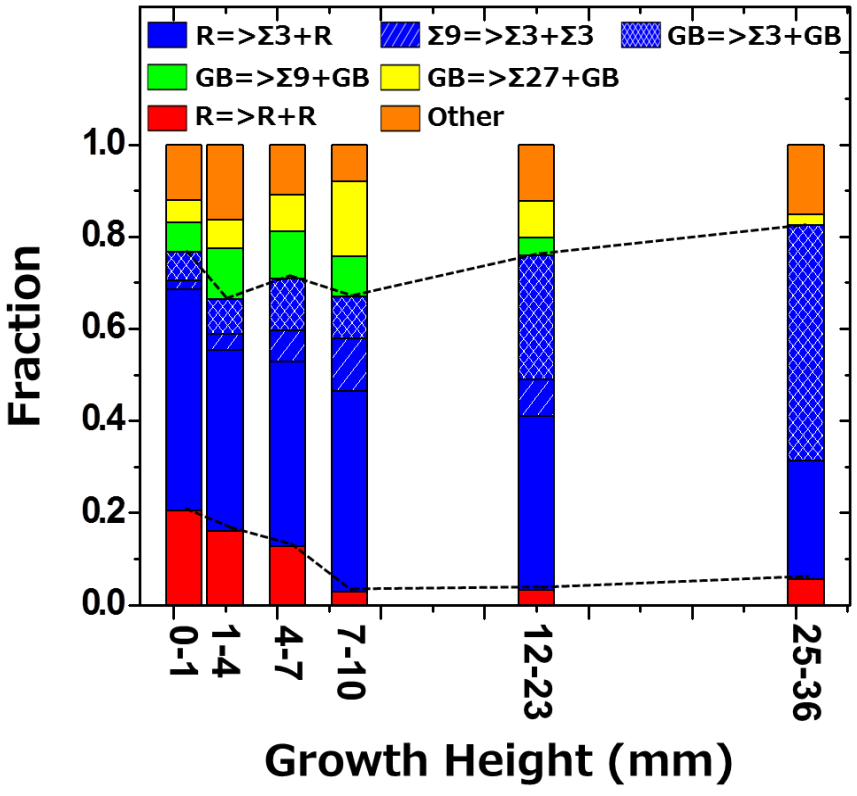

Fig. 6-4. Average fractions of Generation interactions by grain boundary character with respect to growth height. [6-10]

6-3-3-2 Fractions of Annihilation by Grain Boundary Character

Fig. 6-5. shows the average Annihilation by GB character, as a fraction of total Annihilation, with respect to growth height. Major Annihilation for R GBs is R+R=>R. This interaction is high at initial growth stage, decreases rapidly until 10 mm and then slowly thereafter with growth. Total of Σ9, Σ27 and other Annihilations increase until 10 mm however, decreases thereafter with growth. Dominant Annihilation involves Σ3 GBs and total Σ3 Annihilation (i.e. sum of Σ3+R=>R, Σ3+Σ3=>Σ9 and Σ3+GB=>GB) is 43% at 0-1 mm and increases to 75% at 25-36 mm. This results shows that Σ3 GBs dominate Annihilation, while R GB Annihilation fraction decreases with growth.

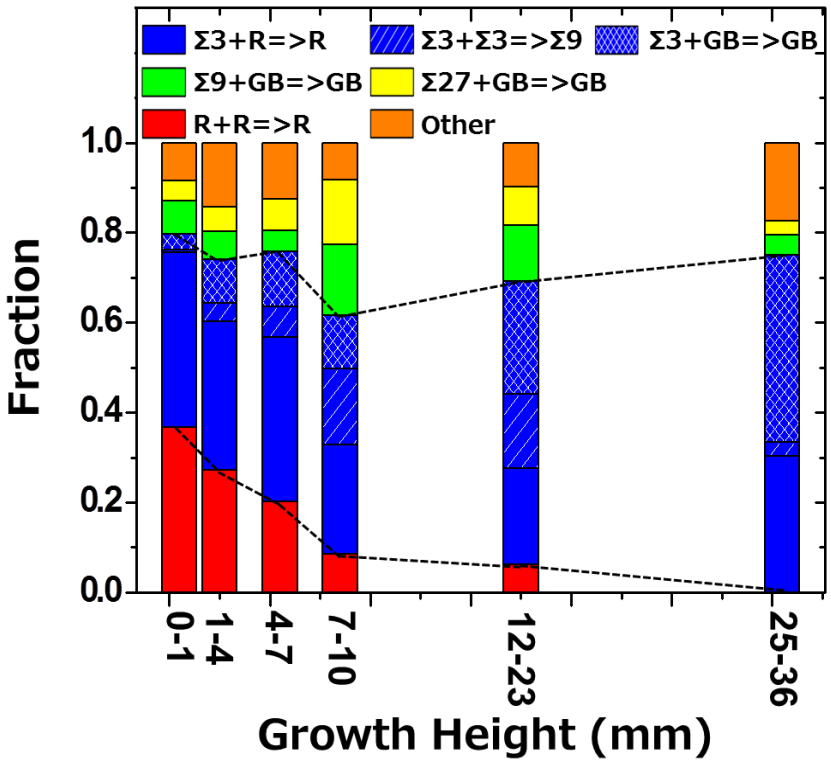

Fig. 6-5. Average fractions of Annihilation interactions by grain boundary character with respect to growth height. [6-10]

6-4 Discussions on Grain Boundary Interactions

It was observed in Fig. 6-2 that the total number of GB interactions is high initially, decreases rapidly and then decreases slowly with growth height. This was consistent with the change in grain size and aspect ratio with growth height, as discussed in Chapter 4 [6-9]. We have defined the three different tendencies, into 3 stages as shown in Fig. 6-3, to explain this phenomenon.

6-4-1 Grain Boundary Interactions at Stage I

In stage **I**, the grain size and the aspect ratio is small, meaning there are small equiaxed grains, as can be seen in Fig. 6-6. This means that the distance between GBs is small; hence the probability of inclined GBs (GBs not parallel to growth direction) to merge is high giving a high number of Annihilation. It was also observed that inclined GBs growing from the template also contributed to the high amount of Annihilation. The total number of Generation is also high in stage **I**, which can be attributed to the high number of R GB splitting, giving a high fraction of R=>R+R (see Fig. 6-4) and also can be seen in Fig. 6-6 (b). Between 0-1 mm the fraction of Annihilation is much higher than Generation, however with growth the impact of the slanted GBs from template decreases

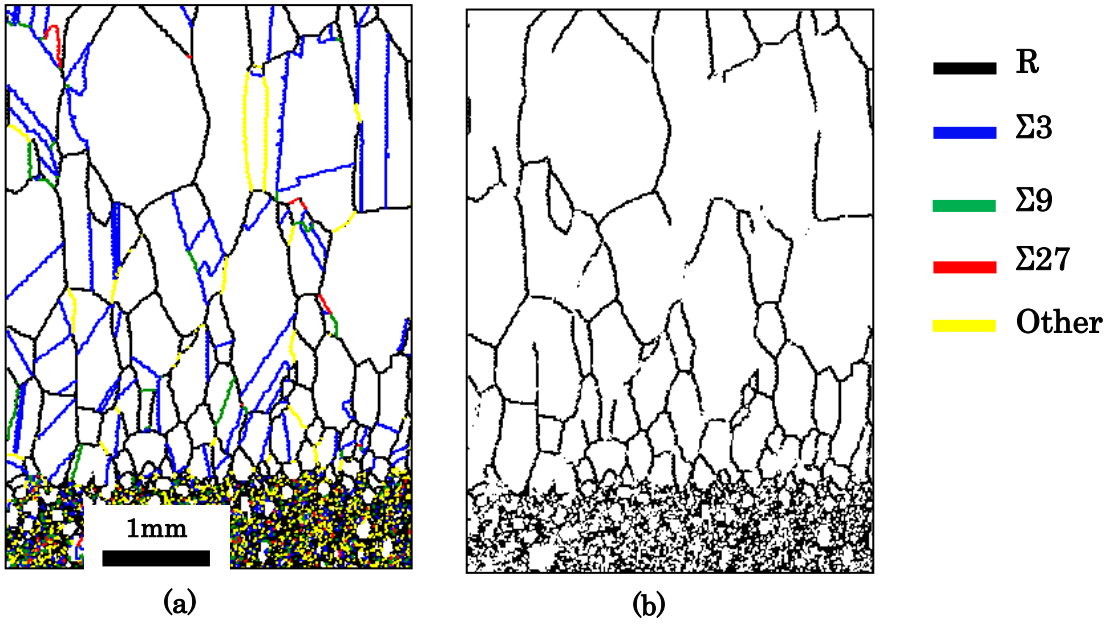

Figure 6-6. Grain boundaries between growth height 0 mm to 4mm (Stage **I**) showing: (a) R, Σ3, Σ9, Σ27, other GBs and (b) only R GBs (color code on the right)

and the grains increase in size leading to a decrease in Annihilation fraction.

6-4-2 Grain Boundary Interactions at Stage II

In stage **II**, there is a rapid decrease in the total number of interactions (Fig. 6-2) and the Annihilation fraction rapidly increases (6-3) with growth height. Looking closely in this region, it can be observed that the grain size increases while R GBs becomes parallel to growth direction as grains become elongated, (see Fig. 6-7). These two factors decrease the probability of R GBs to intersect to cause Annihilation explaining the decrease in fraction of R GB Annihilations as shown in Fig. 6-5. R GB Generation also decreases rapidly in this region contributing to the lower fraction of Generations. In stage **II**, Generation and Annihilation of CSL GBs, especially Σ3 increases rapidly. The Generation of Σ3 is likely due to its significantly low energy [6-11, 6-12, 6-13]. Σ9 and Σ27 is likely due to the interactions of Σ3 GBs as explained in the following equation [6-14]:

$$\Sigma A+\Sigma B\rightarrow\Sigma(A\text{x}B) \quad \text{or} \quad \Sigma A+\Sigma B\rightarrow\Sigma(A/B) \qquad (6\text{-}1)$$

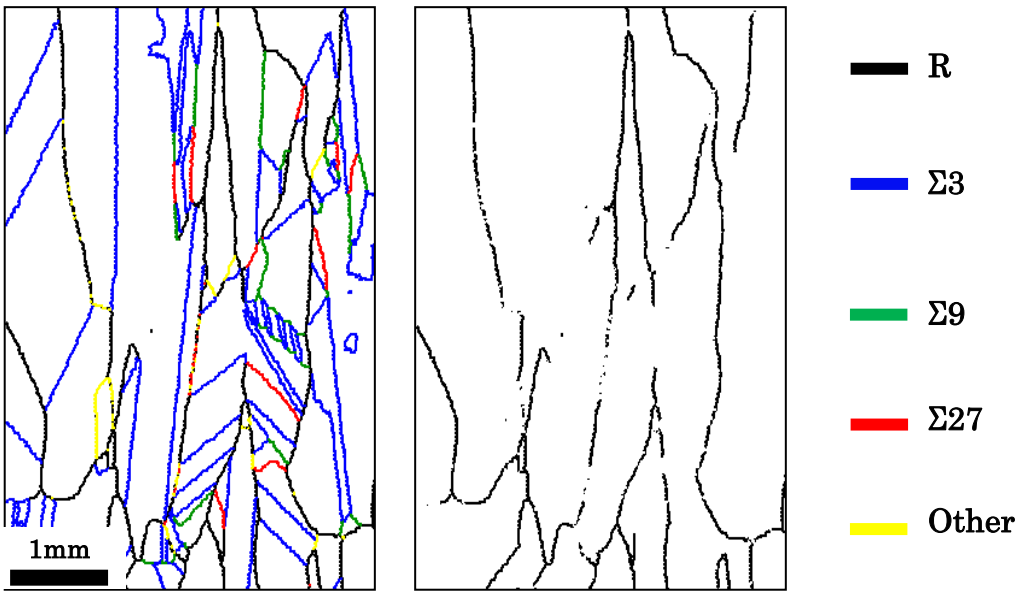

Figure 6-7. Grain boundaries between growth height 4 mm to 10mm (Stage **II**) showing: (a) R, Σ3, Σ9, Σ27, other GBs and (b) only R GBs (color code on the right)

The second relationship applies only if A/B is an integer and $A>B$. Accordingly, the meeting of two Σ3 GBs leads to a Σ9, and if two boundaries at a triple grain junction are Σ3 and Σ9, the third junction is either another Σ3 or Σ27. This relationship also applies with high Σ values involving $\Sigma 3^n$, for example:

$$\Sigma 27+\Sigma 9 \rightarrow \Sigma 243 \qquad (6\text{-}2)$$

Equation 6-2 also explains how Σ9 and Σ27 Generated from R GBs, since in this study very high Σ values were considered as R GBs. Although, the total GB interactions decrease, both in terms of Generation and Annihilation, the fraction of Annihilation increases rapidly in this region showing a decrease in GB density.

6-4-3 Grain Boundary Interactions at Stage III

In stage **III**, the grains are mainly columnar and the R GBs are mostly parallel to growth direction as can be observed in Fig. 6-8. Both Generation and Annihilation for R GBs is low. This can be attributed to the larger grain size and the R GBs parallel to growth direction. Compared to stage **II**, in stage **III** the grains are already columnar so

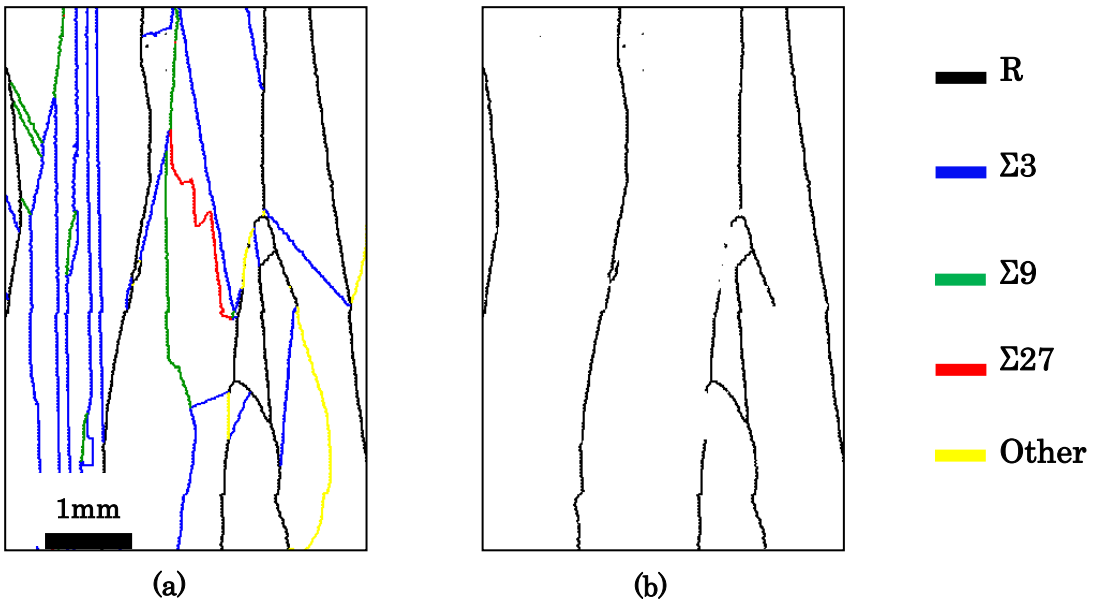

Figure 6-8. Grain boundaries between growth height 14 mm to 20 mm showing: (a) R, Σ3, Σ9, Σ27, other GBs and (b) only R GBs (color code on the right)

there is very little change in the tendency of GB interactions with growth height. The Σ3 GBs dominate the GB interactions similar to stage **II**, since they form easily and are inclined so they have a higher probability of merging with other GBs and Annihilate. The tendency of GB interactions in Stage **III** is steady and it can be expected that at this stage the influence of the template is low, hence the dominance of Σ3 GB interactions is expected to be valid in mc-Si regardless of the template.

6-5 Impact of Grain Boundary Interactions on Grain Structure Evolution: Σ3 and Random Grain Boundaries

In section 6-3, GB interaction was studied in detail and it was established that the dominant GB interaction is that which involves Σ3 GBs, especially at later stage of growth. In this section, the impact of GB interaction on grain structure evolution will be discussed. The GB triple junctions were studied in vertical wafers with respect to change in inclination after GB Generation and Annihilation interactions.

Generally, R GBs without any interaction with other GBs grow parallel to growth direction especially in stages **II** and **III** as defined in section 6-3. For R GBs this is easier because it has zero degrees of freedom fixed, in contrast to coherent GBs, for example Σ3, which has all five degrees of freedom fixed [6-14]. Geometrically, if all GBs are parallel to growth direction, the grain size will remain constant throughout growth as shown in schematics of Fig. 6-9 (a). Therefore the GBs parallel to growth direction limit the change in grain size.

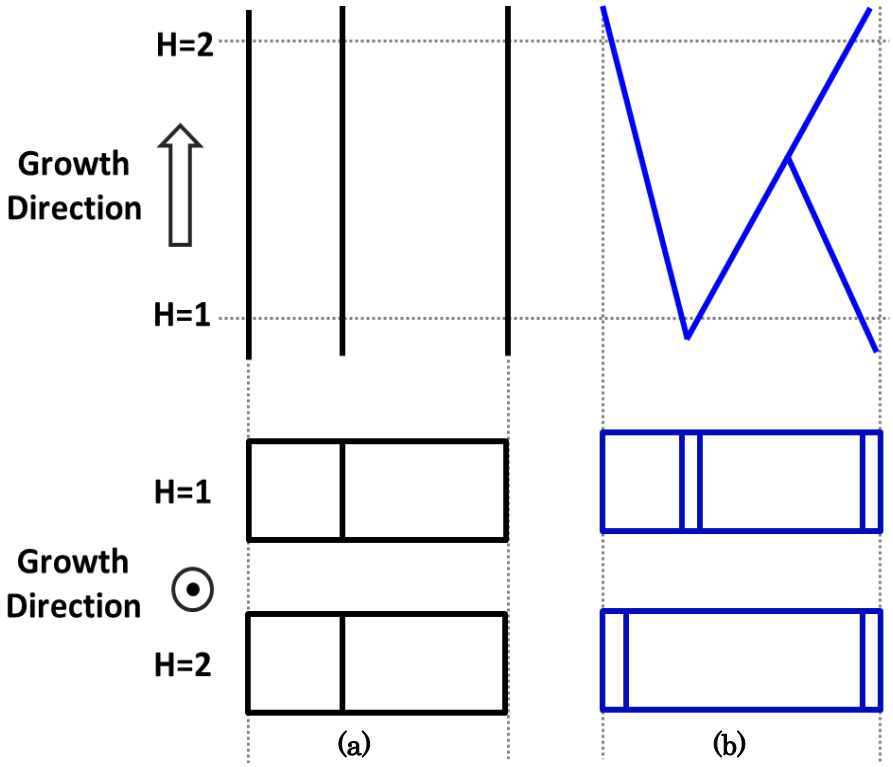

Figure 6-9. Schematics of grain size evolution in case of grain boundaries (a) parallel to growth direction, (b) not parallel to growth direction (inclined). H=1 is near initial region of growth, H=2 is at later stage of growth.

Consequently, if there is a high fraction of R GBs, the grain size will be heavily influenced by the inclination of the R GBs. Since mc-Si grown from small randomly oriented seeds (this sample, HP-mc) have a high fraction of R GBs, especially at initial stage of growth, the inclination of R GBs is an important factor to consider. On the other hand since coherent GBs have fixed degrees of freedom, the GB inclination is determined by the orientation of the grains, and in many cases in this sample the coherent GBs, such as Σ3, are not parallel to growth direction. The different inclinations of coherent GBs due to the different orientations of the grains, lead to change in grain size with growth, as shown in schematics in Fig. 6-9 (b). In mc-Si grown from small randomly oriented seeds, the grain size increases, as well as the fraction of R GBs decrease, as discussed in Chapter 4. Moreover, in Section 6-3 it was statistically illustrated that the dominant R GB Annihilation is merger of two R GBs (R+R=>R). It was also observed that even though a high fraction of Σ3 GBs Annihilate at R GBs, the resulting GB is R GB (Σ3+R=>R), which means this does not decrease the density of R GBS. Therefore it is expected that R GBs would need to become inclined somehow to be able to merge and Annihilate.

In the vertical wafers it was observed that the inclination of R GBs changed when a Σ3 GB was Generated from R GB (R=>Σ3+R). As can be seen in Fig. 6-10 (a), (marked by circles), R GBs inclined towards the opposite direction from which the Σ3 GB was generated. Even though this process does not directly decrease the density of R GBs, the inclination of R GBs that were parallel to growth direction increases the probability of those R GBs to merge with other R GBs. This will lead to an increase in grain size of the grain in which Σ3 was Generated. The inclination of the R GBs after Σ3 GB Generation may be due to the change in the number of fixed degree of freedom of R GBs after interaction with Σ3. Randle discussed that when an R GB interacts with an annealing twin (Σ3), the resulting GB will have four out of five degrees of freedom fixed [6-14]. Since four out of five degrees of freedom is fixed, the inclination of the R GB will depend on the orientation of the grains, hence R GBs follow the orientation of the grains rather than be parallel to the growth direction. It was also observed that even when some inclined R GBs would became parallel to growth direction, subsequent Σ3 Generation led to further R GB inclination, meaning twinned grains grow larger with growth.

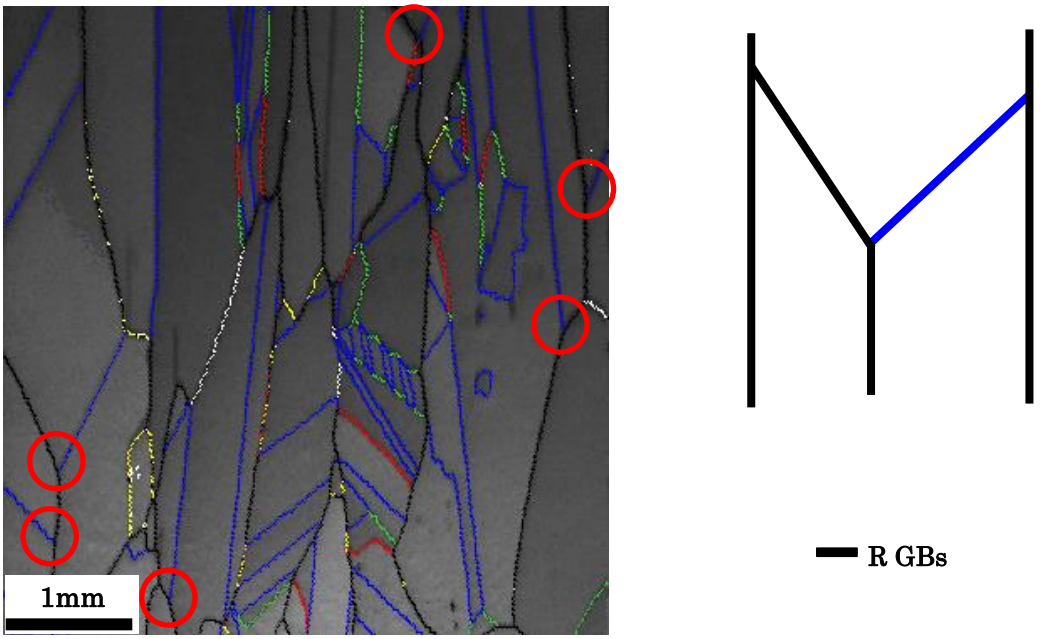

Figure 6-10. Grain boundary network showing (a) R GB inclination towards opposite direction of Generated Σ3 GB (circles), (b) schematic showing R GB Annihilation and consequent grain size increase after due to Σ3 Generation from R GBs.

This was confirmed in horizontal wafers, where some twinned grains grew larger much faster than other grains. Fig. 6-11. shows the inverse pole figure of wafers from growth height 7 mm, 8.5mm and 17 mm, with a twinned grain enclosed in circle. It is clearly observed that this twinned grain increases in size

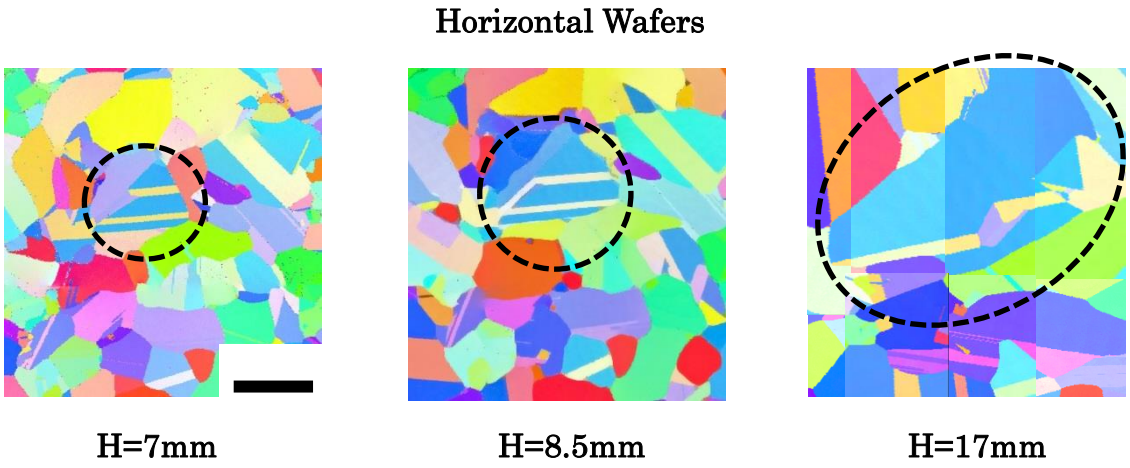

Figure 6-11. Inverse pole figures of horizontal wafers from growth heights 7 mm, 8.5 mm and 17 mm. The enclosed area in each wafer shows twinned grains which grow larger as growth height increases.

6-6 Summary

In mc-Si grown from small randomly oriented seeds the grain size was found to increase with growth height, while the distribution by GB type of changes. To investigate the impact of GB interactions on grain structure evolution, in this Chapter GB interactions were statistically studied in vertical wafers. GB interactions were mainly defined as Generation (increase in GB density) and Annihilation (decrease in GB density).

The total number of GB interactions decreased with growth height as grain size increased. From the tendency of Generation vs Annihilation fraction, 3 stages were defined:

- Stage **I:** High fraction of R GBs exists and inclined GBs from template and spherical grains increase probability of Annihilation.
- Stage **II**: Grains make a transition towards columnar shape and there is a rapid increase in GB Annihilation.
- Stage **III**: Growth is steady and the dominant GB interactions involve Σ3 GBs.

It was also found that Σ3 GB interactions with R GBs contribute to increase in grain size during growth. This could explain the difference between grain size evolution between mc-Si grown from small randomly oriented seeds (HP-mc) and conventional mc-Si.

This study clarifies GB interactions and its impact on the grain structure evolution in mc-Si grown from small randomly oriented grains. This knowledge will enable better optimization of mc-Si, especially HP-mc.

6-7 References

[6-1] Chen, Jun, et al. "Electron-beam-induced current study of small-angle grain boundaries in multicrystalline silicon." *Scripta Materialia* 52.12 (2005): 1211-1215.

[6-2] T. Buonassisi, M. D. Pickett, A. A. Istratov, E. Sauer, T. C. Lommason, E. Marstein, T. Pernau, R. F. Clark, S. Narayanan, S. M. Heald and E. R. Weber, *Proc. 4th World Conf. Photovoltaic Energy Conversion*, 2006, p. 944.

[6-3] Karzel, Philipp, et al. "Dependence of phosphorus gettering and hydrogen passivation efficacy on grain boundary type in multicrystalline silicon." *Journal of Applied Physics* 114.24 (2013): 244902.

[6-4] Zhu, Didi, et al. "Seed-assisted growth of high-quality multi-crystalline silicon in directional solidification." *Journal of Crystal Growth* 386 (2014): 52-56.

[6-5] Y. M. Yang, A. Yu, B. Hsu, W. C. Hsu, A. Yang, C. W. Lan, Prog. Photovolt: Res. Appl. (published online). http://dx.doi.org/10.1002/pip.2437 , 2013

[6-6] Lan, C. W., et al. "Grain control in directional solidification of photovoltaic silicon." *Journal of Crystal Growth* 360 (2012): 68-75.

[6-7] International Technology Roadmap for Photovoltaic, Fifth Edition 2014

[6-8] Wong, Y. T., C. Hsu, and C. W. Lan. "Development of grain structures of multi-crystalline silicon from randomly orientated seeds in directional solidification." *Journal of Crystal Growth* 387 (2014): 10-15.

[6-9] Prakash, Ronit R., et al. "Grain growth of cast-multicrystalline silicon grown from small randomly oriented seed crystal." *Journal of Crystal Growth* 401 (2014): 717-719.

[6-10] Prakash, Ronit R., et al. "Grain boundary interactions in multicrystalline silicon grown from small randomly oriented seeds." *Applied Physics Express* 8.3 (2015): 035502.

[6-11] Kohyama, Masanori, Ryoichi Yamamoto, and Masao Doyama. "Structures and Energies of Symmetrical〈 011〉 Tilt Grain Boundaries in Silicon." *Physica Status Solidi (b)* 137.1 (1986): 11-20.

[6-12] Kohyama, M., R. Yamamoto, and M. Doyama. "Reconstructed Structures of Symmetrical〈 011〉 Tilt Grain Boundaries in Silicon." *Physica Status Solidi (b)* 138.2

(1986): 387-397.

[6-13] Kohyama, M. "Structures and Energies of Symmetrical 〈 001〉 Tilt Grain Boundaries in Silicon." *Physica Status Solidi* (b) 141.1 (1987): 71-83.

[6-14] Randle, Valerie. "Twinning-related grain boundary engineering." *Acta Materialia* 52.14 (2004): 4067-4081.

CHAPTER 7:

Summary

In this work the grain structure evolution in multicrystalline silicon (mc-Si) grown from small randomly oriented seeds was investigated. Mc-Si was grown from a microcrystalline silicon (micro-Si) template, which has randomly oriented grains with an average grain size of 100µm. The grain structure was studied in vertical and horizontal wafers using electron backscatter diffraction. In particular the grain size, boundary, shape and orientation distribution was studied with respect to growth height. Three main areas of this research are: grain structure evolution in mc-Si grown from small random grains (Chapter 4), impact of pulling rate on grain structure evolution (Chapter 5) and grain boundary interactions and its impact on grain structure evolution (Chapter 6).

Grain structure evolution in mc-Si grown from microcrystalline template

In the mc-Si grown from micro-Si template at 15 mm/h crucible pulling rate (PR15), it was found that generally the grain size increased and random grain boundary fraction decreased with growth height. The results suggested a three stage growth process. In stage I (Initial stage), the grains are small and spherical with respect to growth direction and a high density of random grain boundaries exist. However, with growth the grain size increases, and the fraction of random grain boundaries decreases. It was found that this stage is heavily influenced by the template. In stage II, (Transient stage), the average grain size perpendicular to growth direction is almost constant, while grains elongate in growth direction becoming ellipsoidal. The R GBs become mostly parallel to growth direction. In stage III, (Steady stage), the average grain size steadily increases with growth height and the random grain boundary density decreases much faster compare to the Σ3 grain boundaries. The grains elongate towards the growth direction and become columnar. The grains align with growth and grains with near-orientations of <112> and <122> become larger than other grains. The grain structure of the template grown ingot was compared with an ingot grown by the conventional mc-Si growth method. In conventional mc-Si, there seems to be two growth stages. The grains at the initial stage are much larger than those at the same region of the microcrystalline template grown ingot. There is also a high fraction of Σ3 grain boundaries, which are inclined and merge resulting in an increase in grain size, however due to formation of new Σ3 grain boundaries the overall average of grain size remains almost constant at later stage of growth. The comparison between the two growth methods highlighted the impact of the initial growth stage on the evolution of grain structure during growth.

Impact of pulling rate on grain structure evolution

The impact of crucible pulling rate on the grain structure evolution was studied in two ingots grown at different pulling rates. Grain structures were studied in mc-Si ingots grown from microcrystalline Si template at crucible pulling rates of 15 mm/h (PR15) and 45 mm/h (PR45) respectively. It was found that at higher pulling rate, the average grain size decreased and there was an enhancement of grain elongation leading to columnar grains. Moreover, it was found that twinning was also enhanced at higher pulling rate leading to a high fraction of Σ3 GBs. It was also observed that the tendency of decrease in randomness of grain orientations with growth height is less in PR45 compared to PR15. As the growth height increased a higher fraction of near-<112> and <122> appeared in both ingots, however in PR45, near-<111> fraction was also high. The results were discussed in terms of interfacial energy and twinning related to undercooling at GB grooves. However, PR 45 had a convex interface near the initial growth region and this may have affected the results.

Grain boundary interactions and its impact on grain structure evolution

Impact of GB interactions on grain structure evolution, was statistically studied in vertical wafers. GB interactions were mainly defined as Generation (increase in GB density) and Annihilation (decrease in GB density).

The total number of GB interactions decreased with growth height as grain size increased. From the tendency of Generation vs Annihilation fraction, 3 stages were defined:

- Stage **I:** High fraction of R GBs exists and inclined GBs from template and spherical grains increase probability of Annihilation.
- Stage **II**: Grains make a transition towards columnar shape and there is a rapid increase in GB Annihilation.
- Stage **III**: Growth is steady and the dominant GB interactions involve Σ3 GBs.

It was also found that Σ3 GB interactions with R GBs contribute to increase in grain size during growth. This could explain the difference between grain size evolution between mc-Si grown from small randomly oriented seeds (HP-mc) and conventional mc-Si. This study clarifies GB interactions and its impact on the grain structure evolution in mc-Si grown from small randomly oriented grains. This knowledge will enable better optimization of mc-Si, especially HP-mc.

The work in this thesis contributes important information related to the grain structure evolution in mc-Si grown from small randomly oriented seeds. The impact of the initial stage of growth, the pulling rate and the interaction between grain boundaries is shown in detail. Based on these results together with some further work, further optimization of mc-Si, especially HP mc-Si may be achieved.

Further Work

In this thesis the grain structure evolution in mc-Si grown from microcrystalline template was investigated. However, with regards to solar cells, dislocation density and the electrical activity is also very important. For future work, lifetime measurements and electrical activity of the extended defects in the microcrystalline template grown ingot would be helpful to understand the viability of this type of growth with respect to solar cell application. The electrical activity of the grain boundaries at different growth height can be measured by electron beam induced current to identify the highly detrimental grain boundaries. Knowledge on the generation and annihilation of highly detrimental GBs could make it easier to control those GBs leading to further improvements in the quality of the mc-Si wafers.

Moreover, further work could lead to a detailed model explaining grain structure evolution in multicrystalline silicon. The impact of changing the pulling rate during the growth, or studying grain structure evolution using specially organized small seeds with pre-determined orientations are some suggestions to further improve the knowledge of grain structure evolution in mc-Si.

List of Publications

First Author Papers

1. R.R. Prakash, T. Sekiguchi, K. Jiptner, Y. Miyamura, J. Chen, H. Harada and K. Kakimoto, "Grain Growth of cast-multicrystalline silicon grown from small randomly oriented seed crystal", *Journal of Crystal Growth* 401, (2014) 717

2. R.R. Prakash, K. Jiptner, J. Chen, Y. Miyamura, H. Harada and T. Sekiguchi, "Grain boundary interactions in multicrystalline silicon grown from small randomly oriented seeds", *Applied Physics Express* 8, (2015) 035502

3. R. R. Prakash, K. Jiptner, J. Chen, Y. Miyamura, H. Harada and T. Sekiguchi, "Control of extended defects in cast multicrystalline Silicon using polycrystalline template", *Physica Status Solidi,* Submitted

Co-Author Papers

1. Y. Miyamura, J. Chen, R. R. Prakash, K. Jiptner, H. Harada and T. Sekiguchi, "Dislocation generation and propagation across the seed in seed cast-Si ingots", *Acta Physica Polonia A* Vol. 125 (2014) 1024

2. Y. Miyamura, H. Harada, K. Jiptner, J. Chen, R. R. Prakash, S. Nakano, B. Gao, K. Kakimoto and T. Sekiguchi, " Crystal growth of 50 cm square mono-like Si by directional solidification and its characterization", *Journal of Crystal Growth* 401, (2014) 133

3. J. Li, R. R. Prakash, K. Jiptner, J. Chen, Y. Miyamura, H. Harada, K. Kakimoto, A. Ogura and T. Sekiguchi, " Butterfly-shaped distribution of SiNx precipitates in multicrystalline Si for Solar Cells", *Journal of Crystal Growth* 377, (2013) 37

4. J. Chen, R. R. Prakash, J. Li, K. Jiptner, Y. Miyamura, H. Harada, A. Ogura, and T. Sekiguchi, "Analysis of inhomogeneous dislocation distribution in multicrystalline silicon", *Solid State Phenomena* Vol. 205-206 (2013)77

5. Y. Miyamura, H. Harada, K. Jiptner, J. Chen, R. R. Prakash, J. Li, T. Sekiguchi, T. Kojima, Y. Ohshita, A. Ogura, M. Fukuzawa, S. Nakano, B. Gao and K. Kakimoto, *Solid State Phenomena* Vol. 205-206 (2013) 89

List of Presentations

Oral Presentations

1. R. R. Prakash, Y. Miyamura, J. Chen, K. Jiptner, J. Li, H. Harada and T. Sekiguchi, " Directional growth of multicrystalline silicon from crucible and microcrystal template", *7th International Workshop on Crystalline Silicon Solar Cells, Kyushu, Japan 2013.10*
2. R. R. Prakash, Y. Miyamura, J. Chen, K. Jiptner, J. Li, H. Harada and T. Sekiguchi, " Directional growth of multicrystalline silicon from microcrystal feedstock", *74th JSAP Autumn Meeting, Kyoto, Japan 2013.09*
3. R. R. Prakash, Y. Miyamura, J. Chen, K. Jiptner, H. Harada and T. Sekiguchi, "Modelling of unidirectional solidification of multicrystalline silicon", *17th International Conference on Crystal Growth Epitaxy, Warsaw, Poland, 2013.08*
4. R. R. Prakash, Y. Miyamura, J. Chen, K. Jiptner, J. Li, H. Harada and T. Sekiguchi, " Impurity decoration on extended defects in multicrystalline silicon", *73rd Japan Society for Applied Physics (JSAP) Autumn Meeting, Ehime, Japan 2012.09*

Poster Presentation

1. R. R. Prakash, K. Jiptner, Y. Miyamura, J. Chen, H. Harada and T. Sekiguchi, "Impact of growth rate on multicrystalline silicon grown from small randomly oriented seeds", *The 6th World Conference on Photovoltaic Energy Conversion, Japan 2014.11*
2. R. R. Prakash, K. Jiptner, Y. Miyamura, J. Chen, H. Harada and T. Sekiguchi, "Extended defects in multicrystalline silicon grown by directional solidification using polycrystalline template", *The 7th Forum on the Science and Technology of Silicon Materials 2014, Japan 2014.10*
3. R. R. Prakash, Y. Miyamura, J. Chen, K. Jiptner, H. Harada and T. Sekiguchi, "Grain boundary electrical activity and growth in multicrystalline silicon", *75th JSAP Autumn Meeting, Japan 2014.09*
4. R. R. Prakash, Y. Miyamura, J. Chen, K. Jiptner, H. Harada and T. Sekiguchi, "Analysis of grain structure of multicrystalline silicon grown from microcrystal template", *12th International Workshop on Beam Injection Assessment of*

Microstructures in Semiconductors and 12th Joint Symposium on Electronic Materials, Japan 2014.06

5. R. R. Prakash, Y. Miyamura, J. Chen, K. Jiptner, J. Li, H. Harada and T. Sekiguchi, " Grain evolution in multicrystalline silicon grown from small randomly oriented seeds", *61st JSAP Spring Meeting, Kanagawa, Japan 2014.03*
6. R. R. Prakash, Y. Miyamura, J. Chen, K. Jiptner, J. Li, H. Harada and T. Sekiguchi, " Multicrystalline silicon grown from microcrystalline template", *Kinken Wakate 2013 Sendai, Japan, 2013.11*
7. R. R. Prakash, Y. Miyamura, J. Chen, K. Jiptner, J. Li, H. Harada and T. Sekiguchi, " Grain growth behavior of directionally grown multicrystalline silicon", *60th JSAP Spring Meeting, Kanagawa, Japan 2013.03*

List of Figures

List of Tables